MICROCOPY RESOLUTION TEST CHART

NATIONAL BUREAU OF STANDARDS 1963 A

ECAC-TR-83-003

DEPARTMENT OF DEFENSE
Electromagnetic Compatibility Analysis Center
Annapolis, Maryland 21402

ANTENNA PATTERN MEASUREMENTS TO CHARACTERIZE
THE OUT-OF-BAND BEHAVIOR OF REFLECTOR ANTENNAS

Prepared for

Electromagnetic Compatibility Analysis Center
North Severn
Annapolis, MD 21401

DTIC

DEC 1 9 83

DECEMBER 1983

Prepared by

B. J. Cown, C. E. Ryan Jr., and E. E. Weaver
of
Georgia Institute of Technology
Engineering Experiment Station
Atlanta, GA

IIT Research Institute
Under Contract to
Department of Defense

Approved for public release; distribution unlimited.

DTIC FILE COPY

AD-A136199

83 12 19 014

This report was prepared by the Georgia Institute of Technology Engineering Experiment Station as an item of external support to EMC Engineering Development of the IIT Research Institute as part of AF Project 649E under Contract F-19628-80-C-0042 with the Electronic Systems Division of the Air Force Systems Command in support of the DoD Electromagnetic Compatibility Analysis Center, Annapolis, Maryland.

This report has been reviewed and is approved for publication.

Reviewed by

William D. Stuart

WILLIAM D. STUART
Project Manager, IITRI

Kalle R. Kontson

KALLE R. KONTSON
Assistant Director
Contractor Operations

Approved by

Charles L. Flynn

CHARLES L. FLYNN, Col, USAF
Director

Arvel M. Messer

ARVEL M. MESSER
Deputy Director
Plans and Technical Resources

REPORT DOCUMENTATION PAGE		READ INSTRUCTIONS BEFORE COMPLETING FORM
1. REPORT NUMBER ECAC-TR-83-003	2. GOVT ACCESSION NO. AD-A136199	3. RECIPIENT'S CATALOG NUMBER
4. TITLE (and Subtitle) ANTENNA PATTERN MEASUREMENTS TO CHARACTERIZE THE OUT-OF-BAND BEHAVIOR OF REFLECTOR ANTENNAS		5. TYPE OF REPORT & PERIOD COVERED Final Technical Report Dec.21, 1980-Sept.30, 1981
		6. PERFORMING ORG. REPORT NUMBER
7. AUTHOR(s) B. J. Cown, E. E. Weaver, and C. E. Ryan, Jr.		8. CONTRACT OR GRANT NUMBER(s) F-19628-80-C--0042 CDRL # 10P
9. PERFORMING ORGANIZATION NAME AND ADDRESS Electromagnetic Effectiveness Division, Engineering Experiment Station, Georgia Institute of Technology, Atlanta, Georgia 30332		10. PROGRAM ELEMENT, PROJECT, TASK AREA & WORK UNIT NUMBERS
11. CONTROLLING OFFICE NAME AND ADDRESS Electromagnetic Compatibility Analysis Center North Severn		12. REPORT DATE DECEMBER 1983
Annapolis, MD 21402		13. NUMBER OF PAGES 106
14. MONITORING AGENCY NAME & ADDRESS(If different from Controlling Office)		15. SECURITY CLASS. (of this report) UNCLASSIFIED
		15a. DECLASSIFICATION/DOWNGRADING SCHEDULE

16. DISTRIBUTION STATEMENT (of this Report)

Approved for public release; distribution unlimited.

Accession For
NTIS GRA&I
DTIC TAB
Unannounced
Justification

17. DISTRIBUTION STATEMENT (of the abstract entered in Block 20, If different from Report)

By
Distribution/
Availability Codes
Avail and/or
18. SUPPLEMENTARY NOTES
Dist Special

A-1

19. KEY WORDS (Continue on reverse side if necessary and identify by block number)

ANTENNA PATTERN	REFLECTOR ANTENNA	GAIN
OUT-OF-BAND	FEED HORNS	MEDIAN GAIN
HIGHER-ORDER MODES	COMPACT RANGE	ELECTROMAGNETIC COMPATIBILITY
WAVEGUIDE MODES	DATA LOGGER	

20. ABSTRACT (Continue on reverse side if necessary and identify by block number)

Research was conducted to collect and describe out-of-band antenna pattern data. The research efforts were devoted (1) to deriving valid measured data for a reflector antenna for out-of-band frequencies spanning intervals around the second and third harmonics of the in-band design frequency and (2) to statistically characterize the measured data. The second harmonic data were collected for both polarization senses for the out-of-band frequencies of 5.5 GHz to 7.5 GHz in steps

DD FORM 1473 EDITION OF 1 NOV 65 IS OBSOLETE

i

Block 20. Continued.

of 0.1 GHz. The third harmonic data were collected for both polarization
senses for the out-of-band frequencies of 8.0 GHz to 10.0 GHz in
steps of 0.1 GHz. Additionally, in-band data were collected at 2.9,
3.0, and 3.1 GHz for both polarization senses.

The measured data were collected on the Georgia Tech compact antenna
range test facility with the aid of an automated data logger system
designed expressly for efficient collection of broadband antenna data.
The pattern data, recorded directly on magnetic disks, were analyzed
(1) to compute average gain and standard deviation over selected
angular sectors, (2) to construct cumulative probability curves, and
(3) to specify the peak gain and the angular coordinates of the peak at
each frequency. The measured pattern data and associated statistical
data derived therefrom provide a valuable initial data base for EMC
analysis at out-of-band frequencies.

EXECUTIVE SUMMARY

The coupling of electromagnetic energy between pairs of collocated antennas operating in different frequency bands is a problem that is becoming increasingly serious with the growth of antenna density per site. Thus, the electromagnetic compatibility (EMC) analyst must be able to predict and describe the out-of-band antenna coupling phenomena in order to achieve maximum electromagnetic effectiveness for a given antenna installation. The prediction/description of such phenomena is especially difficult because of the existence of higher-order modes in the antenna feed systems. These modes produce far-field patterns representing a complex summation of the individual higher-order mode patterns.

Since it is usually not possible to specify analytically the precise complex excitation coefficients of the higher-order modes, and since very little measured data is available to characterize empirically the out-of-band performance, the Electromagnetic Compatibility Analysis Center engaged the Georgia Institute of Technology (Georgia Tech) to conduct measurement research on a representative reflector antenna at the Georgia Tech compact antenna range.

The antenna selected for testing was a 4-foot-diameter paraboloidal reflector antenna. The antenna was fed at the prime focus with a horn, and had an F/D ratio of 0.32 and a design frequency of 3.0 GHz.

The measurements were conducted on the Georgia Tech compact antenna range, with the aid of a computer-based data-gathering system especially designed for the collection of broadband out-of-band antenna pattern data.

Housing for the compact antenna range was an absorber-lined room 28 feet wide, 26 feet long, and 16 feet high. The transmitting horn projected from the floor and illuminated a silver-painted paraboloidal sector 16 feet wide and 12 feet high. Reflections from this paraboloidal sector were probed to

verify that the quasi-plane wave fields incident on the test antenna were "flat" within 0.5 dB in amplitude and 10 degrees in phase over the extent of the test antenna aperture.

The data logger was initialized so that all patterns were referenced to the electrical boresight at 3.0 GHz. The data was recorded for both polarizations at 2.9 GHz, 3.0 GHz, and 3.1 GHz, and over the ranges of 5.5 GHz to 7.5 GHz and of 8.0 GHz to 10.0 GHz in steps of 0.1 GHz. Data acquisition was limited to a sector of no more than 80 degrees in azimuth and 20 degrees in elevation.

From the measurements it was found that the peak gains of the out-of-band patterns were generally comparable with the peak gain at the in-band design frequency. The peak of the out-of-band radiation was typically shifted in azimuth and elevation away from the in-band electrical boresight direction, but the shifts were usually less than the 3-dB beamwidth of the shifted "beam." Most of these peaks were greater than 25 dBi. Several secondary lobes were also prominent.

A substantial cross-polarized pattern was radiated for the out-of-band frequencies. The peak gains of the cross-polarized patterns were greater than 10 dBi for the majority of the tested frequencies.

Although it is noted that the cumulative probability distributions computed from the measured data differ noticeably from a Gaussian distribution, it is believed that the Gaussian approximation still provides useful engineering estimates for the cumulative probability distributions.

Additional measurements are recommended as being needed for various types and lengths of waveguide transmission components over frequency bands centered about the fundamental, and both the second and third harmonic frequencies. It is further recommended that statistical processing be performed on the data to

determine whether the different transmission line devices result in significant changes in the out-of-band statistical average pattern performance.

It is recommended that both the data measured on this project and the data to be measured in future projects be compared to the mean pattern and standard deviations calculated with the Monte Carlo computer model developed in a companion project. The computer model outputs are presently in K-space and would need to be transformed to azimuth-elevation space to be compared with the data presented herein.

FOREWORD

The research on this program was carried out by personnel of the Electromagnetic Effectiveness Division of the Electronics and Computer Systems Laboratory of the Engineering Experiment Station at the Georgia Institute of Technology, Atlanta, Georgia 30332. The program was sponsored by the Electromagnetic Compatibility Analysis Center, North Severn, Annapolis, Maryland under Contract No. F-19628-80-C-0042. The program is designated by Georgia Tech as Project A-2548. This Final Technical Report covers the period from December 21, 1980 to September 30, 1981. The technical efforts were under the general supervision of Dr. C. E. Ryan, Jr., Chief of the Electromagnetic Effectiveness Division and under the direct supervision of Mr. B. J. Cown, who served as Project Director. The authors gratefully acknowledge the extensive computer programming efforts of Mr. Chris Papanicolopulos and the considerable clerical skills of Ms. Beatriz Gonzalez.

Respectfully submitted,

Barry J. Cown

Barry J. Cown
Project Director

Approved:

Charles E. Ryan Jr.

Charles E. Ryan, Jr.
Chief,
EM Effectiveness Division

ECAC-TR-83-003

TABLE OF CONTENTS

TABLE OF CONTENTS (Continued)

x

TABLE OF CONTENTS (Continued)

TABLE OF CONTENTS (Continued)

LIST OF ILLUSTRATIONS (Continued)

TABLE OF CONTENTS (Continued)

TABLE OF CONTENTS (Continued)

TABLE OF CONTENTS (Continued)

SECTION 1

INTRODUCTION

The results of a 1.8 person-year research effort to collect and describe
out-of-band antenna pattern data are summarized herein. The research efforts
were devoted (1) to deriving valid measured pattern data for a reflector
antenna for out-of-band frequencies spanning intervals around the second and
third harmonics of the in-band design frequency and (2) to characterizing
statistically the measured data. The measured pattern data and the associated
statistical data derived therefrom provide immediately useful baseline
information that can be used in EMC applications. The pattern and statistical
data also serve as validation data for the recently developed out-of-band
reflector model.[1] The measured data may also be used to drive antenna-antenna
coupling prediction models that require the complex (amplitude and phase) far-
field electric field of the antenna as an input.[2]

This research work was motivated by several practical considerations. In
particular, the coupling of electromagnetic energy between cosited antennas
operating in different frequency bands is a serious problem in many
installations today, and one whose importance is likely to increase in the
future as the density of cosited antennas increases. It is, therefore,
imperative that the EMC analyst be able to predict and describe the out-of-
band coupling phenomena in order to achieve the maximum electromagnetic
effectiveness for a given antenna installation. Accurate analysis of antenna

---

[1]Wells, T. B. and Ryan, C. E. Jr., Out-of-Band Reflector Antenna Model,
Georgia Institute of Technology, Final Technical Report, Contract
DAAG29-80-C-0083, May 1981.

[2]Cown, B. J. and Ryan, C. E., Jr., Near-Field Theory and Techniques for
Wideband Radiating Systems at In-Band and Out-of-Band Frequencies, Georgia
Institute of Technology, Interim Technical Report No. 2, Contract No.
DAAG29-78-C-0029, March 1980.

coupling naturally requires a valid characterization of the radiation
properties of antennas at out-of-band frequencies. Of course, the
characterization of the reflector antenna pattern at an out-of-band frequency
presents a difficult problem due to the existence of higher-order modes in the
antenna feed system which produce far-field patterns representing a complex
summation of the individual higher-order mode patterns. Furthermore, very
little measured data is available to characterize empirically the out-of-band
performance of a reflector antenna. It is usually not possible to specify
analytically the precise complex excitation coefficients of the higher-order
modes, and hence a statistical characterization of the antenna excitation was
employed in developing the numerical simulation based upon a Monte Carlo model
for a reflector antenna under the companion research project cited in
Reference 1. However, even sufficient measurement data to validate the
analytical model are lacking. Accordingly, the measurements program described
herein was initiated.

Because the effects of higher-order modes which exist at out-of-band
frequencies are very sensitive to the RF transmission line components,
including the feed horn, attention should be focused on measurements for a
well-defined situation in order (1) to establish valid measurement procedures,
(2) to obtain baseline data for a representative reflector antenna, and (3) to
identify unique problem areas. Toward this end, the measurements were
conducted on the Georgia Tech compact antenna range[3,4] with the aid of a
computer-based data gathering system especially designed for collection of
broadband out-of-band antenna pattern data. This facility and the measurement
procedures are described in the next section. The antenna selected for

[3]Johnson, R. C., "Antenna Range for Providing a Plane Wave for Antenna
Measurements," U.S. Patent 3 302 205, January 31, 1967.

[4]Johnson, R. C., Ecker, A., and Moore, R. A., "Compact Range Techniques and
Measurements," IEEE Transactions on Antennas and Propagation, Vol. AP-17,
pp. 568-576, September 1969.

testing (see Figure 1) was a 4-foot-diameter horn-fed paraboloidal reflector antenna having an F/D ratio of 0.32 and a design frequency of 3.0 GHz. The feed horn is excited by an S-band coax-to-waveguide adapter. The coax-to-waveguide adapter and the straight section of the feed horn waveguide are constructed from standard WR-284 waveguide. The feed horn exit aperture is slightly flared in the TE_{10} E-plane. The feed horn and struts are described in APPENDIX A.

The magnitude of the out-of-band measurement problem can be appreciated by considering the possible higher-order modes (shown in Figure 2) that can exist in the WR-284 waveguide for the second and third harmonic frequency regions. For example, energy can be propagated in five different modes at the second harmonic frequency of 6.0 GHz. These possible modes are the TE_{10}, TE_{20}, TE_{01}, TE_{11}, and TM_{11}. Sketches of the transverse components of the waveguide electric fields for these five modes are shown in Figure 3. Note that the TE_{10} is polarized orthogonal to the TE_{01} mode and that the TE_{11} and TM_{11} modes have a component polarized orthogonal to the TE_{10}. Thus, a substantial cross-polarized radiation pattern may be present at out-of-band frequencies. Similar considerations apply for the third harmonic region where 17 modes are possible at 10.0 GHz.

The actual number of modes that are excited and their relative amplitudes and phases for a particular system depend on the RF transmission line system. Theoretical considerations indicate that a filamentary probe strongly favors excitation of modes which have no magnetic field intensity component parallel with the probe.[5] Thus, if the probe is aligned with, say, the y-axis shown in Figure 3, only the TM^{y}_{nm} modes for (n = 1,3,5,7...) and (m = 0,1,2,3,4...) are excited. Power flow down the guide is associated entirely with the y-polarized electric fields of the allowed TM^{y}_{nm} modes since $E_{y}H_{x} \neq 0$ while $E_{x}H_{y} = 0$. Computations of the power distribution among the

---

[5]Collin, R. E., *Field Theory of Guided Waves*, McGraw-Hill, Inc., 1960.
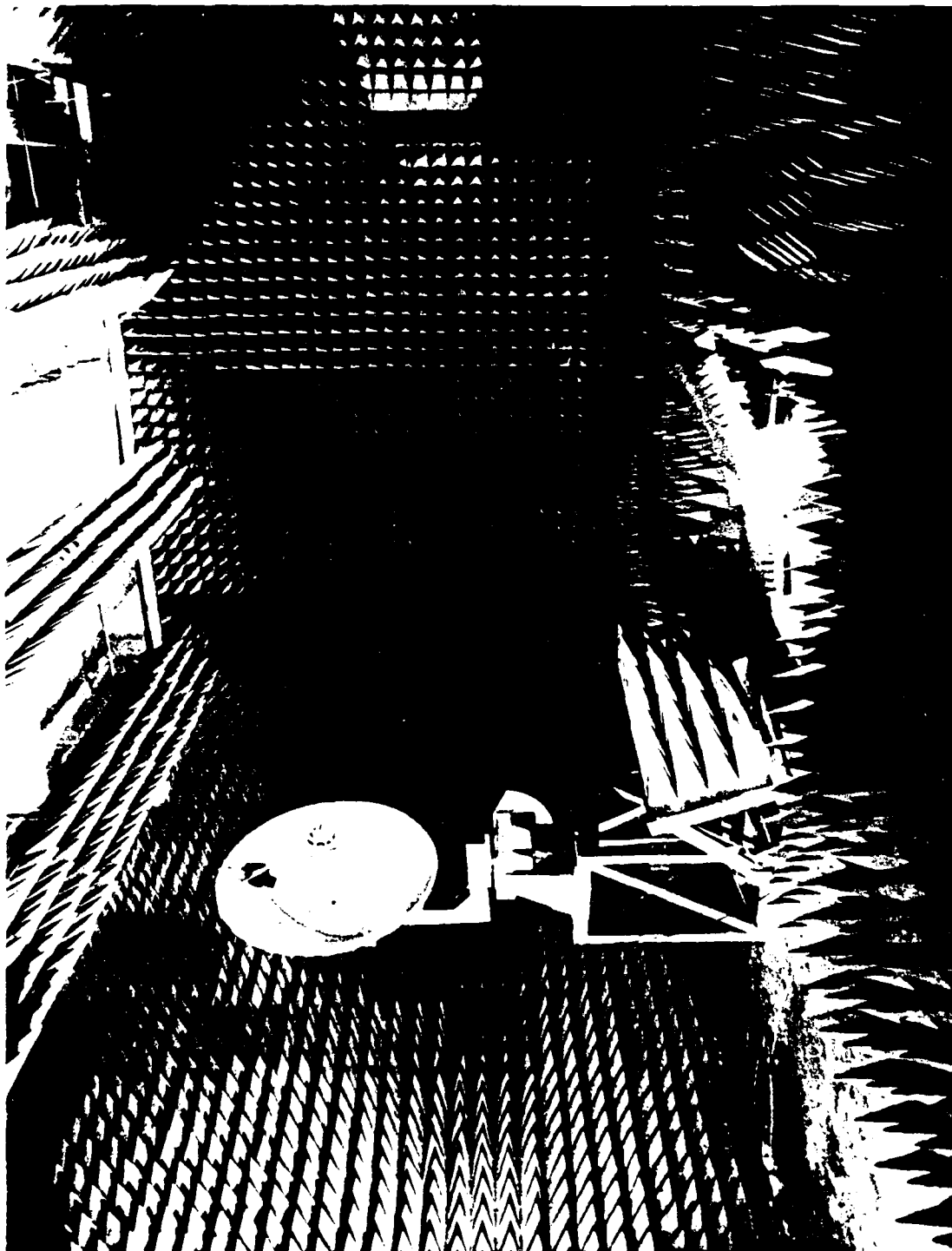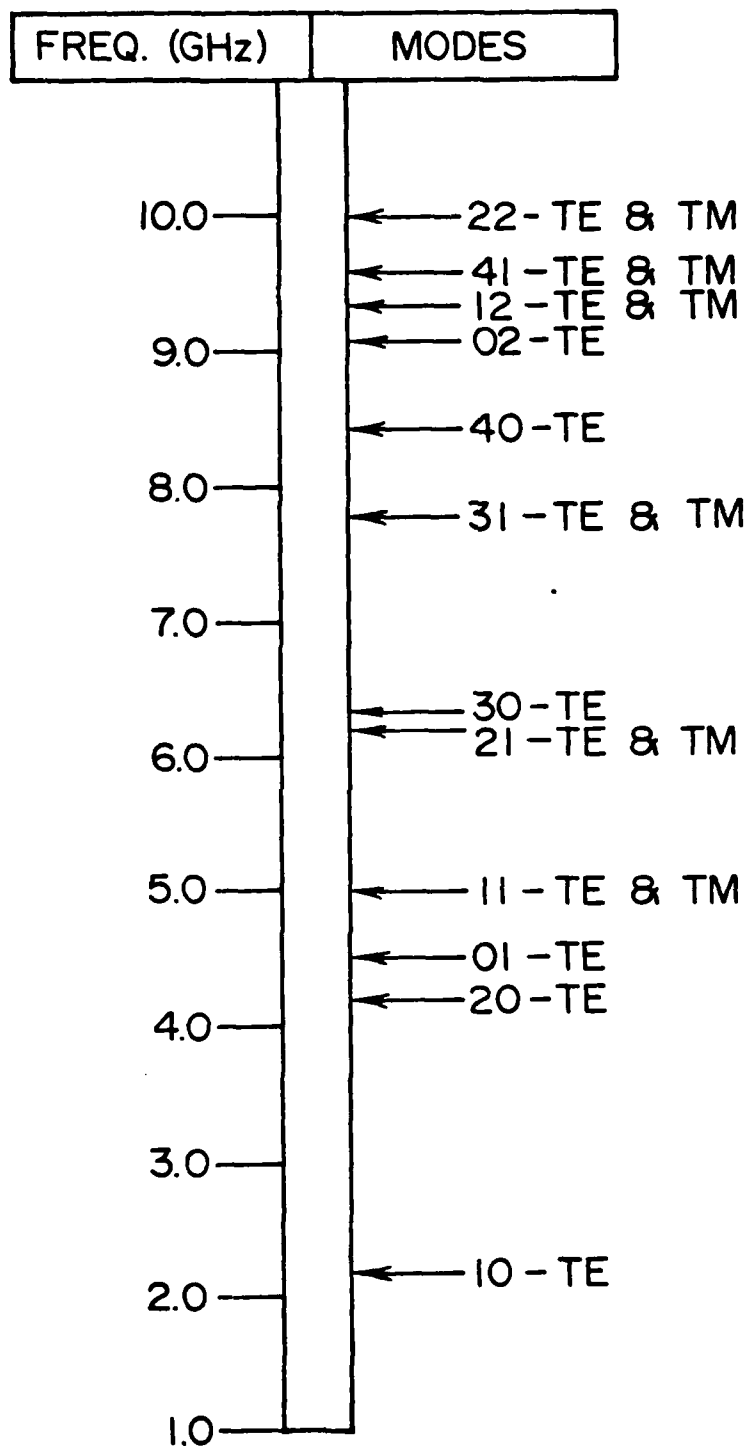
Figure 2.   Allowed higher-order modes versus frequency
for WR-284 S-band rectangular waveguide.
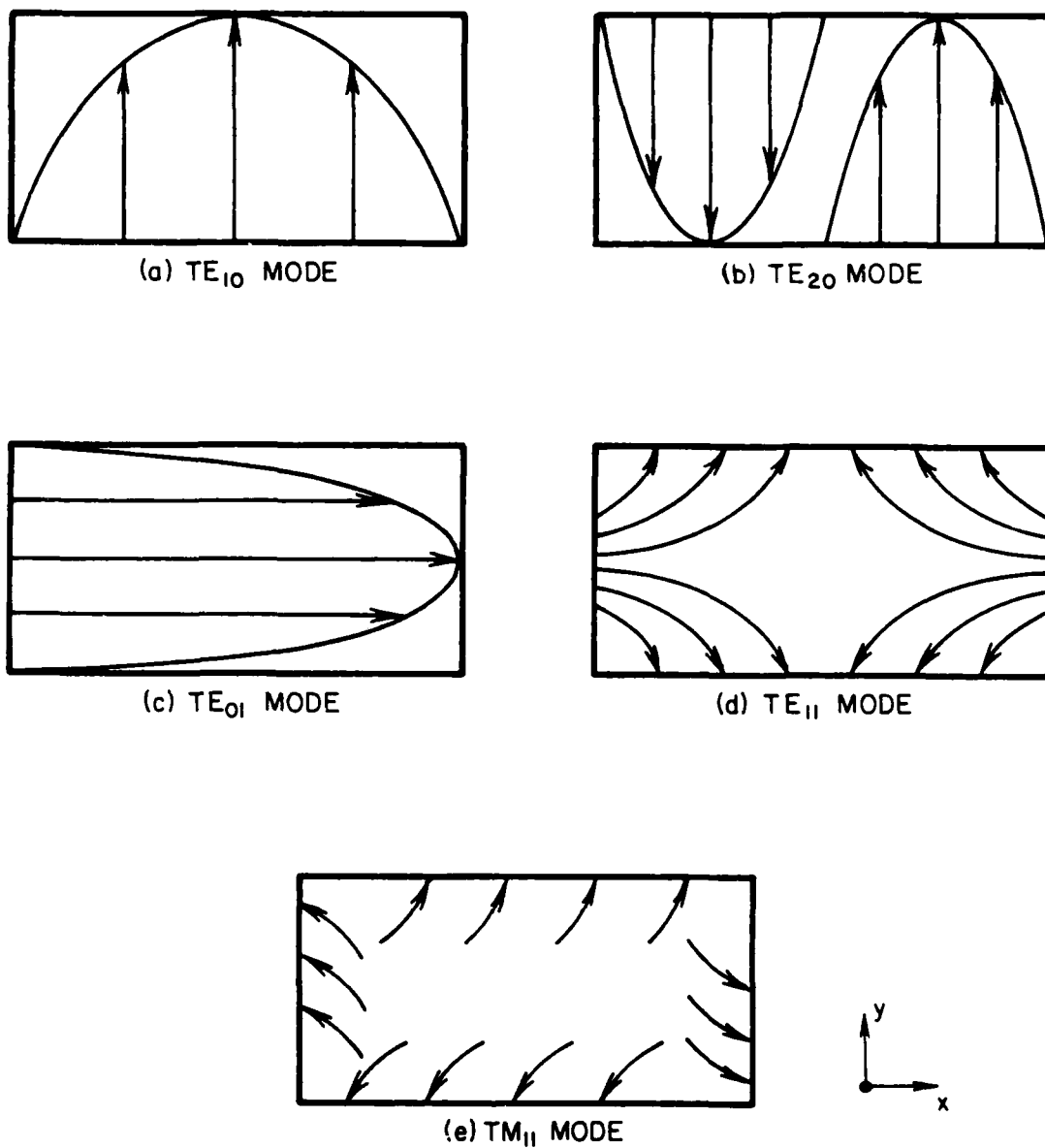
Figure 3.   Transverse electric fields for the indicated
            higher-order modes in rectangular waveguide.

modes are presented by Cown and Ryan[6] for a few selected out-of-band
frequencies for excitation by a filamentary probe. Numerical analyses of
nonfilamentary probes, such as the one used in this measurement program, were
beyond the scope of this research effort. It should be noted that conversion
of some of the electromagnetic energy to other allowed modes can take place in
the feed horn, particularly in the vicinity of the exit aperture. The far-
field pattern of the paraboloidal reflector antenna will, of course, be a
sensitive function of the modal content. It should be noted also that the
relative phases of the modes at the exit aperture are functions of the horn
length and flare angles. This implies a possibly significant frequency
sensitivity.

The foregoing theoretical considerations indicate that the out-of-band
measurements must be performed for both polarization senses for relatively
fine frequency increments within the out-of-band frequency intervals of
interest. Accordingly, the second harmonic measurements were conducted for
both polarization senses for the out-of-band frequencies of 5.5 GHz to 7.5 GHz
in steps of 0.1 GHz. Similarly, the third harmonic measurements were
conducted for both polarization senses for the out-of-band frequencies of
8.0 GHz to 10.0 GHz in steps of 0.1 GHz. However, priority was given to the
acquisition of the out-of-band pattern data for the parallel polarization
sense, and these patterns are more extensively characterized than the cross-
polarized patterns.

The measurement facility and measurement procedures are described in
Section 2; displays of selected measured patterns are presented and discussed
in Section 3. Concluding remarks and recommendations are contained in
Section 4, and a list of references is compiled in Section 5. A description

---

[6]Cown, B. J. and Ryan, C. E., Jr., Near-Field Theory and Techniques for
Wideband Radiating Systems at In-Band and Out-of-Band Frequencies,
Georgia Institute of Technology, Final Technical Report, Contract No.
DAAG29-78-C-0029, January 1982.

of the test antenna is contained in APPENDIX A, a list of professional
engineers/scientists who made significant contributions to the research
project is presented in APPENDIX B, and a list of related research contracts
is contained in APPENDIX C.

SECTION 2

MEASUREMENT FACILITY AND MEASUREMENT PROCEDURES

The measured data were obtained on the Georgia Tech compact range test facility designed expressly for conducting broadband antenna pattern measurements. Far-field antenna radiation patterns from 450 MHz to 18 GHz can be accurately measured at distances usually associated with the Fresnel zone. The measurement setup consisted of (1) the compact range test chamber which housed the compact range reflector and feed system and an azimuth/elevation turntable on which the test antenna was mounted, (2) RF generating and receiving equipment, and (3) the Georgia Tech EMED data logger. Figure 4 shows the compact range reflector and feed system and the test antenna mounted on the turntable as viewed from a vantage point at the back wall of the anechoic test chamber. The RF test equipment and the EMED data logger are shown in Figure 5. A schematic diagram of the basic measurement configuration is contained in Figure 6. The measurement facility and the measurement procedures are described in the following paragraphs.

MEASUREMENT FACILITY AND EQUIPMENT

The Compact Range Facility

The test chamber of the compact range facility is approximately 28 feet wide, 26 feet long, and 16 feet high. A cable trench is used to interconnect the test chamber equipment with the RF equipment in an adjoining control room. There is a specially shaped cavity cut in the floor approximately 3 feet deep to house the feed system in a manner which minimizes scattering from the feed system. Both the range area and the control room are air-conditioned for equipment stability and user comfort. The test chamber is lined with Advanced Absorber Product's 16-inch pyramidal absorber rated at -40 dB reflection for frequencies from 500 MHz to the millimeter region. The compact range consists of (1) a Scientific Atlanta Model 5303-1 azimuth-over-elevation turntable, (2) a precision reflector, (3) a rigidly mounted feed system, and (4) a linear field probe system and positioner.

Figure 1. Test antenna and the compact range reflected parabolic flat reflector.
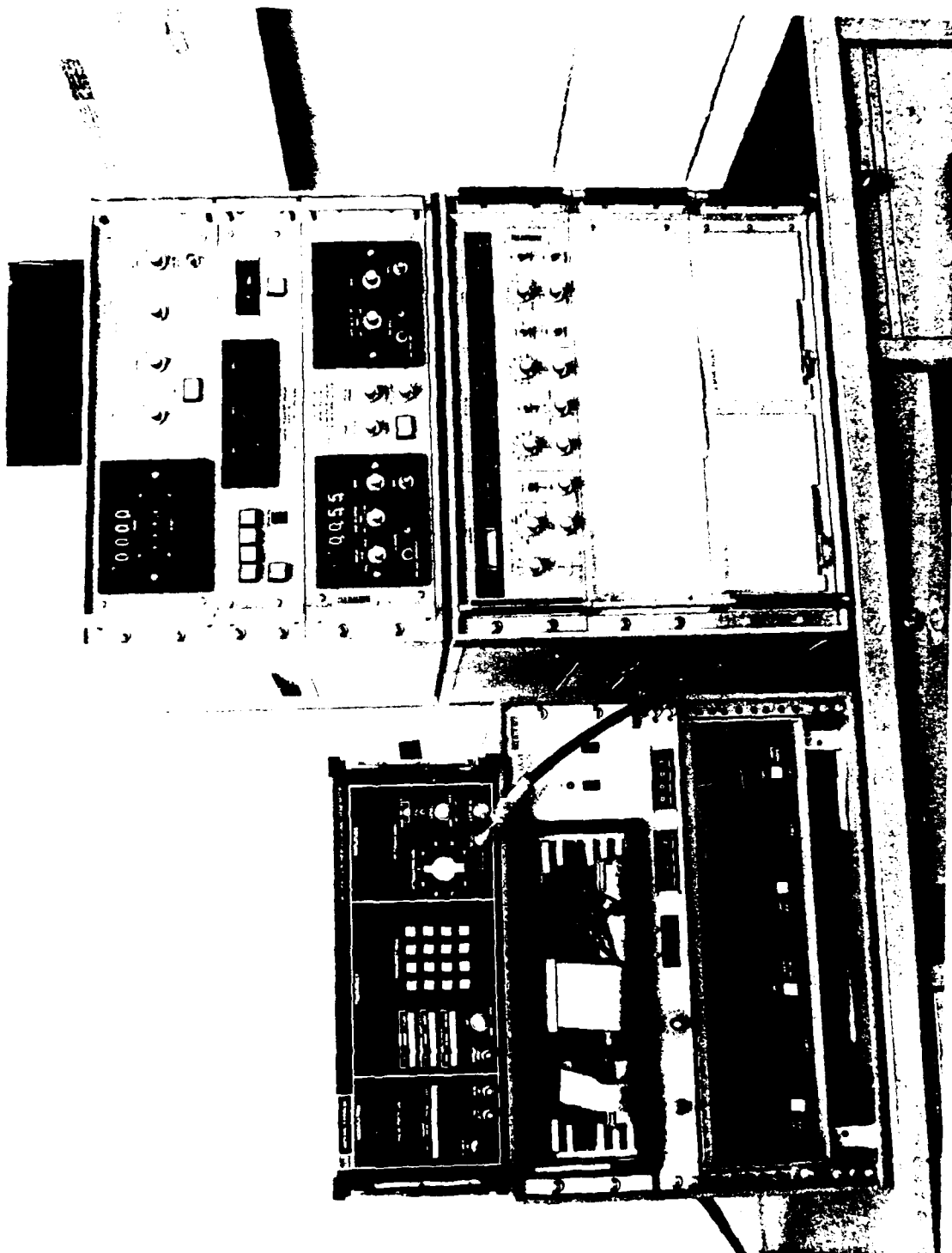
Figure 5. Photographs showing (view from top/left) the RF frequency synthesizer, the 5805 bit logger with computer, and the IF receiving equipment.
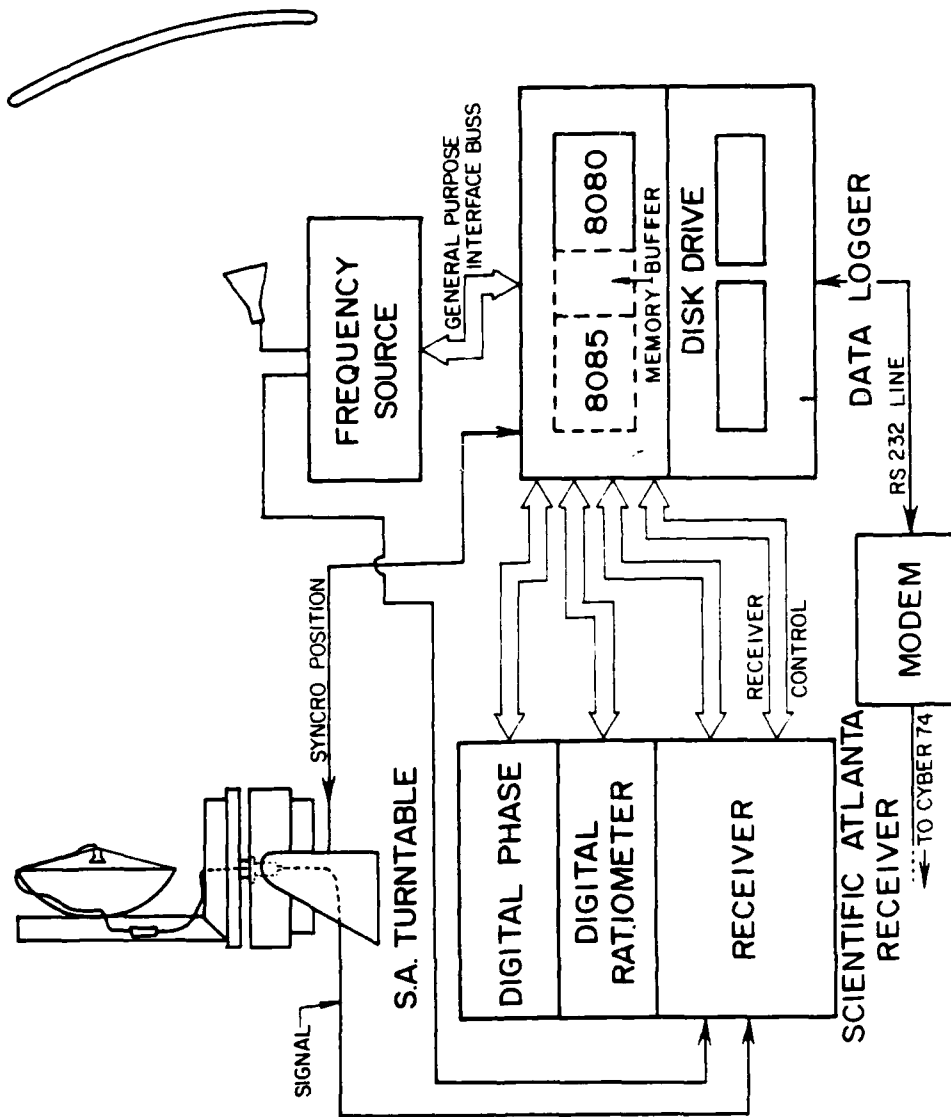
Figure 6. The basic measurement configuration.

The turntable Model 5303-1 has all standard control and output
features. The synchro-motor output is wired to the data logger input, and the
motor control cables are wired to a standard Scientific Atlanta Series 4116-10
motor speed controller. Currently, speed and direction controls are set
manually.

The reflector (shown in Figure 4) is a rectangular offset-fed
paraboloidal section approximately 16 feet wide and 12 feet high. The lower
edge of the reflector lies in a principal plane of the parabola, thus the
focal point is also in this plane approximately 12 feet from the reflector and
3 feet above ground level. The reflector consists of a rigid steel backing
structure with a precision-machined epoxy surface. The epoxy suface has
several coats of metallic silver paint. The dark semicircular region was left
unpainted in order to reduce unwanted reflections.

The feed system is designed to be used for many types of experiments.
Feeds are available to cover from 500 MHz to 18 GHz. Each feed horn has a
mounting bracket with guide pins that mate with the feed positioner. The feed
positioner can be moved in orthogonal "X,Y,Z" directions as well as in azimuth
in order to permit precise adjustment of each feed. Each axis of motion has
precision dials so that feeds may be exchanged without loss of the precise
location of the proper point of any feed.

The linear field probe is used to position a small horn type antenna
along a 10-foot pole. The field probe is used in conjunction with the feed
positioner to adjust the feed in order to obtain fields incident on the test
antenna aperture that are "flat" in both magnitude and phase. The positioner
can be mounted either vertically or horizontally within the plane of the
aperture of the test antenna.

RF Generating and Receiving Equipment

For this series of experiments, the RF generating and receiving equipment
was housed in the control room adjacent to the compact range facility. Each

piece of RF equipment was attached to the Georgia Tech EMED data logger via
special data lines. For discussion purposes, in the following paragraphs, the
RF equipment is divided into signal generating and receiving components.

The RF signal generating equipment consisted of a Watkins Johnson 1204
frequency synthesizer, associated transmission lines, and a directional
coupler. The synthesizer was connected to the data logger via its IEEE
488-1975 general-purpose data bus. The RF output of the frequency synthesizer
was connected to the compact range feed system by a coaxial cable length and a
directional coupler for frequencies below 8.0 GHz. For frequencies above 8.0
GHz, a waveguide transmission line and coupler were used. The coupler for
both setups was attached to the range feed horn, and the receiver reference
mixer was attached to the coupled arm. This arrangement ensures that the
reference signal obtained includes amplitude or phase fluctuations caused by
the source or transmission line.

The RF receiving equipment included Scientific Atlanta's 1770
programmable receiver, 1833 digital ratiometer, and 1800 digital phase
display. Ancillary equipment included RF cables, coaxial mixers, a coaxial
rotary joint, and various digital data cables. It is beyond the scope of this
report section to describe all innerconnections between the various Scientific
Atlanta equipment or between these devices and the data logger. However, the
following discussion will describe the RF channels and features necessary to
understand the general flow of the data.

The receiver system was configured as shown in Figure 6. The RF
reference channel was connected as described previously, with the reference
mixer located at the range feed. The signal channel mixer was affixed behind
the test antenna with a short cable connecting it to the test antenna feed.
Another cable run connected to the mixer through the rotary joint to the
receiver, thus this cable and the rotary joint, as well as the reference
cable, carried only the receiver LO (1-2 GHz) and IF (45 MHz). This RF
configuration has a minimum RF transmission line-length between mixers. Since
the recorded phase is the relative phase between the signals in the two

channels and the recorded amplitude is the ratio between the two channels, this configuration minimizes data distortion caused by RF transmission line effects or RF power variations.

Georgia Tech EMED Data Logger

The Georgia Tech EMED data logger is a computer system assembled in-house and designed specifically to interface and control experiments and measurements using the above-described Scientific Atlanta receiving equipment and turntables. The data logger is a dual CPU system. The tasks of the Intel 8080 (master) and the 8085 (slave) CPU are described below (see also Figure 7).

The 8085 is the interface between the 8080 and the various equipments. Unless interrupted by commands from the 8080 or the comparator, the 8085 is locked in a loop in which it continuously reads data from the receiving equipment and writes this data into the "first-in, first-out" (FIFO) memory chip. Upon command from the 8080, the 8085 controls any controllable function of the receiver, interprets and responds with any data it has, and performs any IEEE-488 bus function (for these experiments it controlled the RF source). In addition, the 8085 also reads angle information from two syncro-motor-to-digital (S to D) converters. The digital outputs from the S-to-D chips are also multiplexed (switched) to a latched comparator chip. The other input to the comparator is written by the 8085. Under the normal pattern recording mode, an azimuth or elevation angle is passed from the 8080 to the 8085 to the comparator chip. The mux is then latched for either azimuth or elevation data. When the 8085 written angle and the input azimuth or elevation match, the comparator chip interrupts the 8085. The 8085 interrupt routine then reads the data buffered in the FIFO chip, converts the numbers into binary format, and sends the data via the high speed data bus to the 8080.
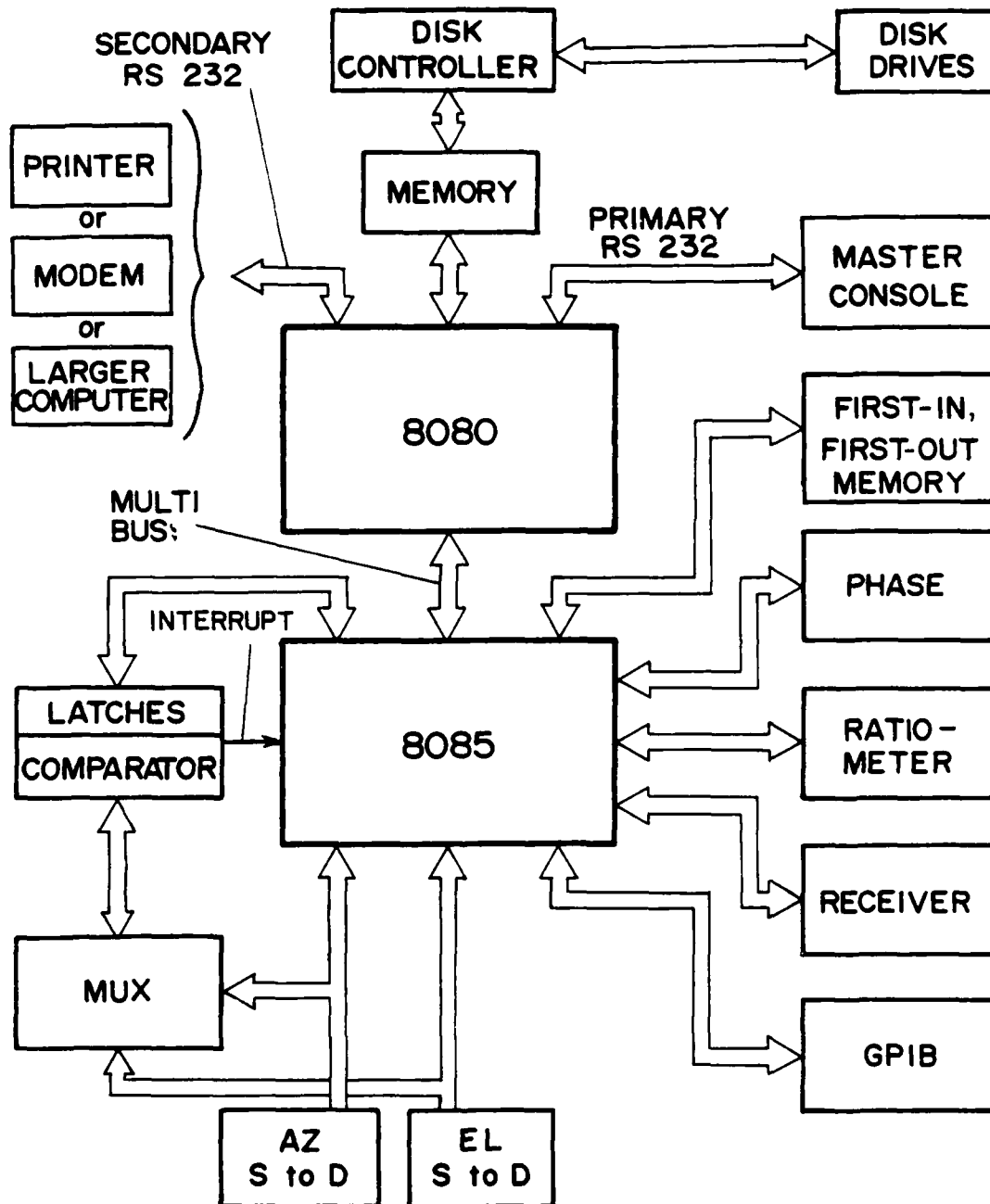
Figure 7.   EMED data logger block diagram.

The Intel 8080 card, the 64K memory card, the disk controller, and the disk drives are stock equipment. As presently configured, the 8080 has several text editors, an assember, a FORTRAN compiler, a library generator, and many other software routines all stored on disk. The 8080 runs under a comprehensive control language. In general, the 8080 is a "stand-alone" computer with CRT console and printer.

All control function routines written for the 8080 to control the 8085 are contained in a series of FORTRAN-callable libraries, and the data-logger control program for this program is written in FORTRAN. A functional description of the main data-logger control program is presented below. Since motor control is not currently implemented on this system, all azimuth data is recorded for a single elevation angle in a single program execution.

The data-logger program first asks the user for all run parameters. These parameters include the elevation angle, the azimuth sector over which data will be recorded, the frequency increment data, the beginning frequency, and the ending frequency. The system then tunes the source and the receiver to the beginning frequency and checks for frequency lock. Next, the receiver's reference channel attenuator is set. This is accomplished by incrementally reducing the attenuator setting and checking the receiver for saturation and amplitude "out of range" errors. If an error is detected, the attenuator is increased by 10 dB. Next, the signal channel attenuator is set in a similar fashion except that the highest point in the pattern is found first and then the signal attenuator is set so that the received signal is 10 dB below saturation at the highest point. After the attenuators are set, all status lines are checked once more and then the data are taken and stored in an array. Once the data array is filled, the data are corrected for attenuator settings and written on a disk file. The system then goes to the next frequency and repeats the process until all frequency data have been taken for the selected elevation angle.

MEASUREMENT PROCEDURES

The main steps involved in conducting the broadband antenna measurements
were (1) aligning the compact range feed horn to produce a plane-wave field
over the extent of the aperture of the test antenna, (2) recording the
measured amplitude and phase responses of the test antenna via the data-logger
system and measuring the peak gain at each frequency, and (3) computer
processing of the pattern and gain data to generate pattern plots and to
calculate statistical parameters of the pattern data.

Compact Range Feed Horn Alignment

The compact range feed horn was aligned with aid of the linear field
probe previously described in this section. The probe was oriented
horizontally in the plane later to be occupied by the test antenna. The field
was then probed with the in-band (S-band) range feed, and the feed was
adjusted until the quasi-plane was "flat" within 0.5 dB in amplitude and
10.0 degrees in phase over the extent of the test antenna aperture. This
process was repeated with the probe positioned vertically and, finally,
several linear cuts were made through the field to ensure the flatness of the
incident wave through the entire plane of the test antenna. The final feed
positions were then recorded for later use in positioning the S-band feed.
The above procedures were repeated for selected frequencies in each frequency
band with an appropriate waveguide feed that operates only in the TE_{10} mode
over the harmonic region under test.

Data Collection and Processing

The test antenna was first positioned manually in azimuth and elevation
via the turntable controller for the maximum received signal at the in-band
frequency of 3.0 GHz. The data-logger azimuth and elevation offset thumb-
wheel switches were then adjusted so that the output angles (as read from the
logger LED displays) were zero degrees. These in-band reference angles were

then used for all frequency ranges. Thus, all of the out-of-band patterns were referenced to the electrical boresight at 3.0 GHz.

The data logger is initialized with the appropriate frequency and angle information. The data logger then records the antenna responses in amplitude and phase for all frequencies within the desired frequency range at the prescribed elevation angle. The in-band data were recorded for the frequencies of 2.9 GHz, 3.0 GHz, and 3.1 GHz for both polarization senses. The second harmonic data were recorded for both polarization senses for frequencies from 5.5 GHz to 7.5 GHz in steps of 0.1 GHz. Similarly, the third harmonic data were recorded for both polarization senses for frequencies from 8.0 GHz to 10.0 GHz in steps of 0.1 GHz. The elevation angle was then incremented manually and the above procedures were repeated until all data were recorded for all prescribed elevation angles.

The in-band patterns data, as well as the second and third harmonic out-of-band pattern data, were recorded over the front 80-degree azimuth sector for prescribed elevation angles. The center of the azimuth sector was always aligned with the electrical boresight defined by the peak of the mainbeam at 3.0 GHz. The in-band pattern data were recorded every 0.5 degree in azimuth. The azimuth pattern data for the in-band and second harmonic frequency regions for the parallel polarization were collected every 1.0 degree over a 20-degree elevation sector centered about the 3.0 GHz electrical boresight. The cross-polarized data were collected only for ±2.0 degrees and 0 degrees. Similarly, the third harmonic azimuth pattern data were collected every 0.5 degree over a 10-degree elevation sector for parallel polarization, and the cross-polarized data were collected only for ±1.0 degrees and 0 degree.

Appropriate standard gain horns were employed to determine a reference gain level relative to an isotropic radiator over each band of test frequencies. The appropriate standard gain horn was mounted on a tripod and

positioned at the spot where the center of the test antenna aperture was
located. The reference gain level was then recorded versus frequency via the
data logger.

The recorded pattern data and reference gain data were transferred via
phone lines from the data-logger system disks to the Georgia Tech-owned
Control Data Corporation Cyber 74 computer system for processing. Special-
purpose FORTRAN IV computer programs were employed to create pattern plots for
each frequency and to compute the peak gain, the median and standard
deviation, and statistical average patterns (discussed in the next section).

SECTION 3

OUT-OF-BAND PATTERN CHARACTERISTICS

The general characteristics of the measured patterns are described in the
following paragraphs with the aid of (1) tabulations of the selected key EMC
descriptive parameters for the measured patterns of the measured frequencies for
both polarization senses, (2) power pattern plots at selected out-of-band
frequencies for both polarization senses, and (3) plots of the statistical
average patterns for the second and third harmonic regions for the parallel
polarization sense. The selected EMC descriptors were the peak gain, the angular
coordinates of the peak, and the average gain and standard deviation over the
front 80-degree angular sector for the azimuth pattern that cuts through the
highest peak, i.e., the maximum azimuth pattern. These EMC descriptors are
tabulated in TABLES 1 through 4. The selected power pattern plots are displayed
in Figures 8 through 44, and the statistical average patterns are shown in
Figures 45 and 46. Positive azimuth angles for the patterns open
counterclockwise from the in-band electrical boresight direction as viewed from a
vantage point behind the antenna. Similarly, positive elevation angles for the
patterns open upward from the in-band electrical boresight direction.

TABLES 1 and 2 present data for the parallel polarization patterns for the
second and third harmonic frequency intervals, respectively. Similarly, TABLES 3
and 4 present data for the cross polarization for the second and third harmonics,
respectively.

The power pattern plots presented in Figures 8 through 37 contain plots for
the parallel polarization sense. Those shown in Figures 38 through 44 contain
plots for the cross polarization sense. Each one of the even-number figures,
numbers 8 through 36, shows plots of the azimuth patterns for the 21 elevation
angles for the parallel polarization. Each of these plots is followed by
 plots of the azimuth and elevation patterns obtained by cutting through the
overall pattern maximum. The figures are grouped according to frequency in
ascending order from 3.0 GHz to 10.0 GHz. For the cross polarization, only

TABLE 1

TABULATION OF THE PEAK GAIN, THE ANGULAR
COORDINATES OF THE PEAK, AND THE AVERAGE GAIN AND STANDARD
DEVIATION FOR THE OUT-OF-BAND FREQUENCIES FROM 5.5 GHz TO 7.5 GHz
FOR THE PARALLEL POLARIZATION SENSE

Frequency (GHz)	Peak Gain (dB/iso)	Angular Coordinates[a] (degrees)		Average Gain (dB/iso)	Standard Deviation (±dB)
		ϕ_o	θ_o		
5.5	31.0	+0.5	+2.0	+4.5	11.7
5.6	30.7	+0.5	-3.0	+3.4	10.4
5.7	31.0	+0.5	-4.0	+5.8	10.4
5.8	31.2	+0.0	-3.0	+2.6	11.3
5.9	31.5	+0.5	-4.0	+5.1	11.7
6.0	32.7	-0.5	-3.0	+3.2	11.3
6.1	31.0	+0.5	-4.0	+4.5	11.0
6.2	31.0	0.0	-2.0	+1.5	12.7
6.3	27.7	+0.5	0.0	+4.2	12.0
6.4	30.8	0.0	+1.0	+0.6	10.4
6.5	31.8	0.0	+2.0	+3.1	9.8
6.6	31.6	0.0	+2.0	+3.0	9.7
6.7	31.7	+0.5	+2.0	-1.0	12.2
6.8	31.2	0.0	+3.0	+0.6	11.4
6.9	32.2	0.0	+3.0	-0.3	12.0
7.0	32.3	0.0	+2.0	+0.4	12.6
7.1	31.7	0.0	+3.0	+0.5	11.5
7.2	31.3	0.0	+3.0	+2.3	11.2
7.3	33.7	0.0	+1.0	+3.2	12.2
7.4	31.1	+0.5	-4.0	+0.6	9.9
7.5	30.2	+3.0	+2.0	+1.1	11.7

[a]The symbols ϕ_o and θ_o denote the azimuth and elevation angles, respectively, of the highest peak.

TABLE 2

TABULATION OF THE PEAK GAIN, THE ANGULAR
COORDINATES OF THE PEAK, AND THE AVERAGE GAIN AND STANDARD
DEVIATION FOR THE OUT-OF-BAND FREQUENCIES FROM 8.0 GHz TO 10.0 GHz
FOR THE PARALLEL POLARIZATION SENSE

Frequency (GHz)	Peak Gain (dB/iso)	Angular Coordinates[a] (degrees)		Average Gain (dB/iso)	Standard Deviation ($\pm$dB)
		ϕ_o	θ_o		
8.0	33.5	-0.5	-1.5	-3.1	14.3
8.1	27.5	-0.5	-1.0	-9.0	14.6
8.2	25.0	-0.5	-2.0	-13.0	14.9
8.3	26.5	-0.5	-0.5	-10.9	14.1
8.4	21.5	-0.5	-1.0	-14.7	13.2
8.5	23.0	-0.5	0.0	-13.9	14.3
8.6	26.5	-1.0	+1.0	-11.5	14.4
8.7	16.5	-1.0	+1.0	-19.8	14.2
8.8	19.0	-0.5	+1.0	-18.5	14.5
8.9	27.0	-0.5	+0.5	-10.5	12.7
9.0	24.0	-0.5	+1.0	-14.6	14.3
9.1	20.5	-0.5	+1.0	-17.3	13.2
9.2	27.5	-0.5	-2.0	-5.1	12.0
9.3	31.0	-1.0	+1.0	+1.2	13.6
9.4	31.5	-0.5	0.0	-8.8	14.9
9.5	27.5	-0.5	0.0	-13.1	15.0
9.6	30.5	-1.0	+2.0	-5.2	13.5
9.7	26.0	-0.5	-0.5	-9.3	13.4
9.8	33.5	-0.5	0.0	-2.8	13.6
9.9	30.5	-1.0	+3.5	-8.4	13.5
10.0	20.0	-1.5	0.0	-17.4	14.1

[a]The symbols ϕ_o and θ_o denote the azimuth and elevation angles, respectively, of the highest peak.

TABLE 3

TABULATION OF THE PEAK GAIN, THE ANGULAR
COORDINATES OF THE PEAK, AND THE AVERAGE GAIN AND STANDARD
DEVIATION FOR THE OUT-OF-BAND FREQUENCIES FROM 5.5 GHz TO 7.5 GHz
FOR THE CROSS POLARIZATION SENSE

Frequency (GHz)	Peak Gain (dB/iso)	Angular Coordinates[a] (degrees) ϕ_o	θ_o	Average Gain (dB/iso)	Standard Deviation (±dB)
5.5	22.7	+2.5	-1.0	-3.0	11.7
5.6	23.9	+2.5	-1.0	-3.0	13.3
5.7	23.6	+2.5	-1.0	-5.5	13.3
5.8	21.4	+2.5	0.0	-3.1	10.2
5.9	21.9	+2.5	-1.0	-2.1	10.5
6.0	18.8	+2.5	-1.0	-7.5	12.6
6.1	20.8	+2.5	-1.0	-5.0	11.4
6.2	17.9	+2.5	-1.0	-6.9	9.7
6.3	13.1	-3.5	+1.0	-11.0	9.0
6.4	12.6	+1.5	-1.0	-12.0	10.4
6.5	17.2	+2.5	-1.0	-8.1	12.1
6.6	16.3	+3.0	-1.0	-8.3	10.1
6.7	24.4	+2.0	+1.0	+0.7	9.0
6.8	17.0	+2.0	+1.0	-10.3	13.6
6.9	23.9	+1.5	+1.0	-6.2	11.9
7.0	17.8	-2.0	+1.0	-10.3	10.2
7.1	19.9	-2.0	+1.0	-5.3	9.7
7.2	20.4	+2.5	-1.0	-7.1	13.2
7.3	22.9	+2.5	-1.0	-6.7	14.2
7.4	19.1	-1.5	+1.0	-8.6	12.0
7.5	16.8	-1.5	+1.0	-10.0	11.0

[a]The symbols ϕ_o and θ_o denote the azimuth and elevation angles, respectively, of the highest peak.

TABLE 4

TABULATION OF THE PEAK GAIN, THE ANGULAR
COORDINATES OF THE PEAK, AND THE AVERAGE GAIN AND STANDARD
DEVIATION FOR THE OUT-OF-BAND FREQUENCIES FROM 8.0 GHz TO 10.0 GHz
FOR THE CROSS POLARIZATION SENSE

Frequency (GHz)	Peak Gain (dB/iso)	Angular Coordinates[a] (degrees) ϕ_o	θ_o	Average Gain (dB/iso)	Standard Deviation (±dB)
8.0	22.0	+1.0	−1.0	−8.3	11.9
8.1	17.7	+1.0	−1.0	−12.9	11.7
8.2	21.3	+1.0	−1.0	−11.0	13.8
8.3	17.7	−1.0	−1.0	−10.8	12.2
8.4	10.8	−1.0	−1.0	−17.2	10.9
8.5	10.1	+1.0	−1.0	−19.5	12.2
8.6	15.1	+1.0	−1.0	−16.4	13.8
8.7	7.3	−2.0	0.0	−21.4	12.0
8.8	8.6	+2.0	+1.0	−21.8	11.6
8.9	19.9	−2.0	+1.0	−11.0	12.1
9.0	19.9	−2.0	+1.0	−13.8	13.2
9.1	20.9	+2.0	+1.0	−12.9	13.8
9.2	21.5	+2.0	+1.0	−14.2	15.3
9.3	22.5	−3.0	+1.0	−10.4	13.7
9.4	7.3	+3.0	+1.0	−22.6	12.9
9.5	14.5	+3.0	+1.0	−15.5	12.4
9.6	20.4	−4.0	+1.0	−10.0	12.5
9.7	17.2	−3.0	+1.0	−11.5	12.0
9.8	16.4	+2.0	−1.0	−10.9	11.7
9.9	21.3	−3.0	−1.0	−8.3	12.6
10.0	10.6	−3.0	−1.0	−21.8	13.0

[a]The symbols ϕ_o and θ_o denote the azimuth and elevation angles, respectively, of the highest peak.

Figure 8.   Axonometric view showing plots of the measured azimuth patterns recorded
for 21 elevation angles for the parallel polarization for the in-band
frequency of 3.0 GHz. The gain at the highest peak is 28.2 dB relative
to an isotropic radiator.

Figure 9. Principal plane azimuth pattern for the parallel
           polarization for the in-band frequency of 3.0 GHz.
           The gain at the highest peak is 28.2 dB relative
           to an isotropic radiator.

Figure 10.   Axonometric view showing plots of the azimuth patterns recorded for 21 elevation angles for the parallel polarization for the out-of-band frequency of 5.5 GHz. The gain at the highest peak is 31.0 dB relative to an isotropic radiator.

Figure 11.   Azimuth and elevation patterns corresponding to the
             overall recorded pattern maximum for the parallel
             polarization for the out-of-band frequency of 5.5 GHz.
             The gain at the top of the charts is 31.0 dB relative
             to an isotropic radiator.

Figure 12. Axonometric view showing plots of the azimuth patterns recorded for the 21 elevation angles for the parallel polarization for the out-of-band frequency of 6.0 GHz. The gain at the highest peak is 32.7 dB relative to an isotropic radiator.

Figure 13.   Azimuth and elevation patterns corresponding to the
              overall recorded pattern maximum for the parallel
              polarization for the out-of-band frequency of 6.0 GHz.
              The gain at the top of each chart is 32.7 dB relative
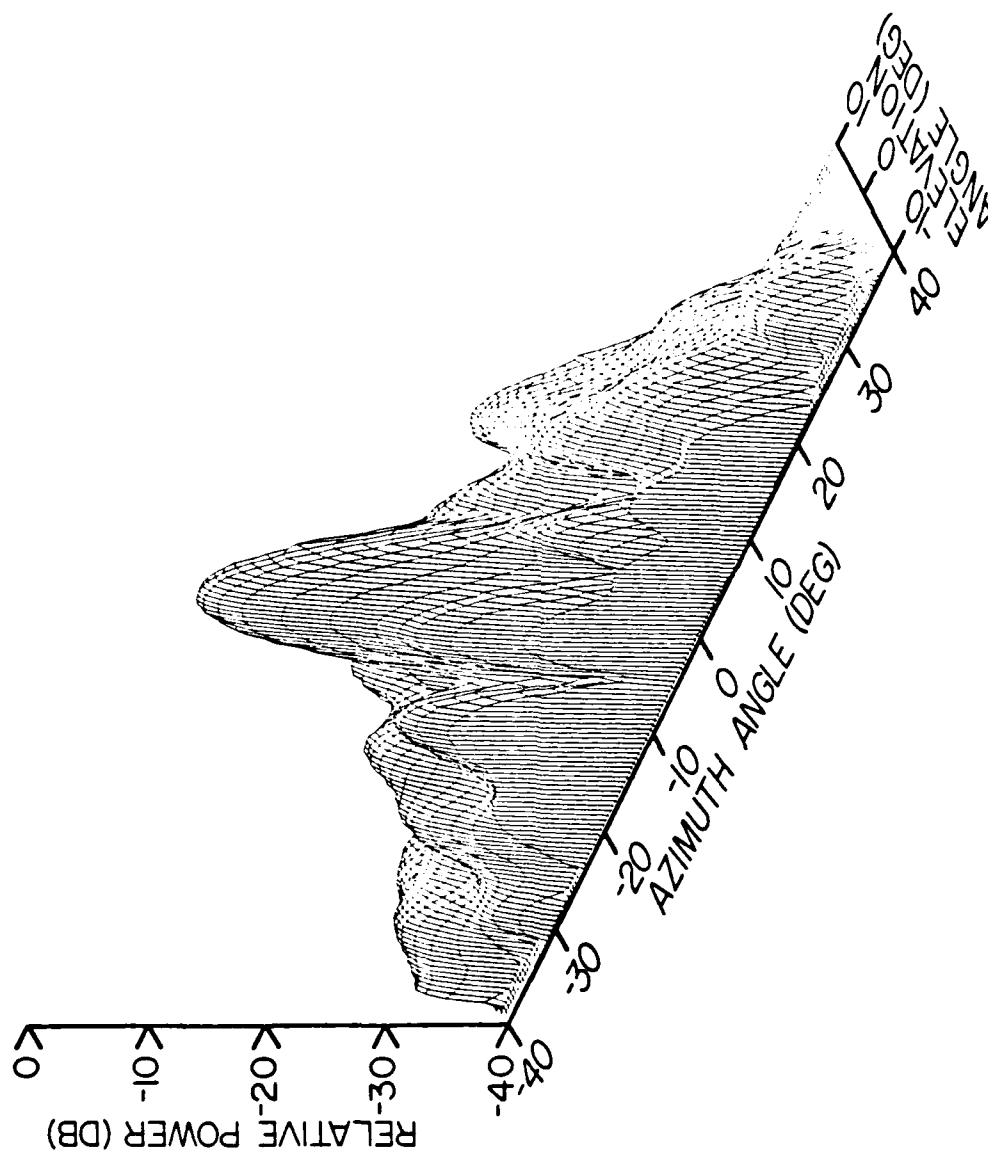   to an isotropic radiator.

Figure 14. Axonometric view showing plots of the azimuth patterns recorded
for 21 elevation angles for the parallel polarization for the
out-of-band frequency of 6.2 GHz. The gain at the highest peak
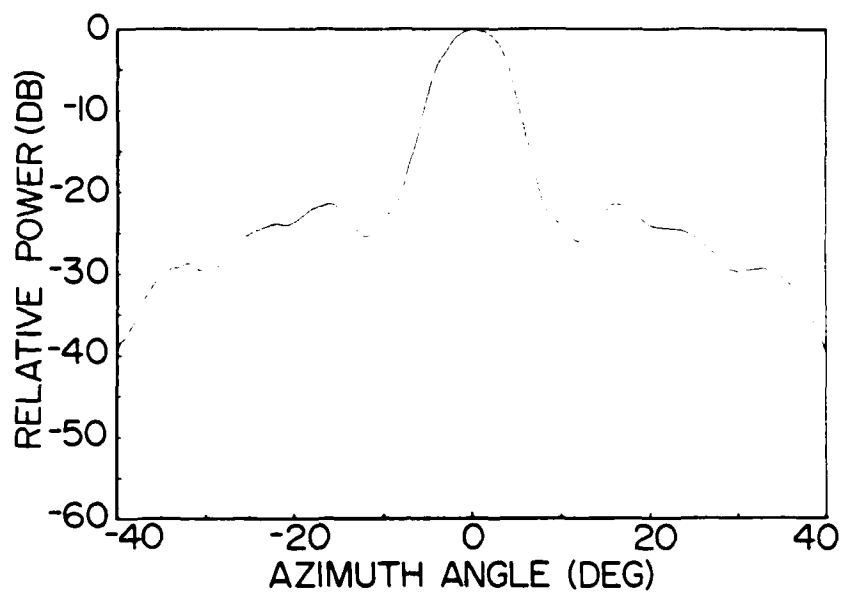is 31.0 dB relative to an isotropic radiator.

Figure 15.   Azimuth and elevation patterns corresponding to the
             overall recorded pattern maximum for the parallel
             polarization for the out-of-band frequency of 6.2 GHz.
             The gain at the top of each chart is 31.0 dB relative
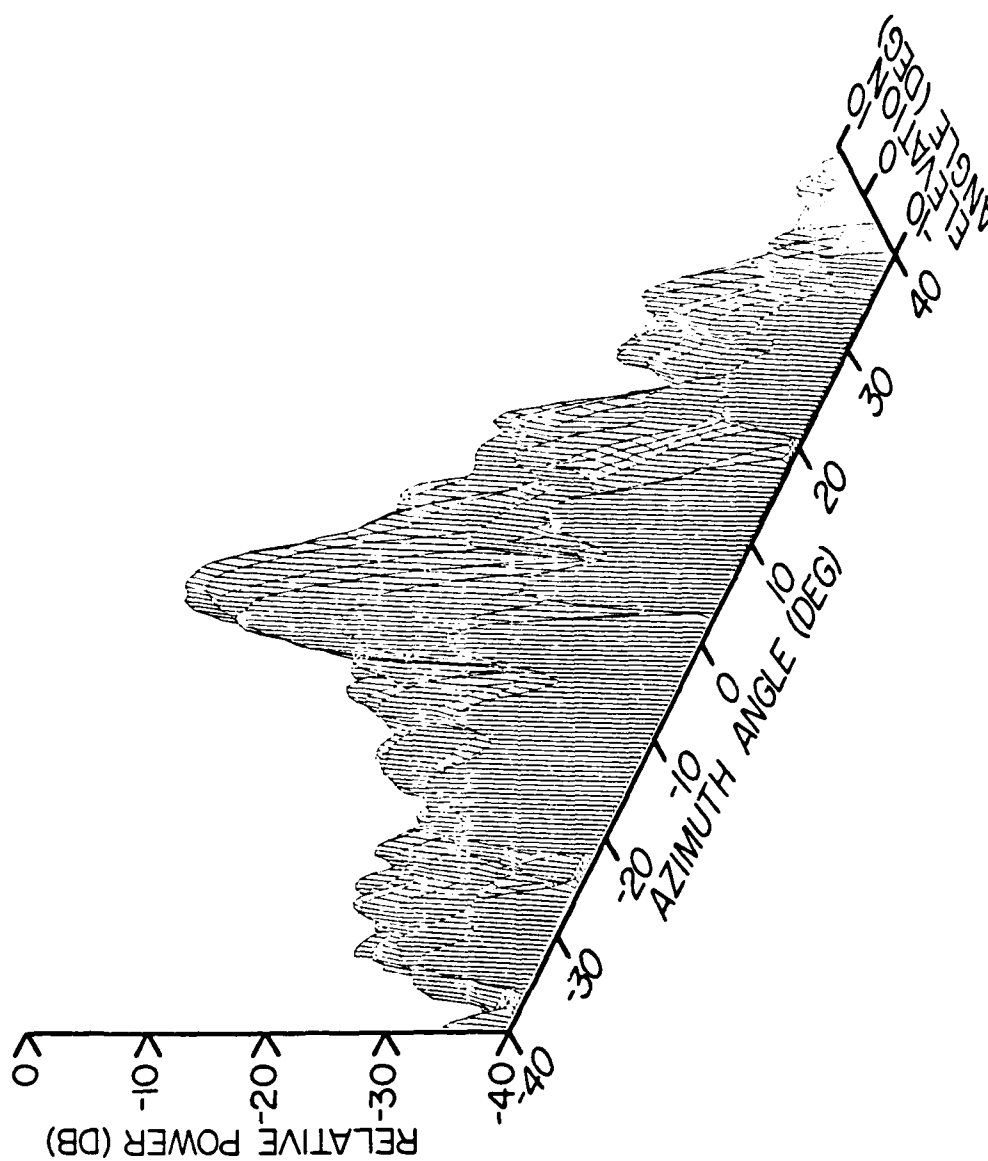   to an isotropic radiator.

Figure 16. Axonometric view showing plots of the azimuth patterns recorded for 21 elevation angles for the parallel polarization for the out-of-band frequency of 6.3 GHz. The gain at the highest peak is 31.0 dB relative to an isotropic radiator.
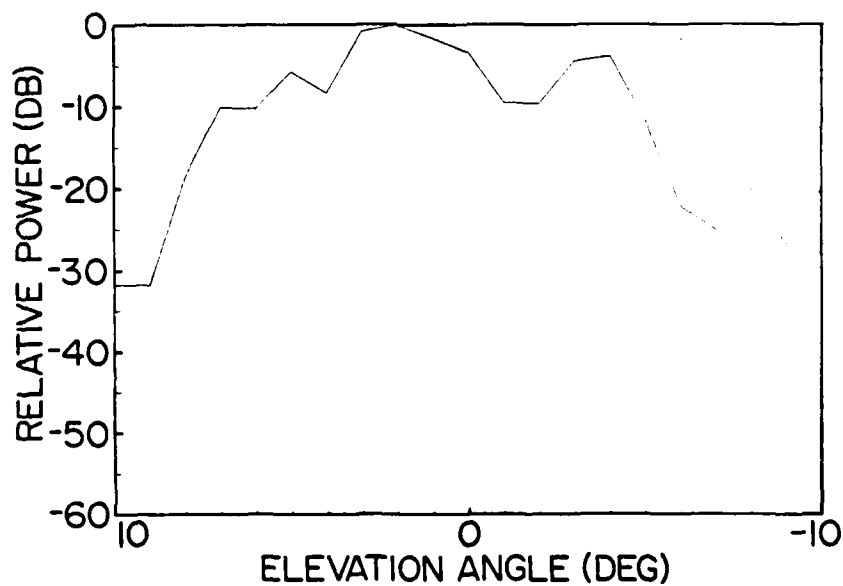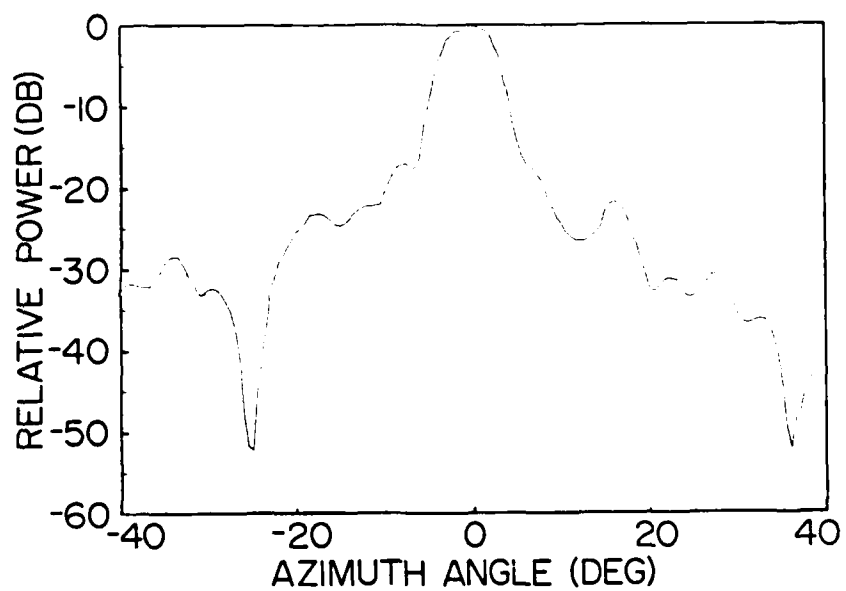
Figure 17.   Azimuth and elevation patterns corresponding to the
             overall recorded pattern maximum for the parallel
             polarization for the out-of-band frequency of 6.3 GHz.
             The gain at the top of each chart is 27.7 dB relative
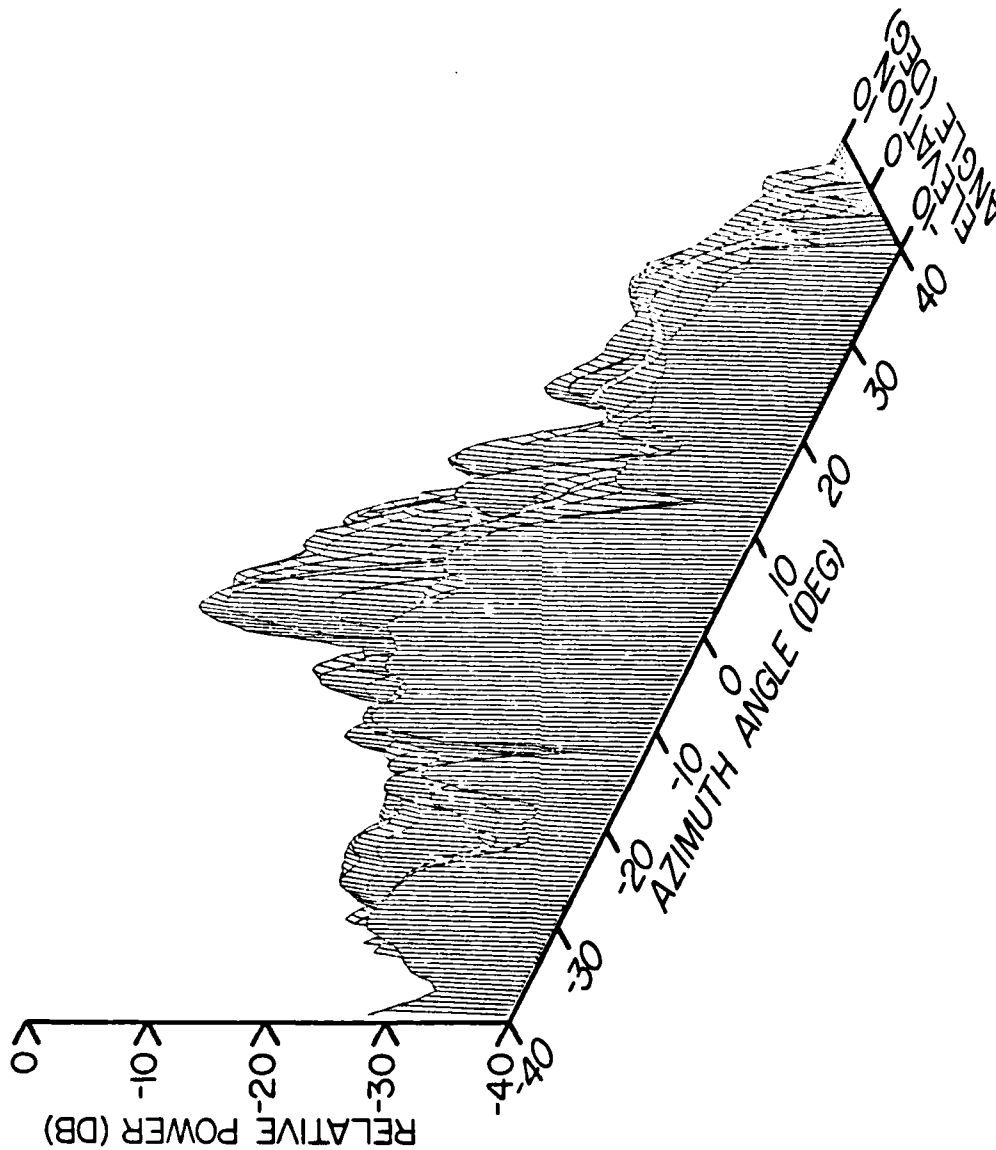   to an isotropic radiator.

Figure 18. Axonometric view showing plots of the azimuth patterns recorded for 21 elevation angles for the parallel polarization for the out-of-band frequency of 6.4 GHz. The gain at the highest peak is 30.8 dB relative to an isotropic radiator.
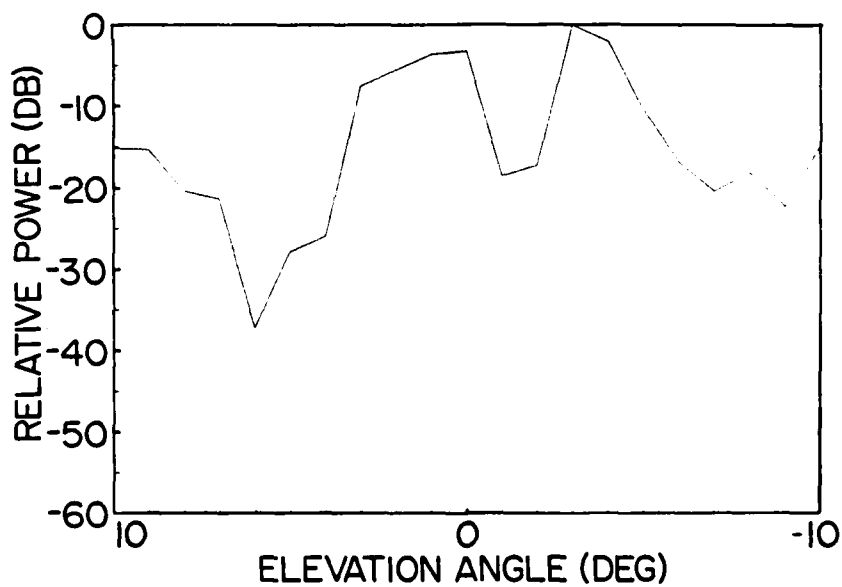
Figure 19. Azimuth and elevation patterns corresponding to the
            overall recorded pattern maximum for the parallel
            polarization for the out-of-band frequency of 6.4 GHz.
            The gain at the top of the charts is 30.8 dB relative
            to an isotropic radiator.

Figure 20. Axonometric view showing plots of the azimuth patterns recorded for 21 elevation angles for the parallel polarization for the out-of-band frequency of 6.5 GHz. The gain at the highest peak is 31.8 dB relative to an isotropic radiator.
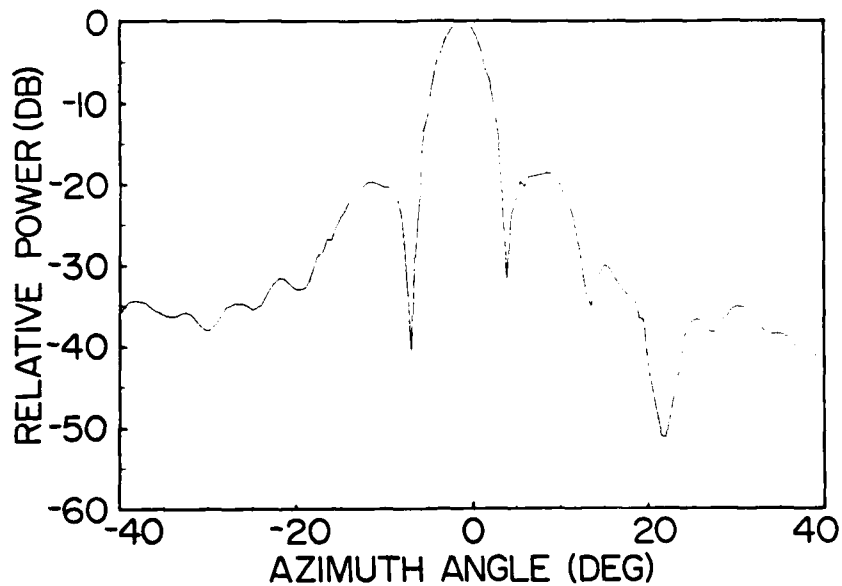
Figure 21. Azimuth and elevation patterns corresponding to the
overall recorded pattern maximum for the parallel
polarization for the out-of-band frequency of 6.5 GHz.
The gain at the top of each chart is 31.8 dB relative
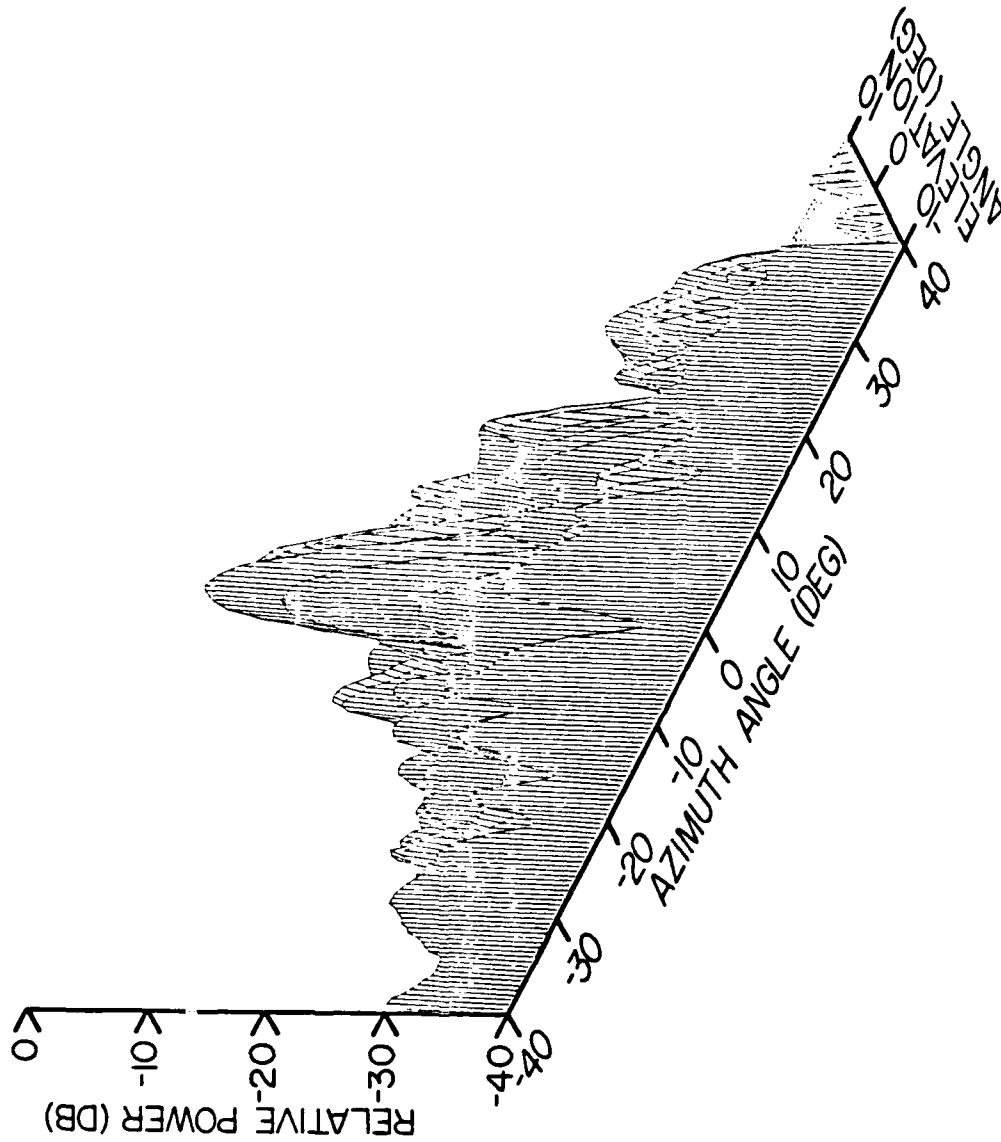to an isotropic radiator.

Figure 22.   Axonometric view showing plots of the azimuth patterns recorded for
21 elevation angles for the parallel polarization for the out-ot-band
frequency of 6.6 GHz.   The gain at the highest peak is 31.6 dB relative
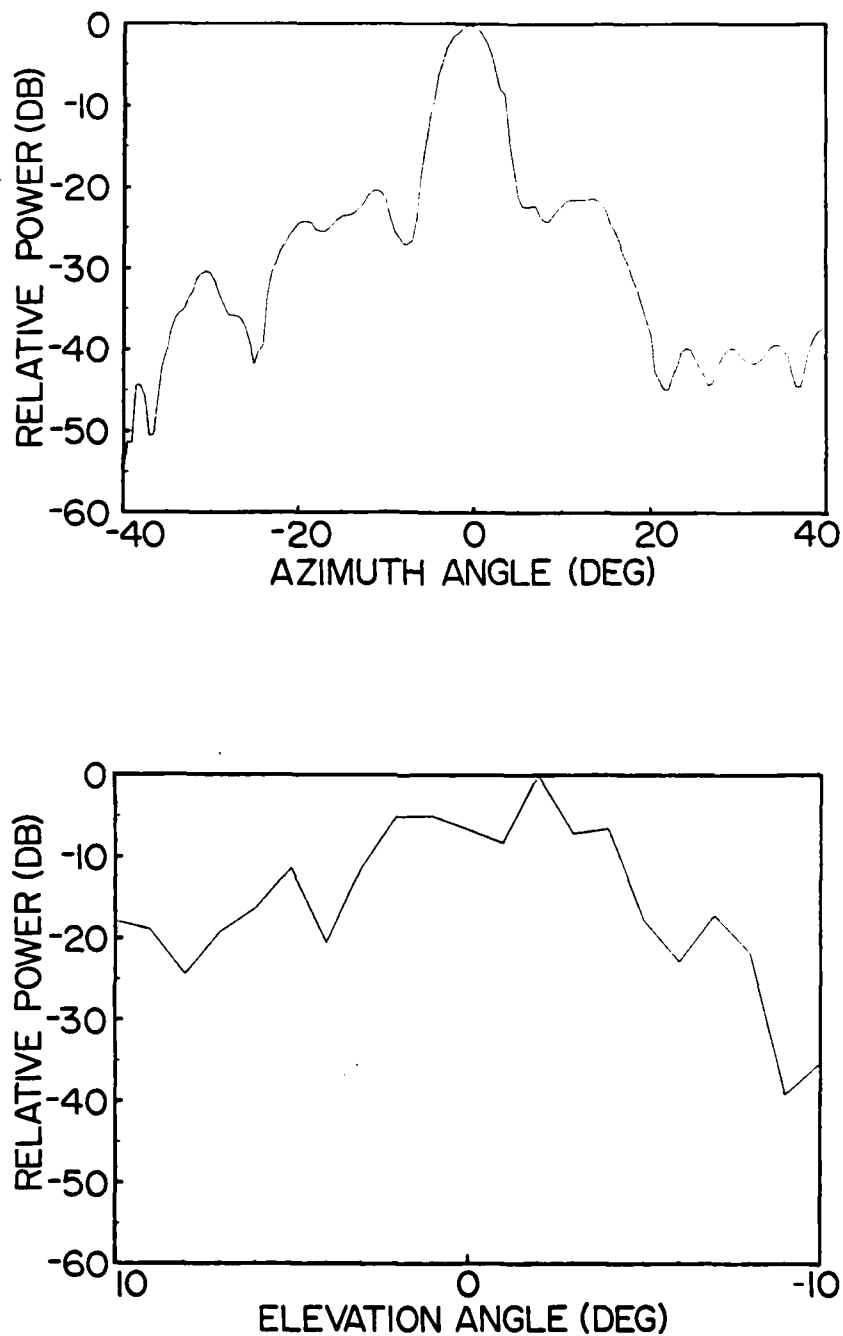to an isotropic radiator.

Figure 23. Azimuth and elevation patterns corresponding to the
            overall recorded pattern maximum for the parallel
            polarization for the out-of-band frequency of 6.6 GHz.
            The gain at the top of each chart is 31.6 dB relative
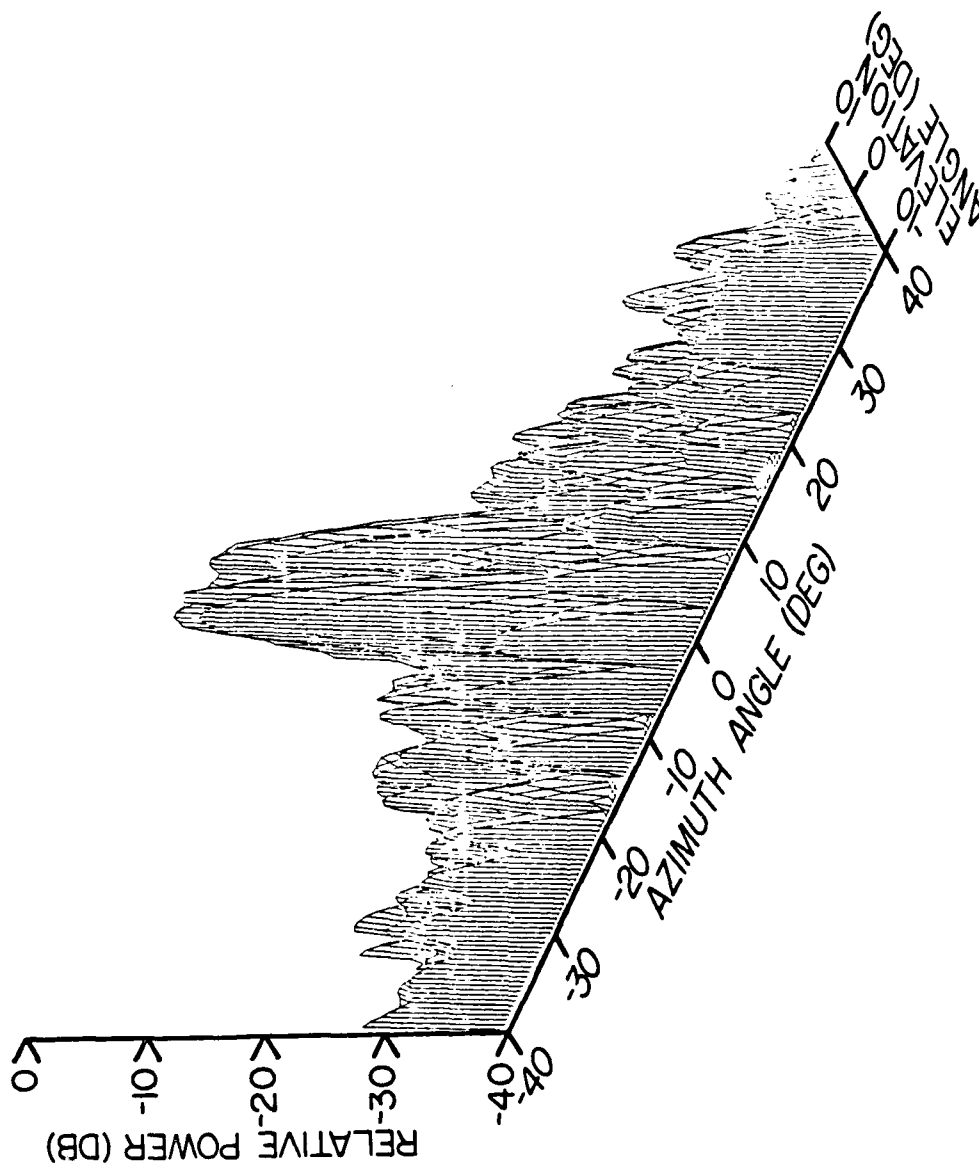   to an isotropic radiator.

Figure 24. Axonometric view showing plots of the azimuth patterns recorded for 21 elevation angles for the parallel polarization for the out-of-band frequency of 8.0 GHz. The gain at the highest peak is 33.5 dB relative to an isotropic radiator.
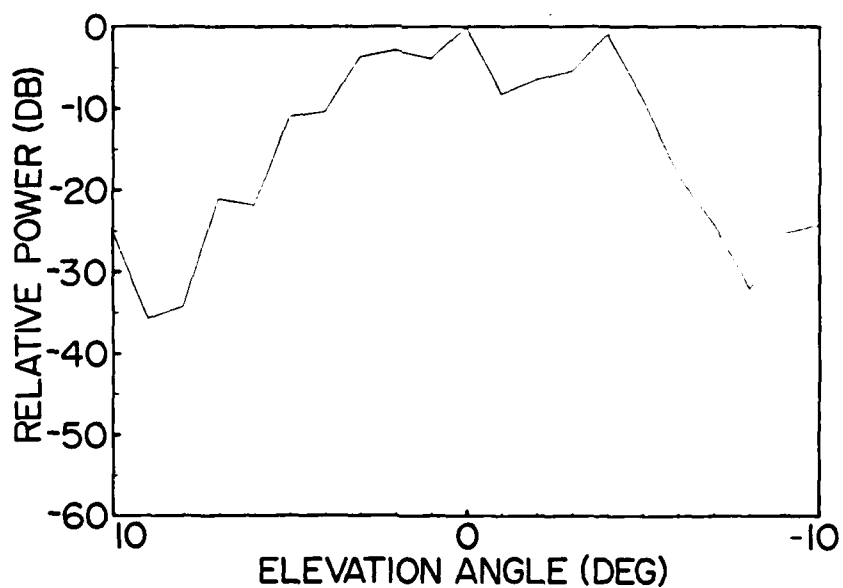
Figure 25. Azimuth and elevation patterns corresponding to the
            overall recorded pattern maximum for the parallel
            polarization for the out-of-band frequency of 8.0 GHz.
            The gain at the top of each chart is 33.5 dB relative
            to an isotropic radiator.

3-23

Figure 26. Axonometric view showing plots of the azimuth patterns recorded for 21 elevation angles for the parallel polarization for the out-of-band frequency of 8.8 GHz. The gain at the highest peak is 19.0 dB relative to an isotropic radiator.
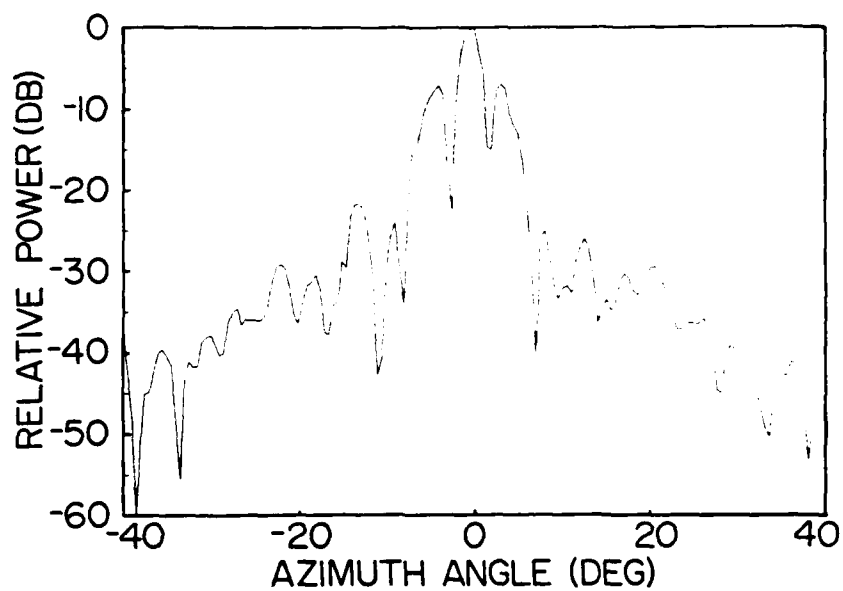
Figure 27. Azimuth and elevation patterns corresponding to the
overall recorded pattern maximum for the parallel
polarization for the out-of-band frequency of 8.8 GHz.
The gain at the top of each chart is 19.0 dB relative
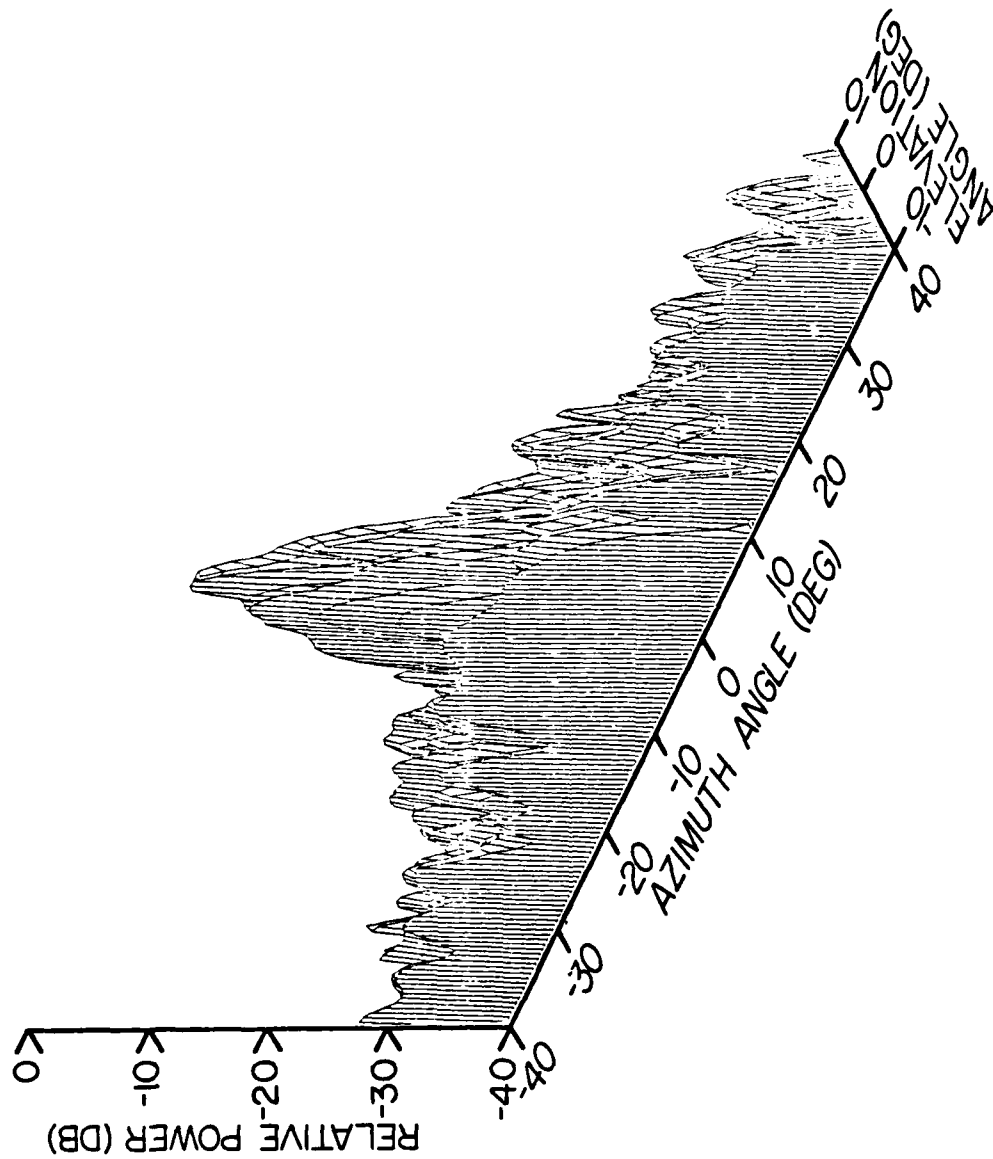to an isotropic radiator.

Figure 28.   Axonometric view showing plots of the azimuth patterns recorded for
21 elevation angles for the parallel polarization for the out-of-band
frequency of 9.0 GHz. The gain at the highest peak is 24.0 dB relative
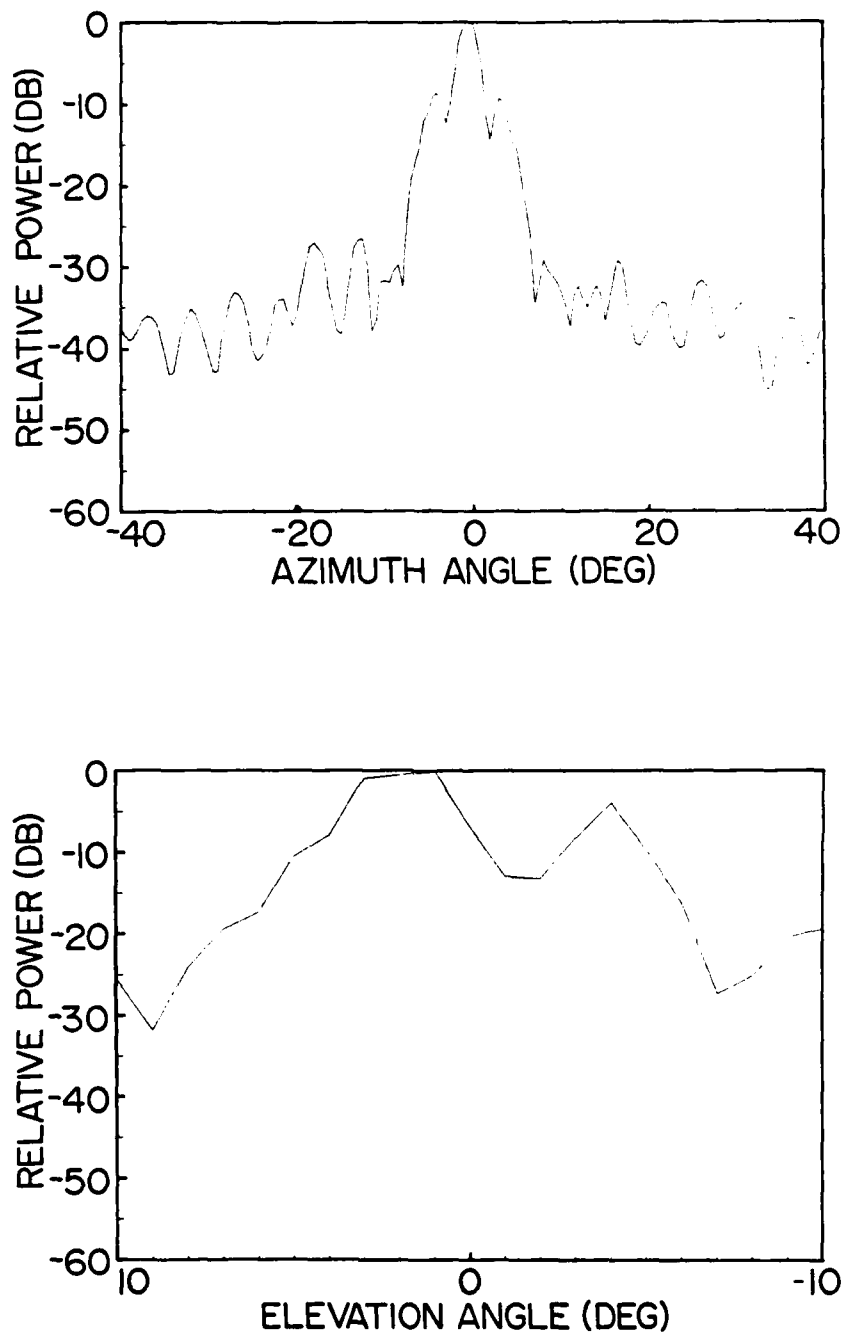to an isotropic radiator.

Figure 29. Azimuth and elevation patterns corresponding to the
overall recorded pattern maximum for the parallel
polarization for the out-of-band frequency of 9.0 GHz.
The gain at the top of each chart is 24.0 dB relative
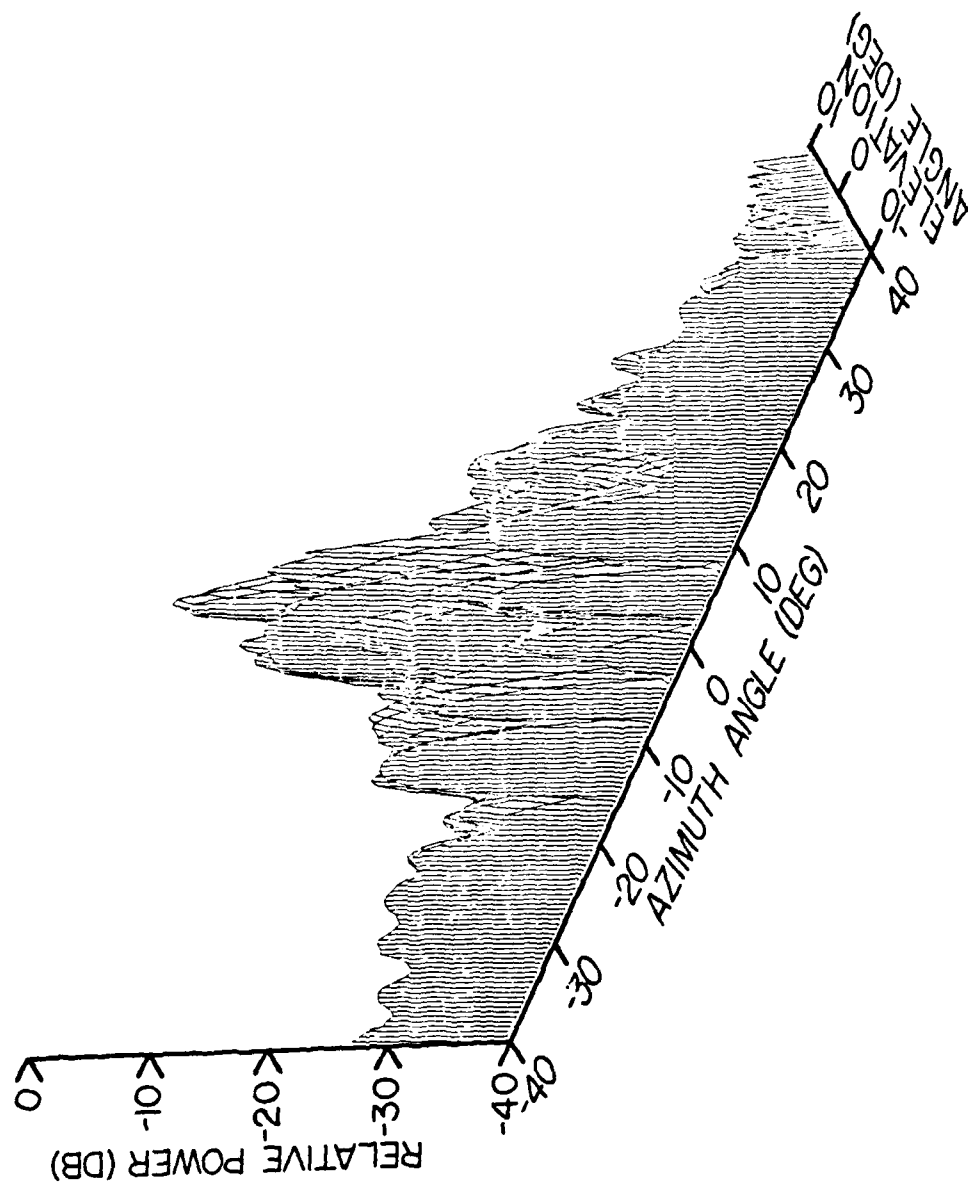to an isotropic radiator.

Figure 30. Axonometric view showing plots of the azimuth patterns recorded for 21 elevation angles for the parallel polarization for the out-of-band frequency of 9.2 GHz. The gain at the highest peak is 27.5 dB relative to an isotropic radiator.
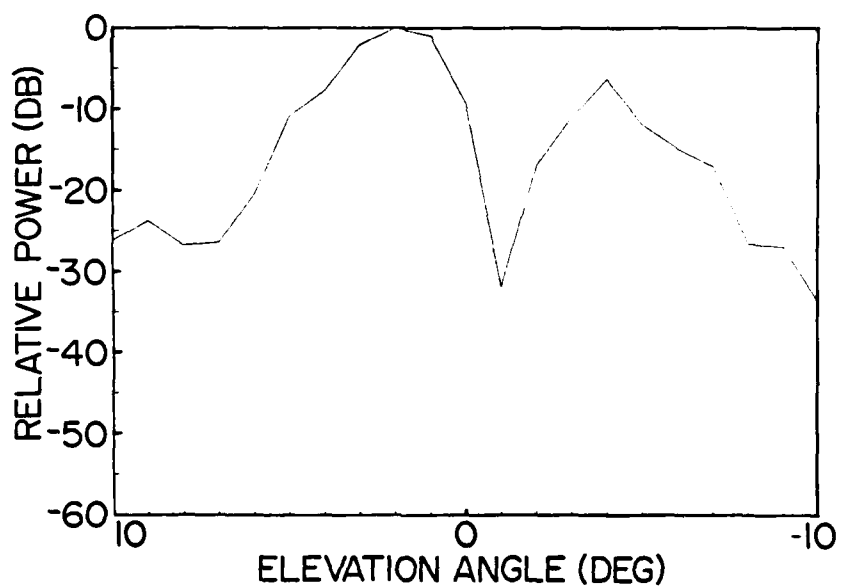
Figure 31. Azimuth and elevation patterns corresponding to the
            overall recorded pattern maximum for the parallel
            polarization for the out-of-band frequency of 9.2 GHz.
            The gain at the top of each chart is 27.5 dB relative
            to an isotropic radiator.
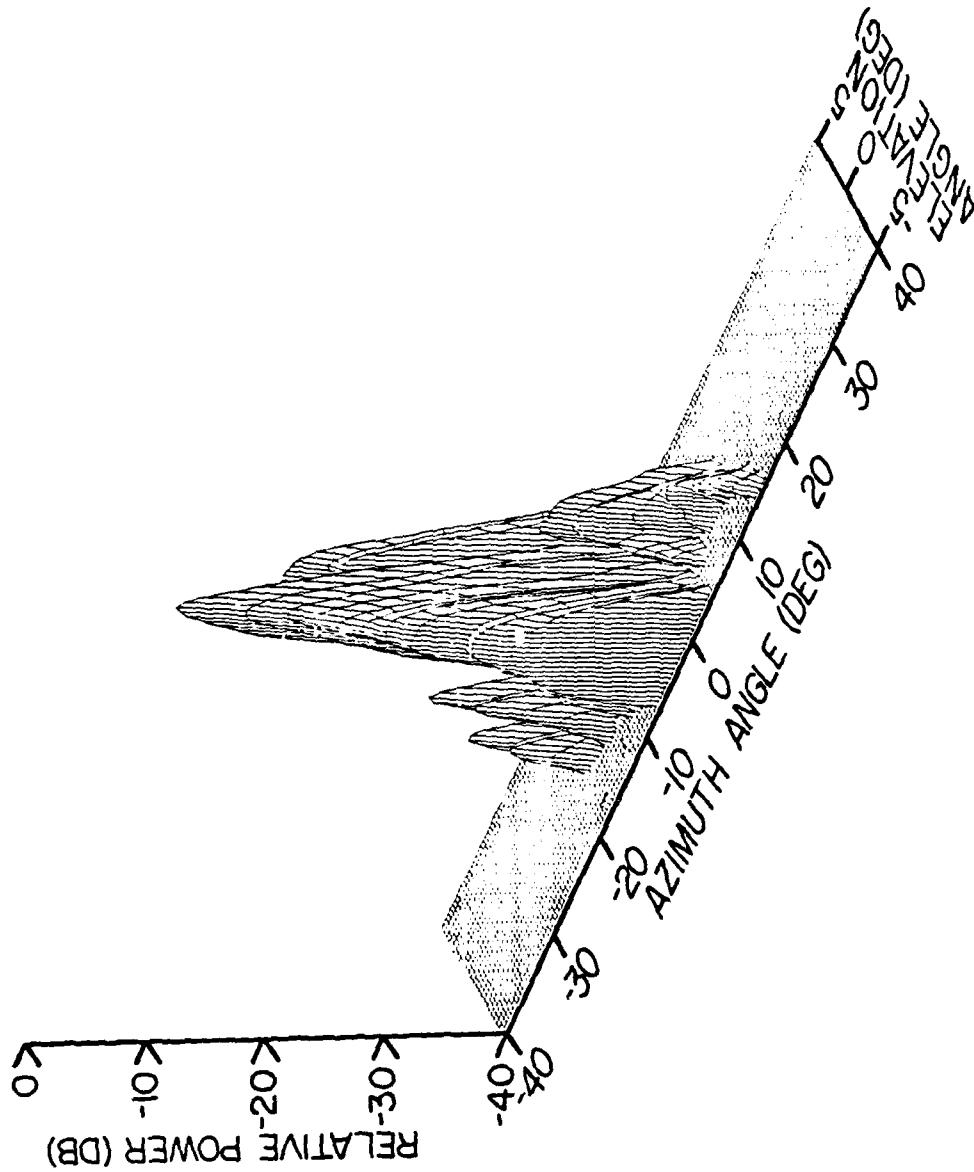
Figure 32. Axonometric view showing plots of the azimuth patterns recorded for 21 elevation angles for the parallel polarization for the out-of-band frequency of 9.4 GHz. The gain at the highest peak is 31.5 dB relative to an isotropic radiator.
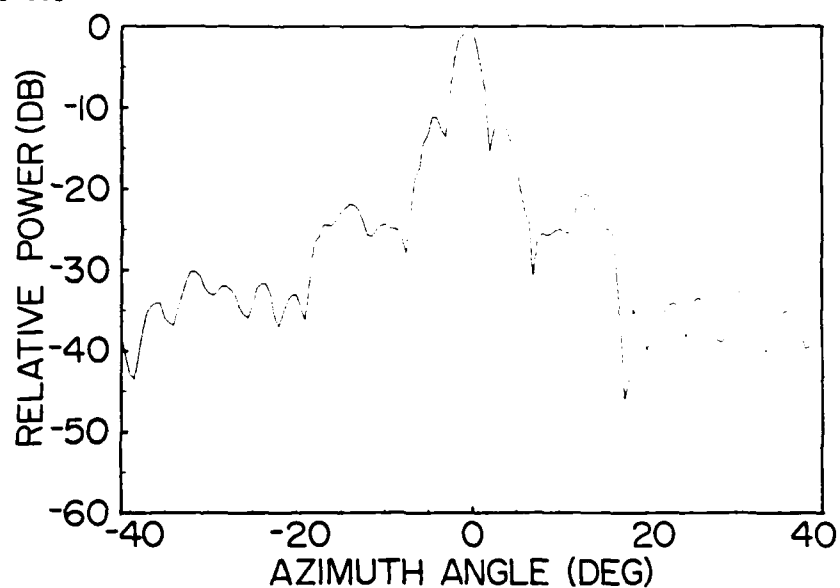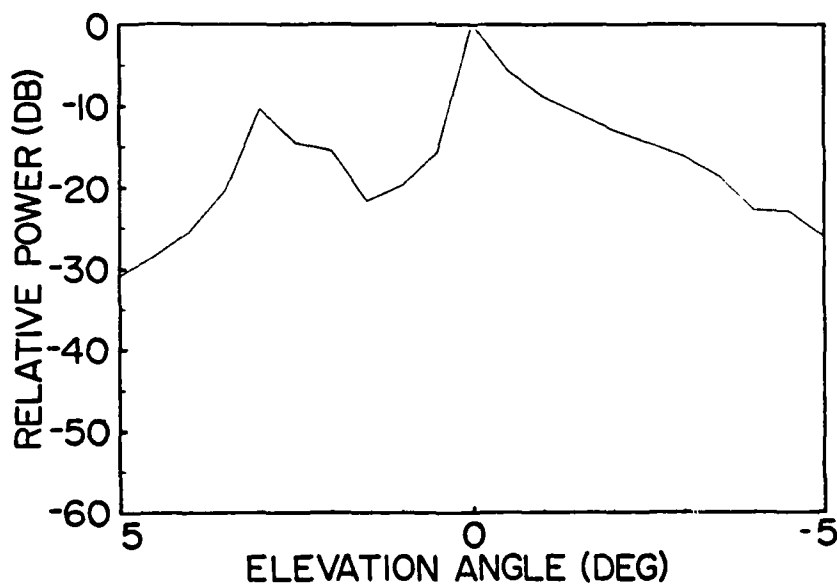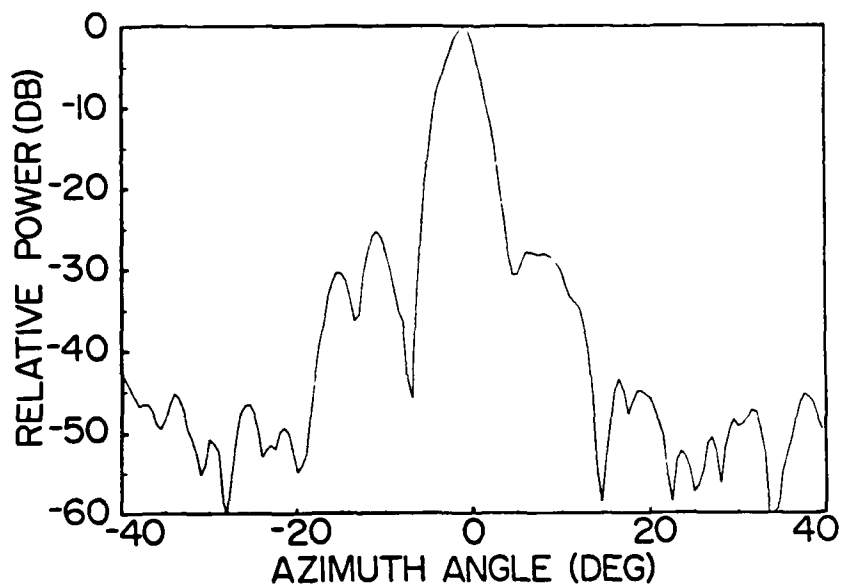
Figure 33.   Azimuth and elevation patterns corresponding to the
             overall recorded pattern maximum for the parallel
             polarization for the out-of-band frequency of 9.4 GHz.
             The gain at the top of each chart is 31.5 dB relative
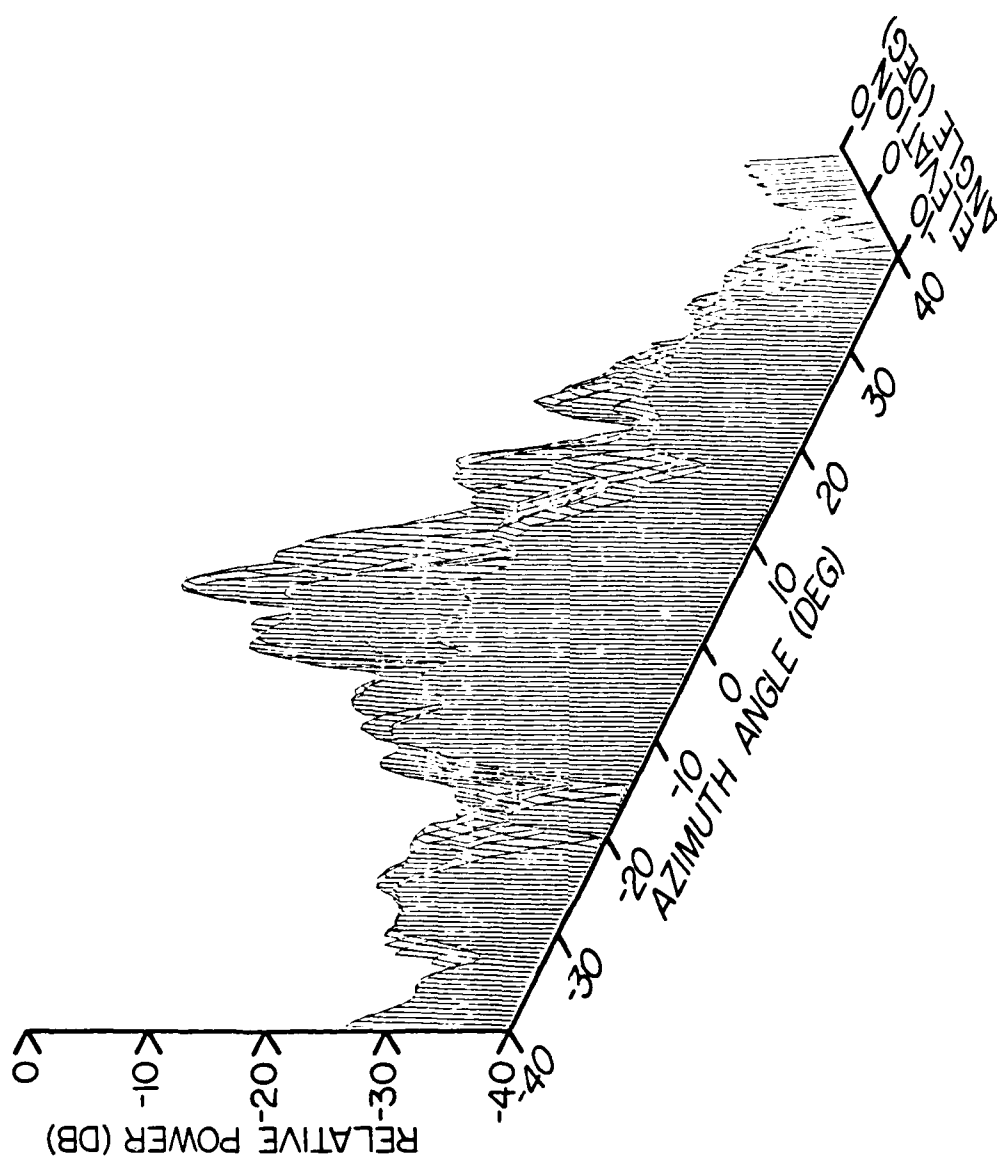   to an isotropic radiator.
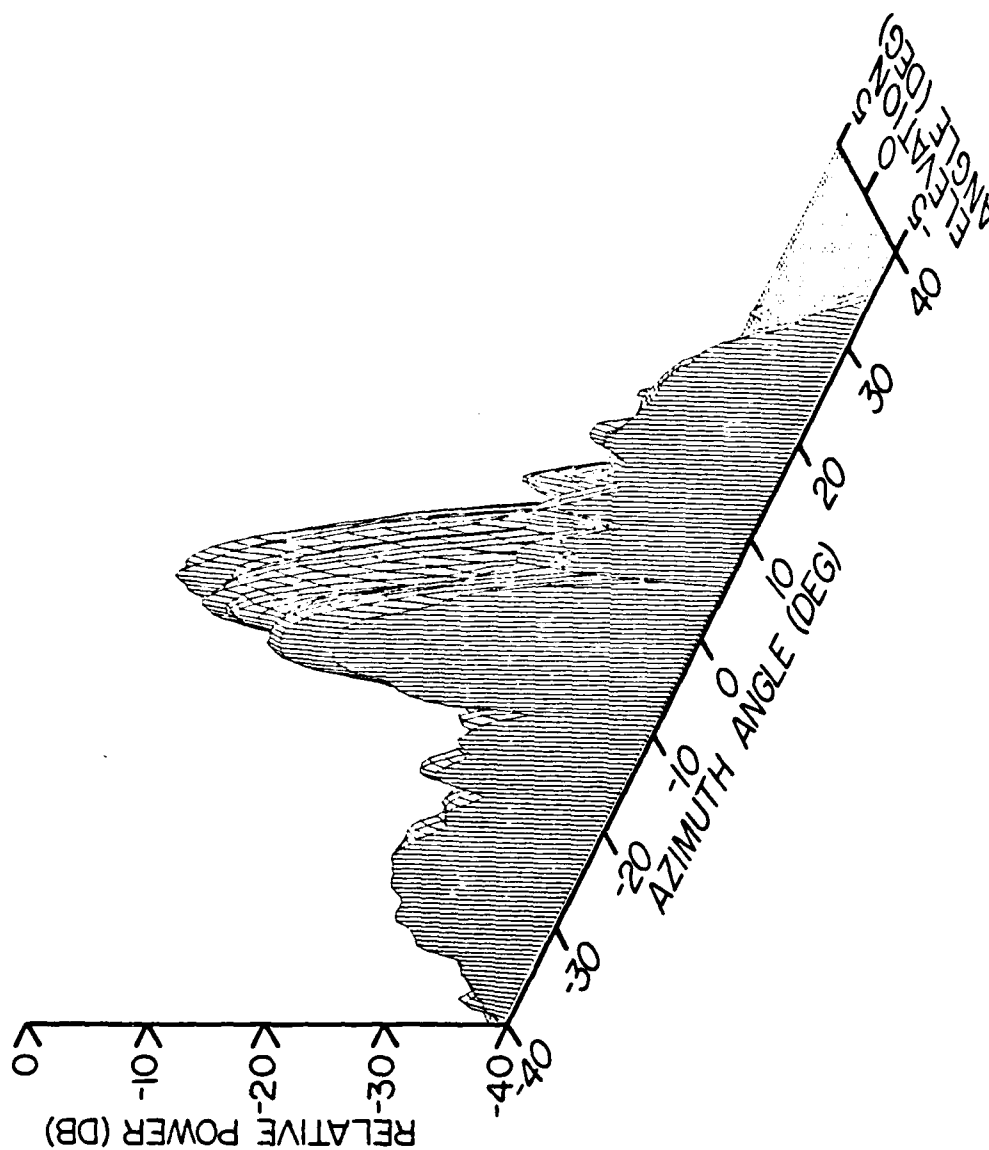
Figure 34.   Axonometric view showing plots of the azimuth patterns recorded for 21 elevation angles for the parallel polarization for the out-of-band frequency of 9.6 GHz. The gain at the highest peak is 30.5 dB relative to an isotropic radiator.
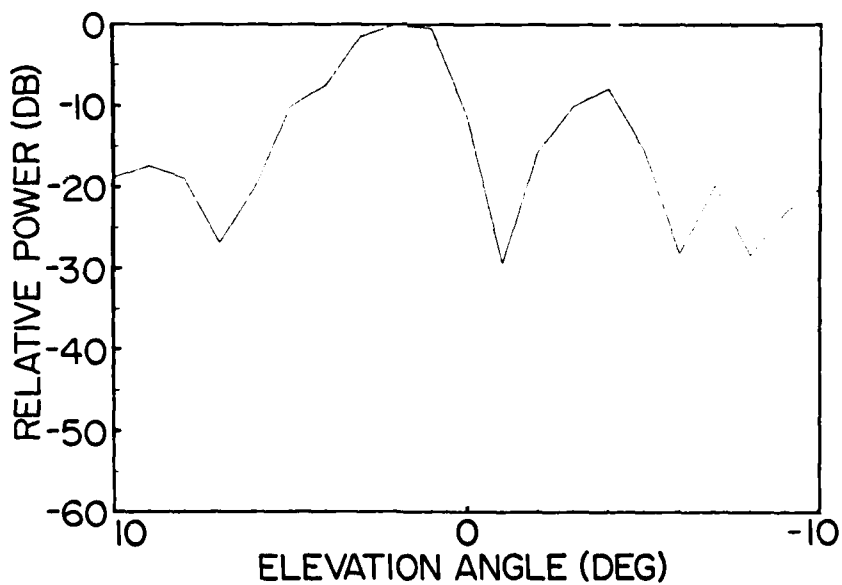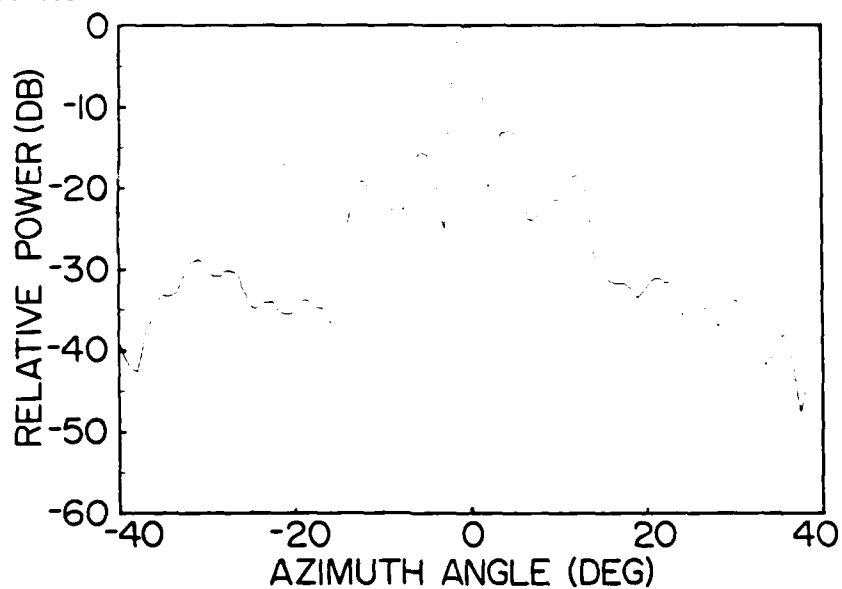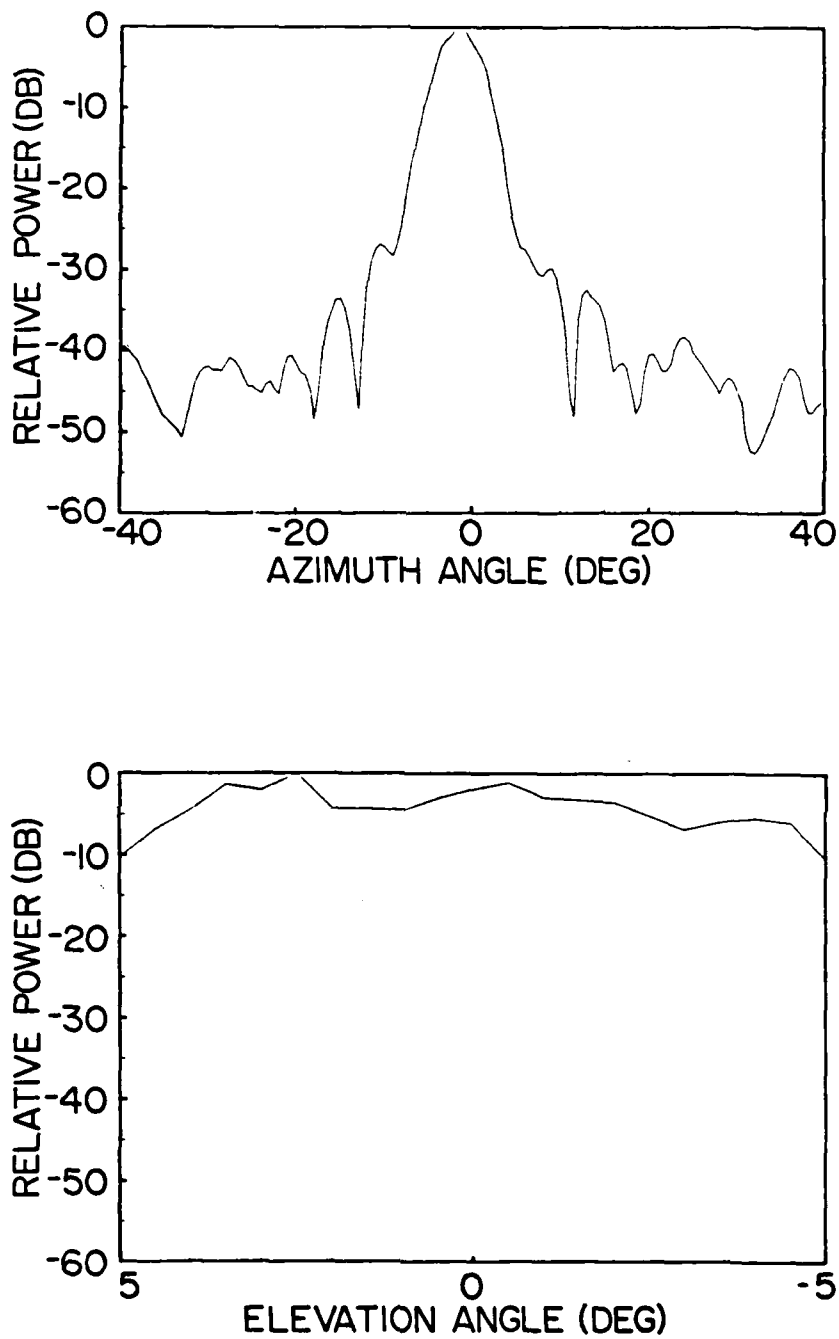
Figure 35. Azimuth and elevation patterns corresponding to the
            overall recorded pattern maximum for the parallel
            polarization for the out-of-band frequency of 9.6 GHz.
            The gain at the top of each chart is 30.5 dB relative
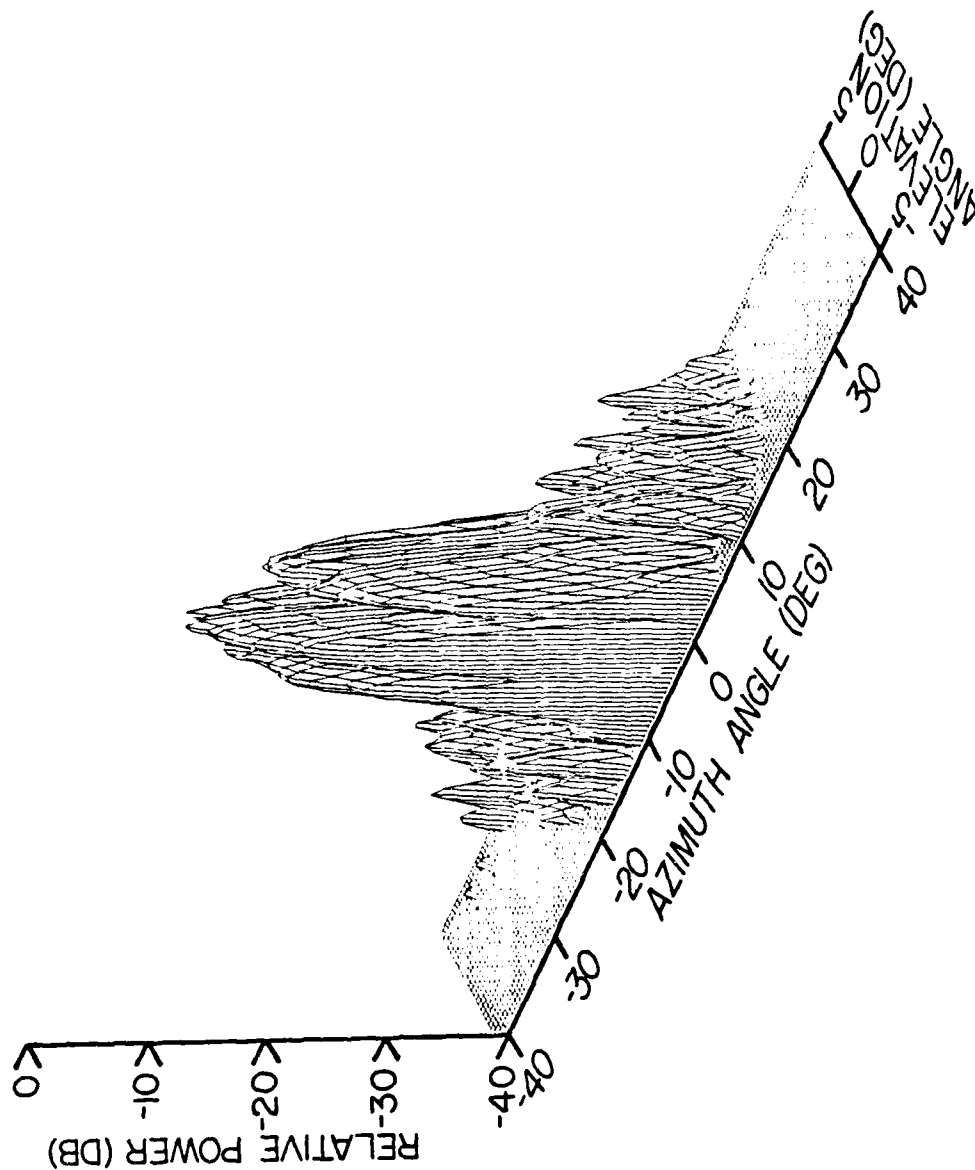   to an isotropic radiator.
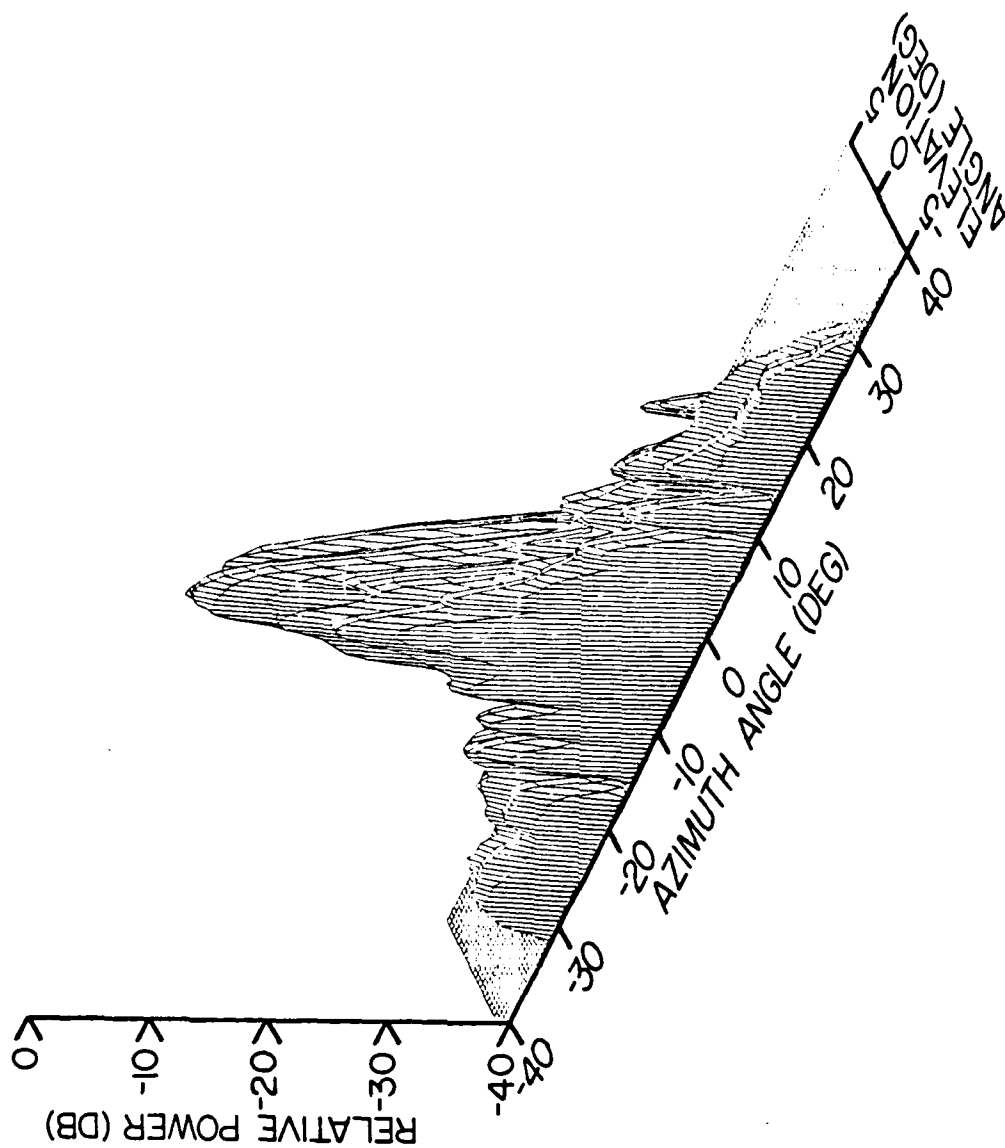
Figure 36. Axonometric view showing plots of the azimuth patterns recorded for 21 elevation angles for the parallel polarization for the out-of-band frequency of 10.0 GHz. The gain at the highest peak is 20.0 dB relative to an isotropic radiator.
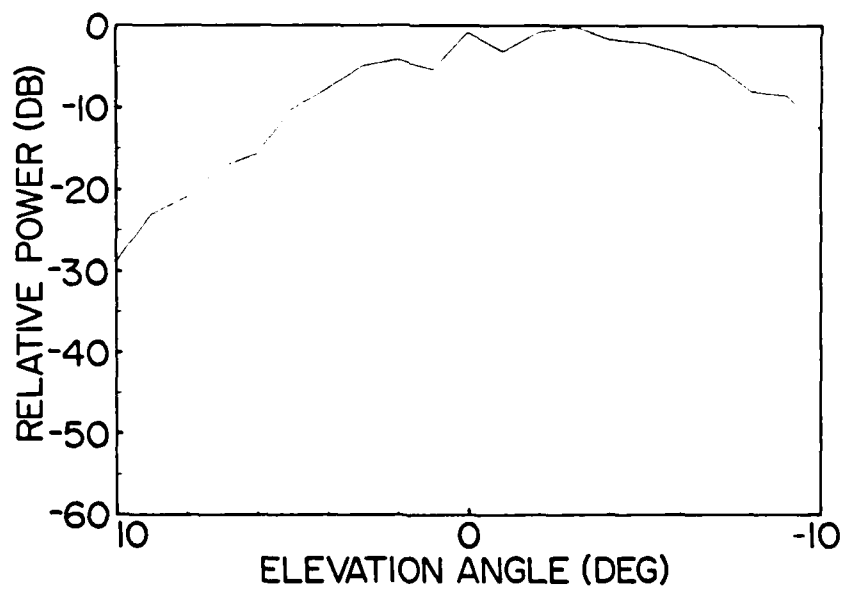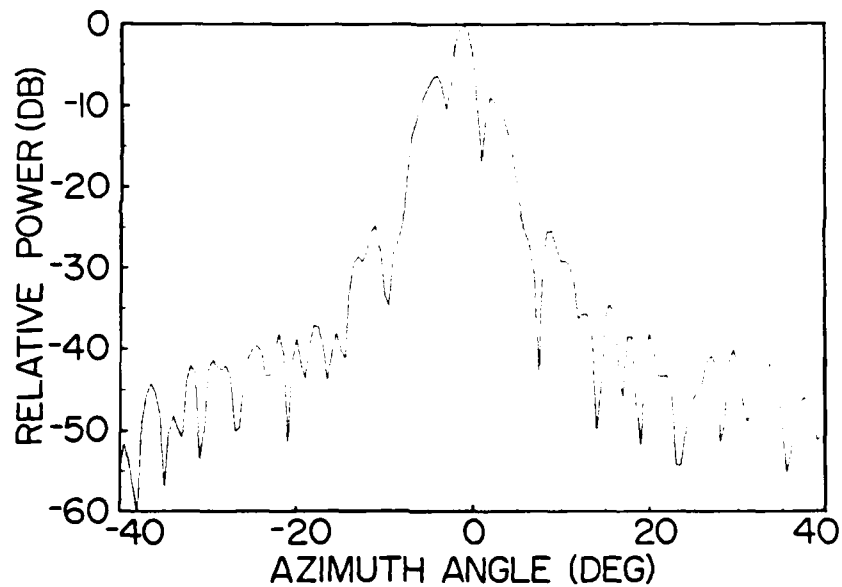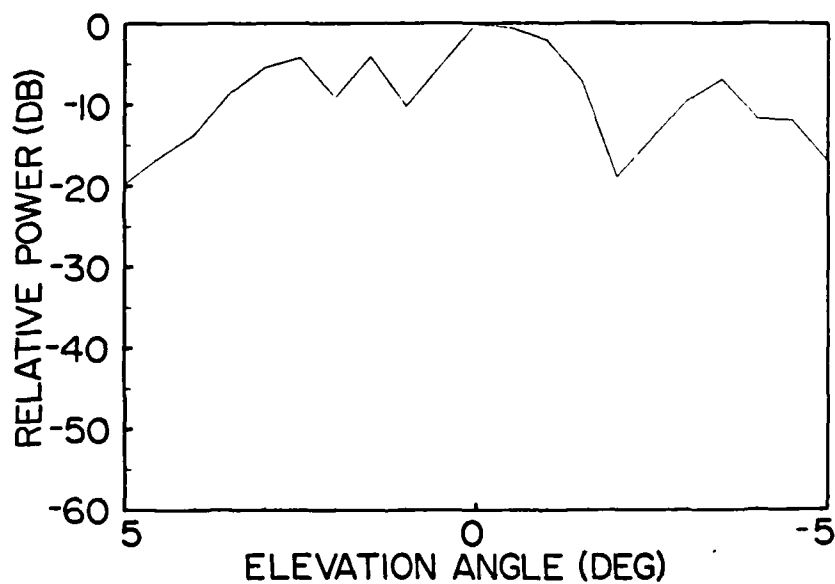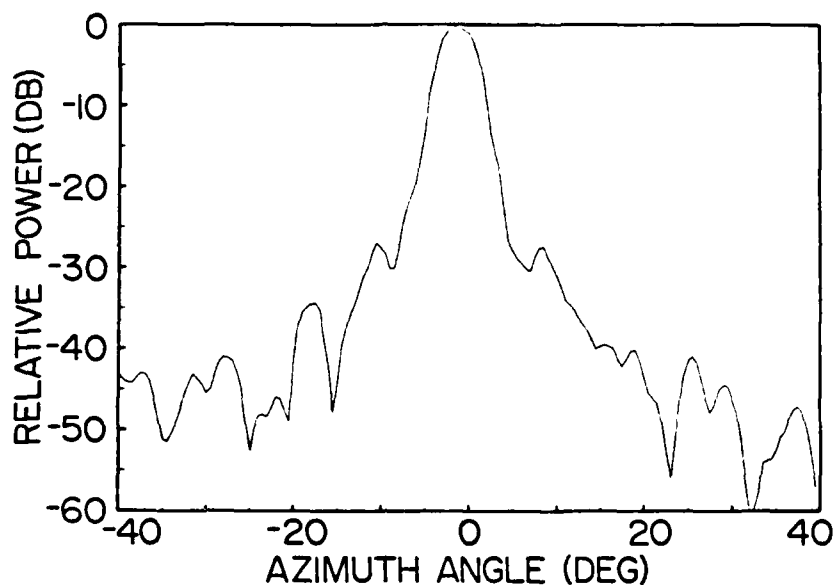
Figure 37.   Azimuth and elevation patterns corresponding to the
              overall recorded pattern maximum for the parallel
              polarization for the out-of-band frequency of 10.0 GHz.
              The gain at the top of each chart is 20.0 dB relative
              to an isotropic radiator.
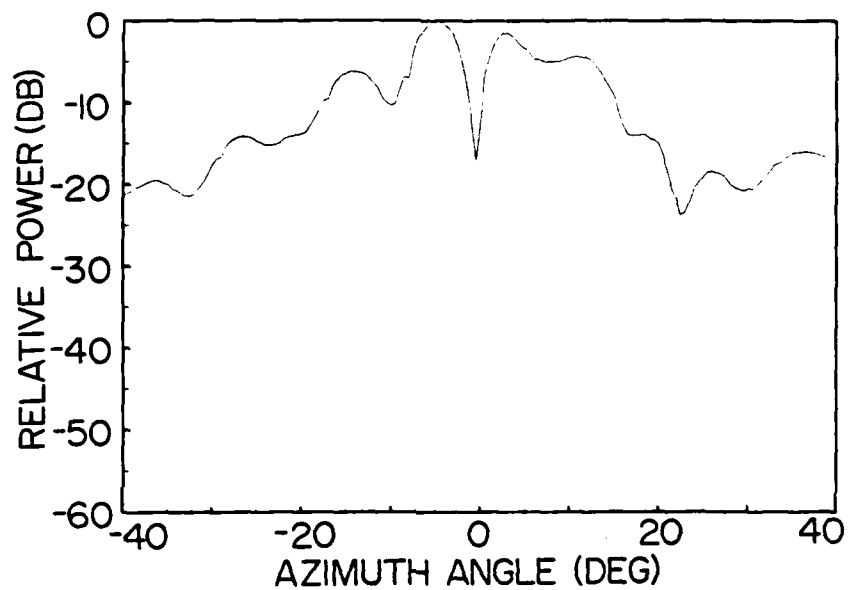
Figure 38.   Azimuth and elevation patterns corresponding to the
             overall recorded pattern maximum for the cross
             polarization for the in-band frequency of 3.0 GHz.
             The gain at the top of each chart is 6.8 dB relative
             to an isotropic radiator.
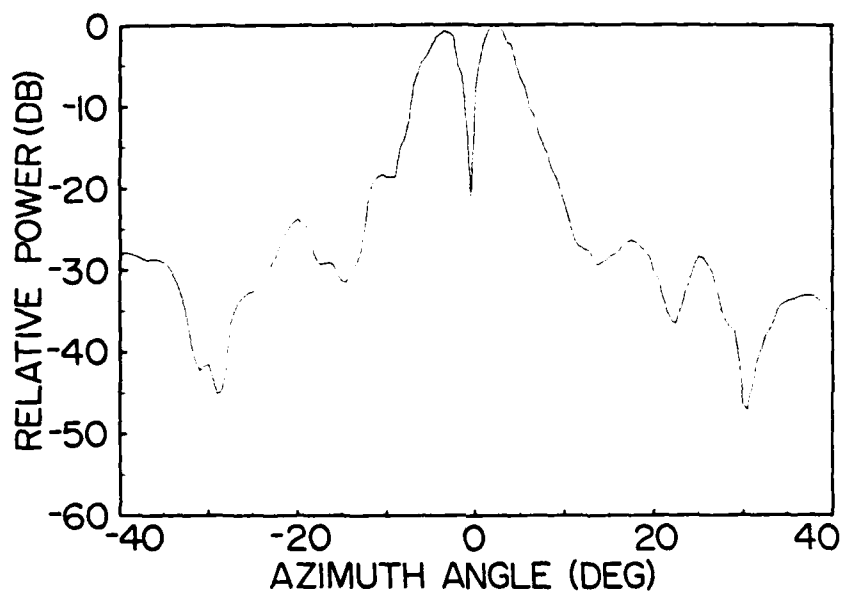
Figure 39.   Azimuth and elevation patterns corresponding to the
             overall recorded pattern maximum for the cross
             polarization for the out-of-band frequency of 5.5 GHz.
             The gain at the top of each chart is 22.7 dB relative
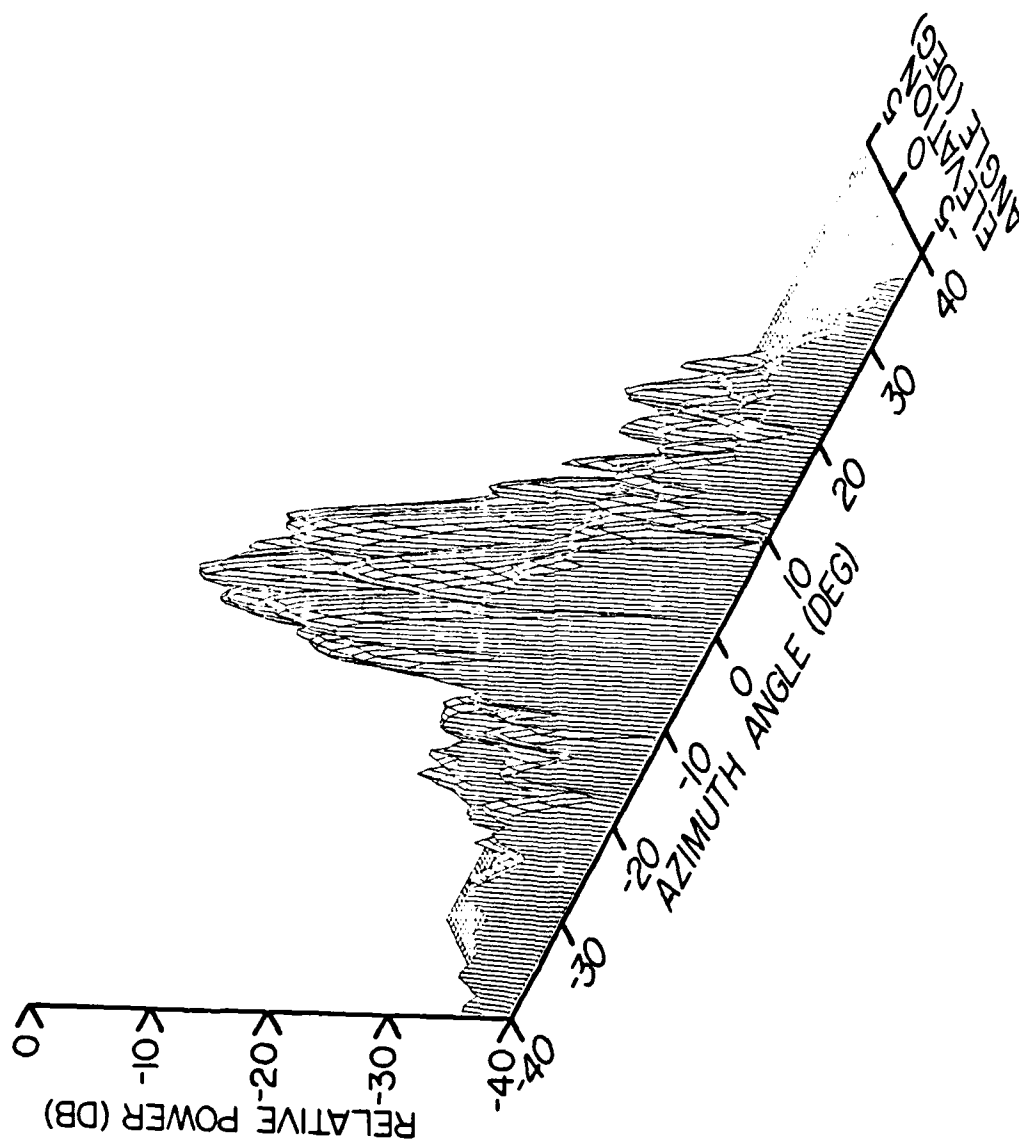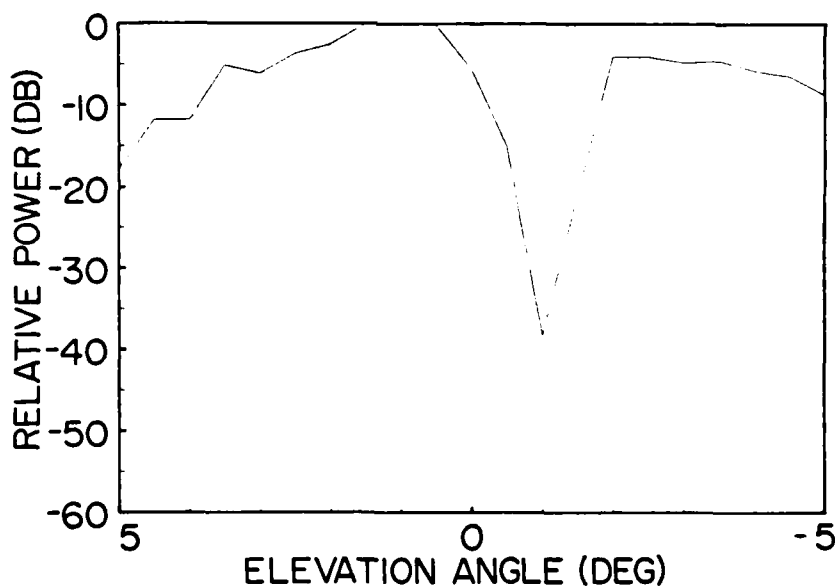   to an isotropic radiator.
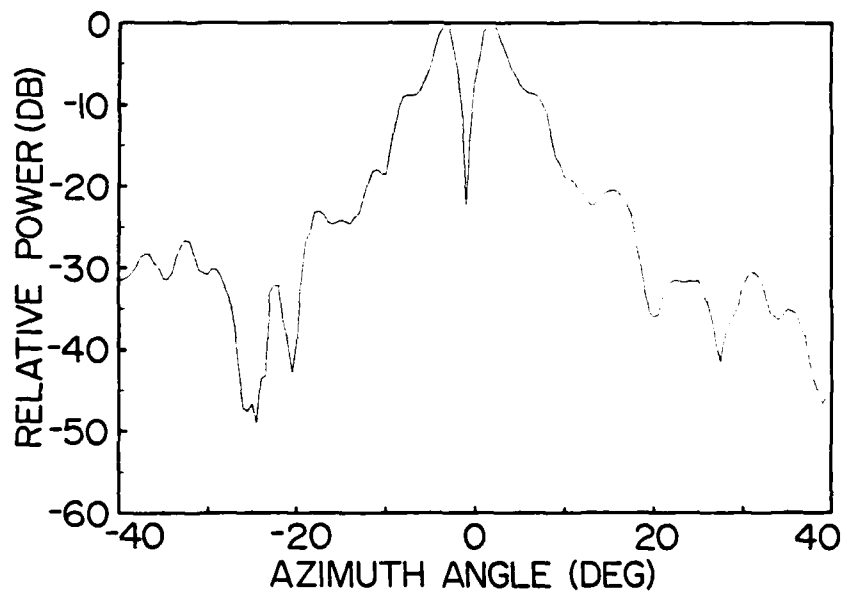
Figure 40. Azimuth and elevation patterns corresponding to the
            overall recorded pattern maximum for the cross
            polarization for the out-of-band frequency of 6.5 GHz.
            The gain at the top of each chart is 17.2 dB relative
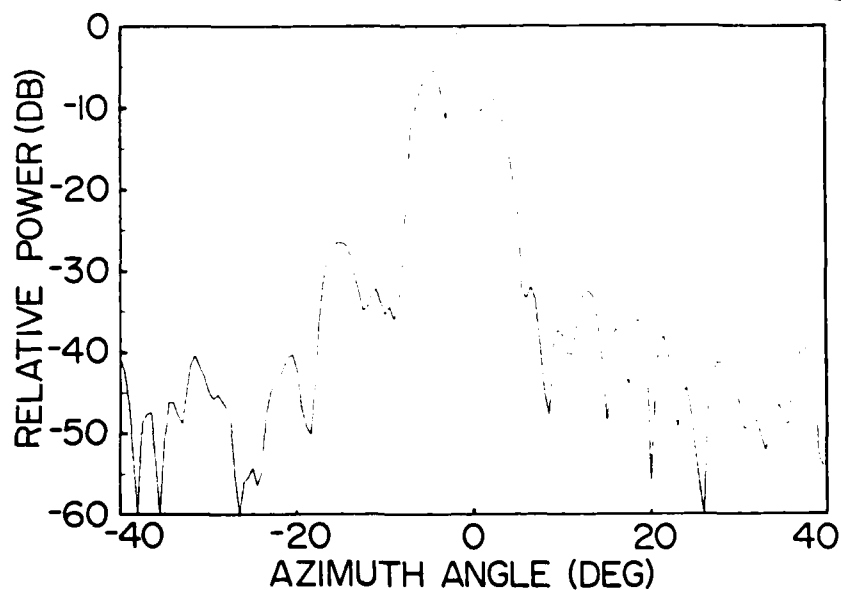   to an isotropic radiator.
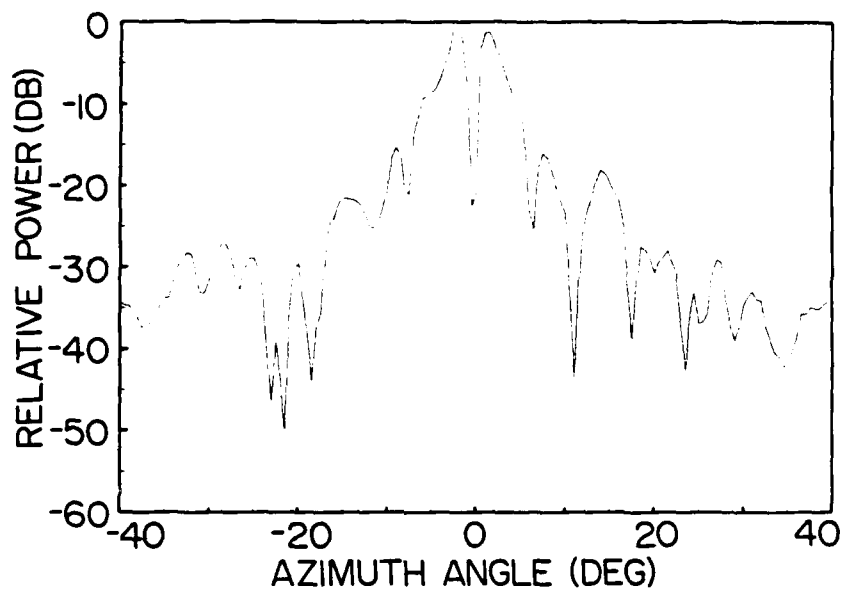
Figure 41.   Azimuth and elevation patterns corresponding to the
             overall recorded pattern maximum for the cross
             polarization for the out-of-band frequency of 7.5 GHz.
             The gain at the top of each chart is 16.8 dB relative
             to an isotropic radiator.
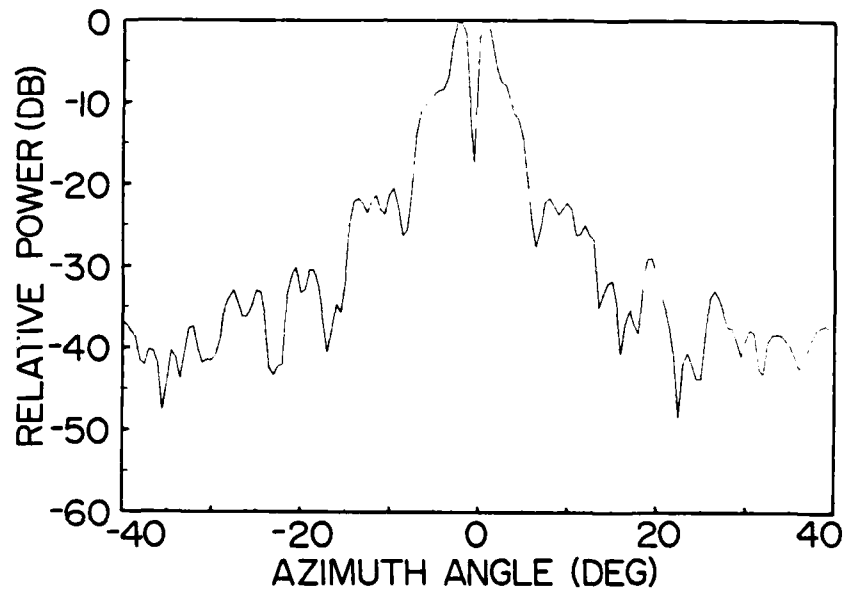
Figure 42. Azimuth and elevation patterns corresponding to the
overall recorded pattern maximum for the cross
polarization for the out-of-band frequency of 8.0 GHz.
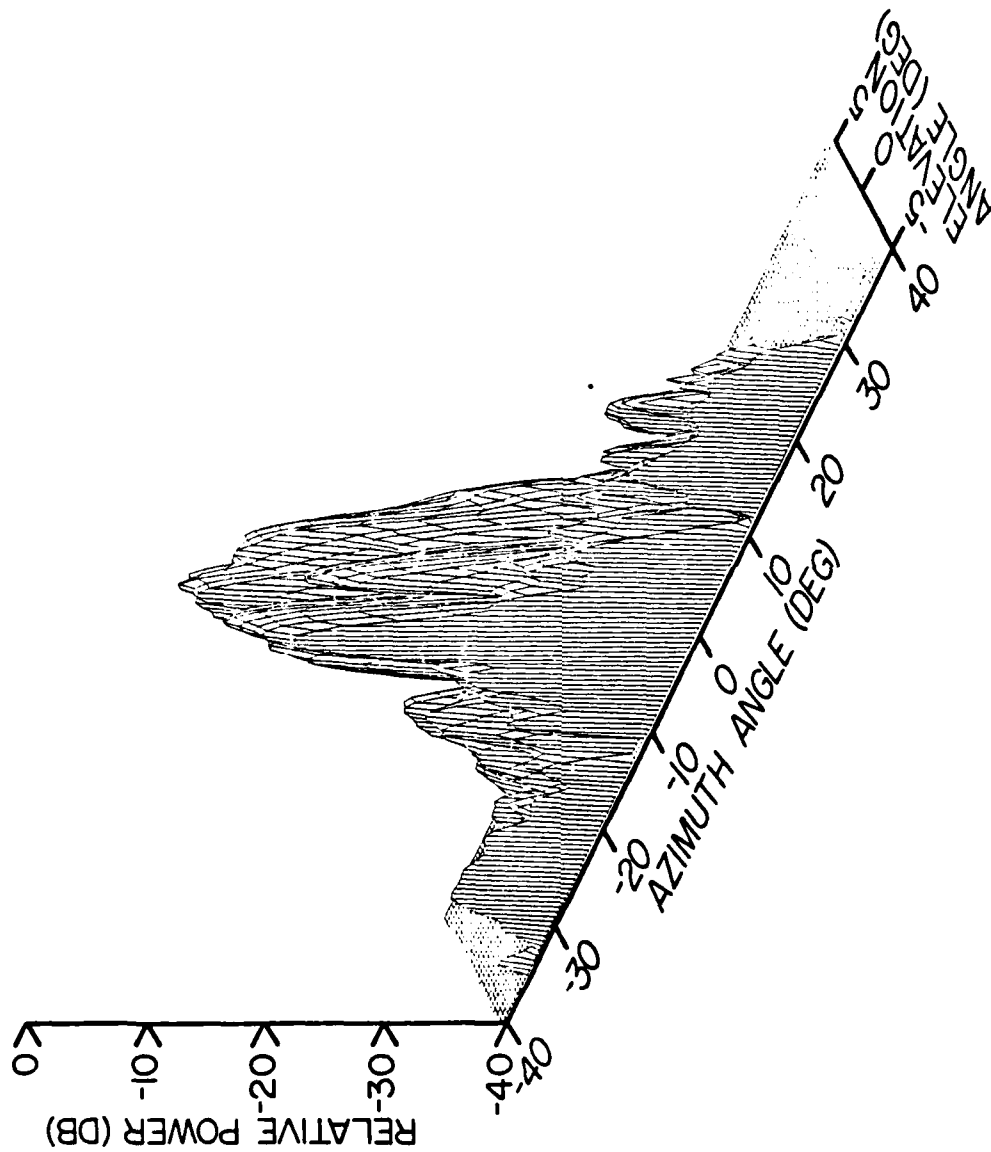The gain at the top of each chart is 22.0 dB relative
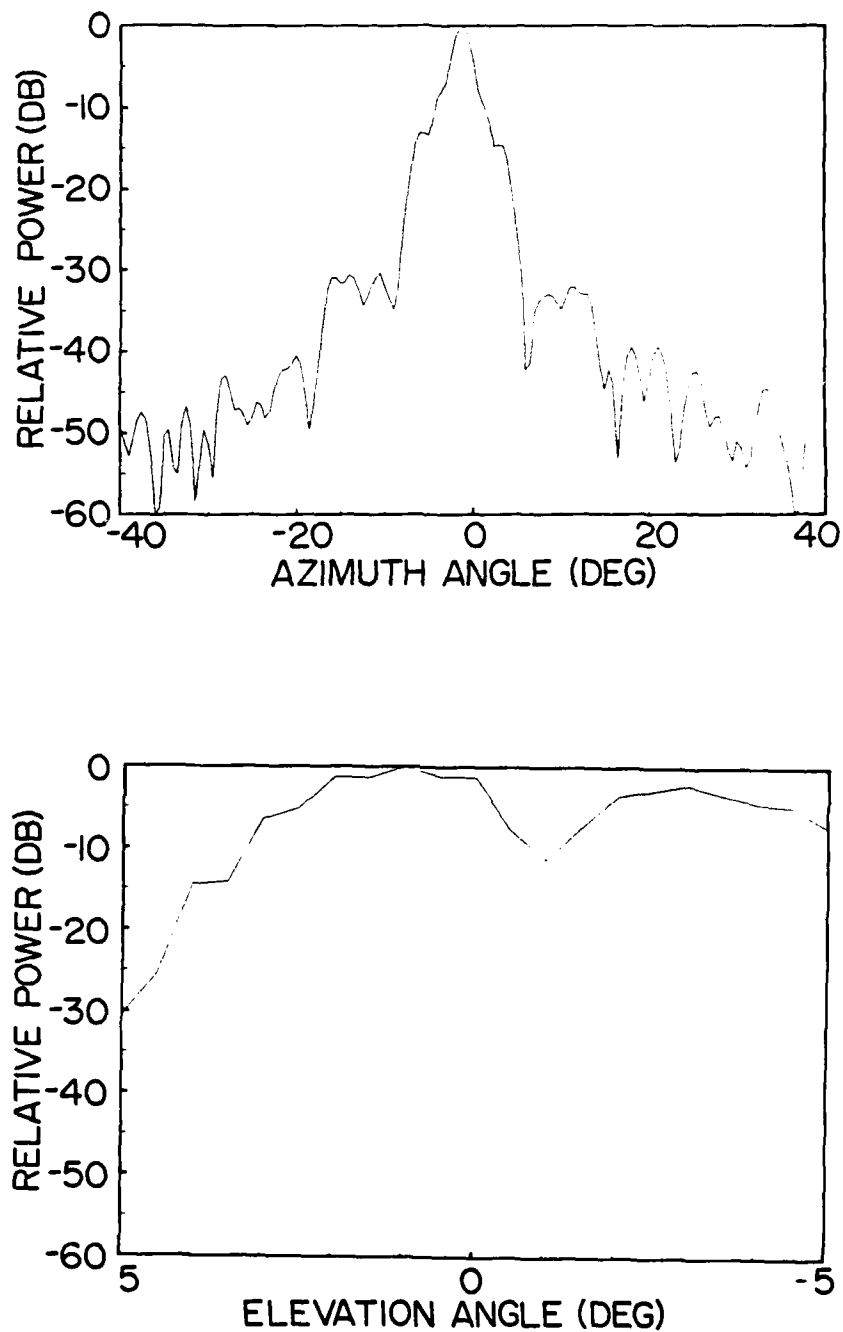to an isotropic radiator.
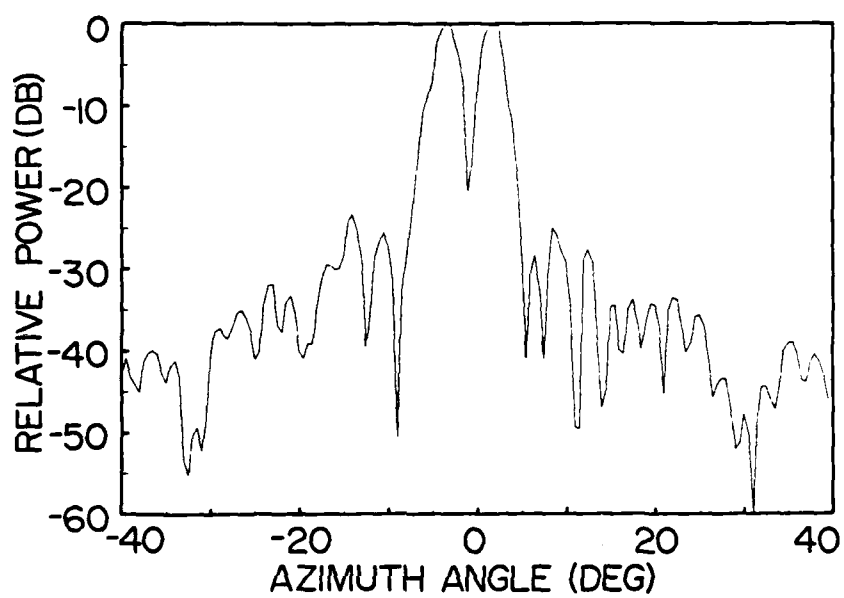
Figure 43.   Azimuth and elevation patterns corresponding to the
             overall recorded pattern maximum for the cross
             polarization for the out-of-band frequency of 9.0 GHz.
             The gain at the top of each chart is 19.9 dB relative
             to an isotropic radiator.
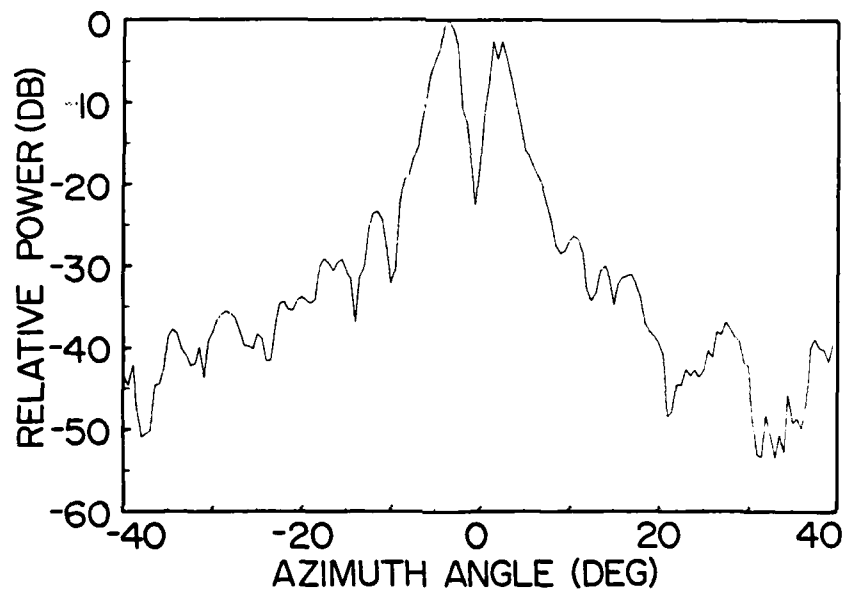
Figure 44.   Azimuth and elevation patterns corresponding to the
             overall recorded pattern maximum for the cross
             polarization for the out-of-band frequency of 10.0 GHz.
             The gain at the top of each chart is 10.6 dB relative
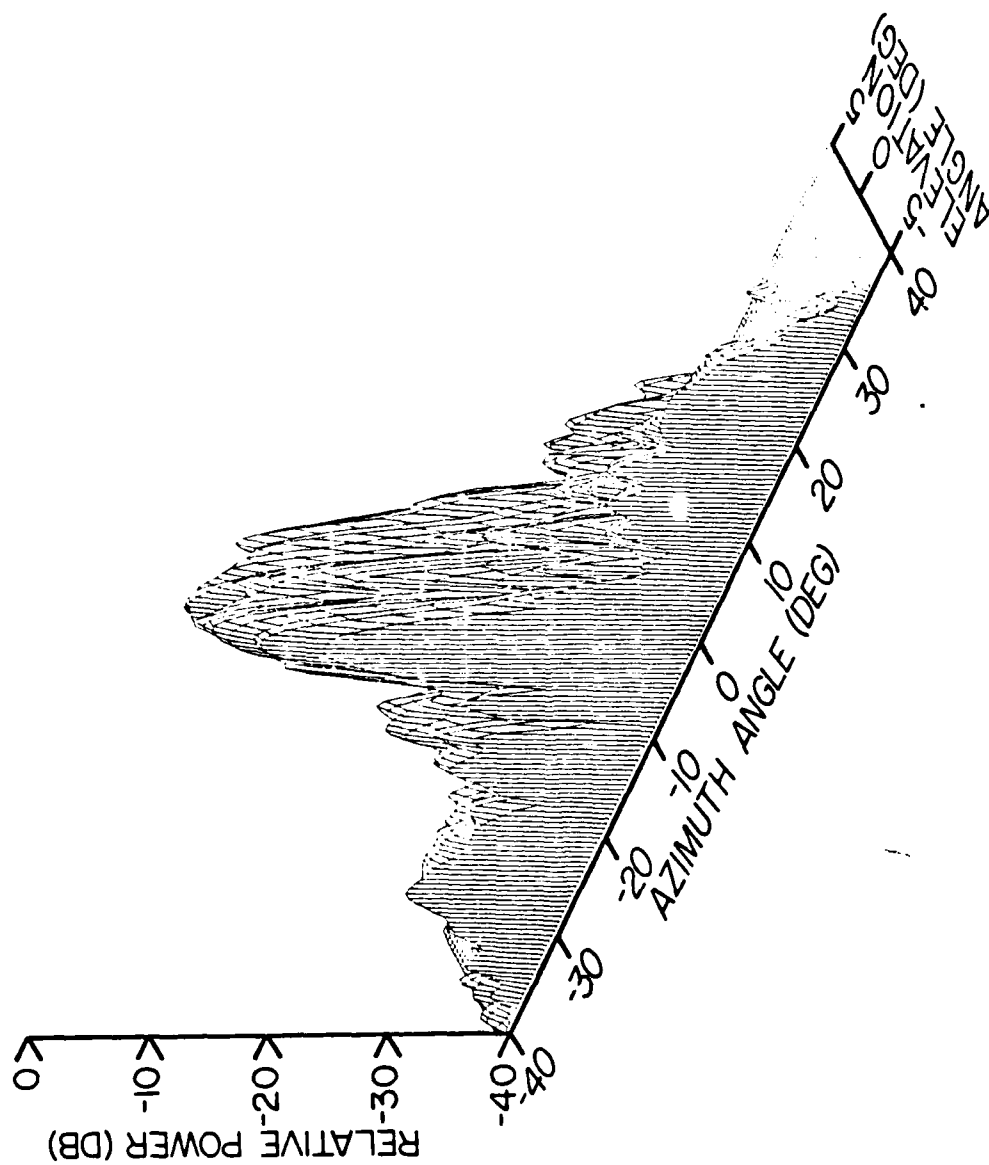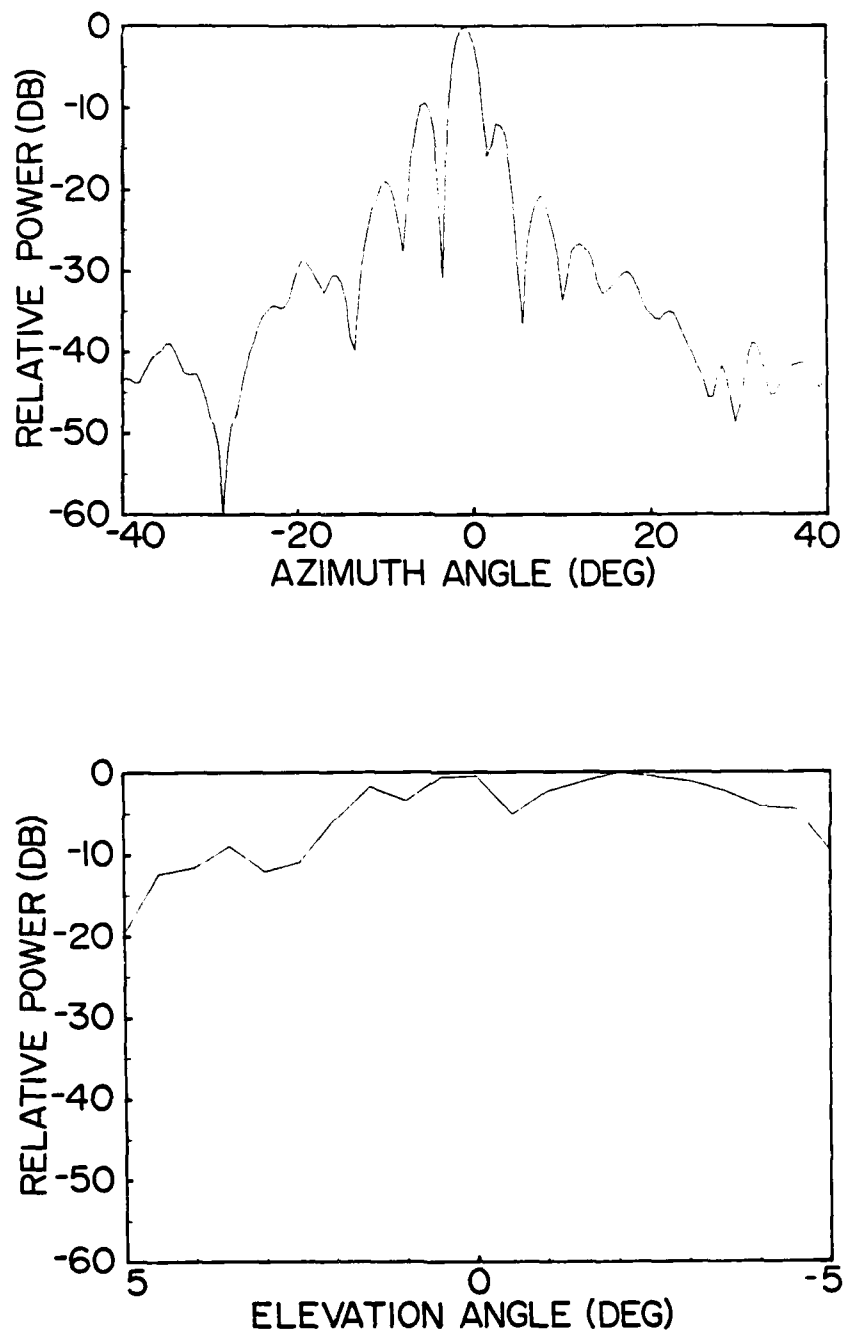   to an isotropic radiator.
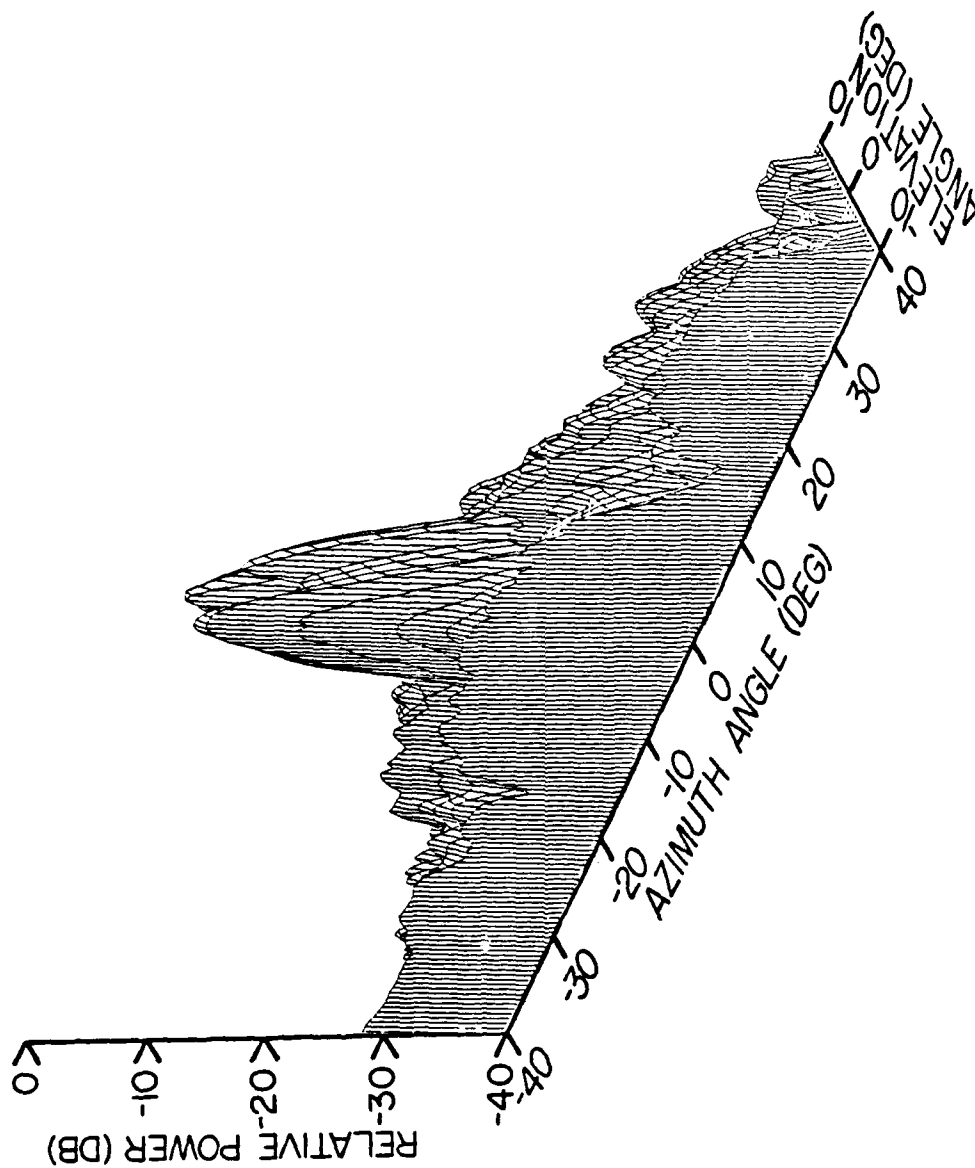
Figure 45. Axonometric view showing plots of the average azimuth patterns computed for the parallel polarization sense for the out-of-band second harmonic frequencies from 5.5 GHz to 7.5 GHz. The average gain at the highest peak is 28.2 dB relative to an isotropic radiator.
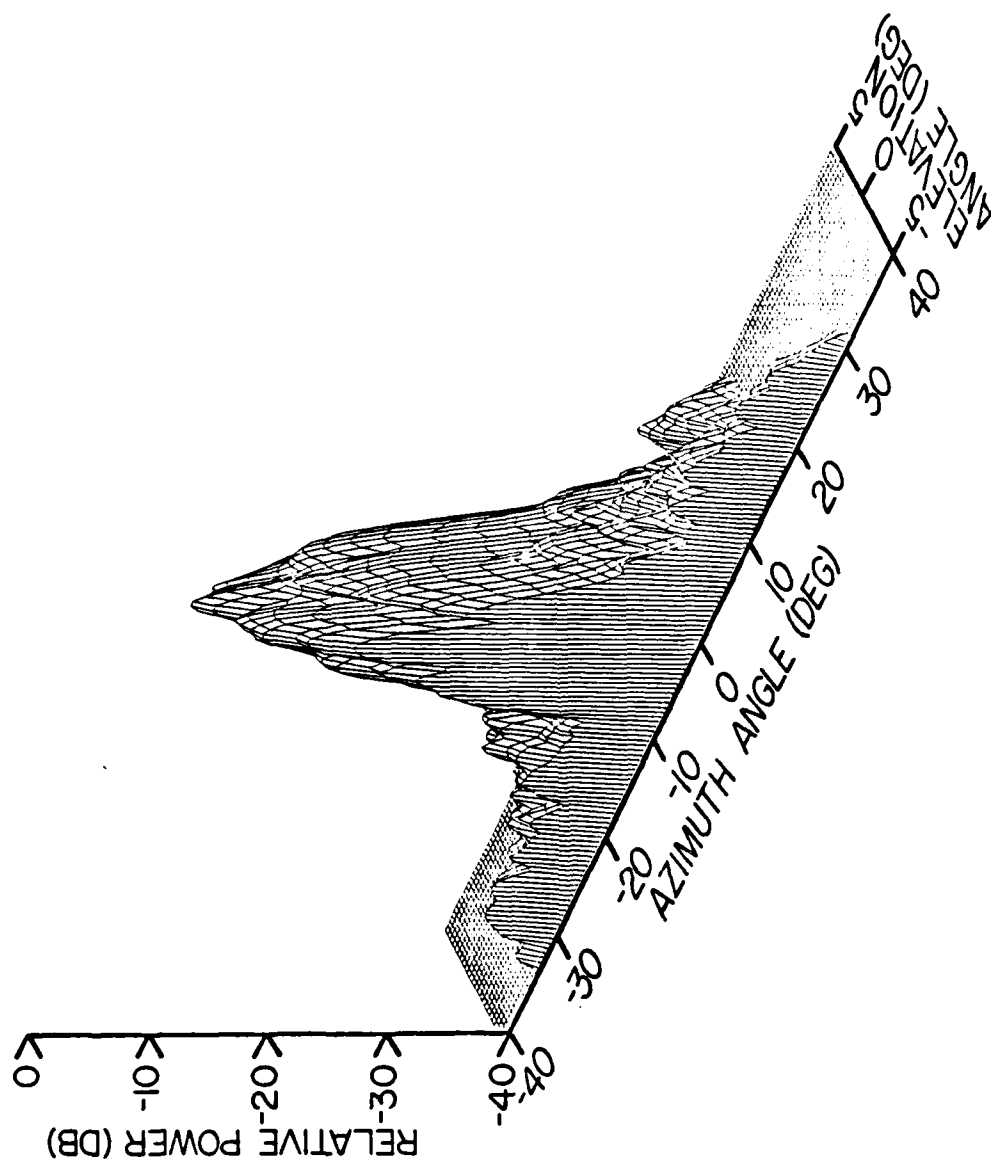
Figure 46.   Axonometric view showing plots of the average azimuth patterns computed for the parallel polarization sense for the out-of-band second harmonic frequencies from 8.0 GHz to 10.0 GHz. The average gain at the highest peak is 24.0 dB relative to an isotropic radiator.

plots of the maximum recorded azimuth pattern are displayed in Figures 38
through 44. Again, the figures are sequenced by frequency in ascending order
from 3.0 to 10.0 GHz.

TABULATIONS OF KEY EMC PARAMETERS

The data tabulated in TABLES 1 through 4 provide an overview of the
selected EMC parameters versus frequency and polarization sense, particularly
for the parallel polarization sense. The peak gain and the angular
coordinates of the peak for parallel polarization are accurately determined
because the measured data were recorded every 1.0 degree for elevation angles
from -10.0 degrees to +10.0 degrees for the second harmonic region, and every
0.5 degree from -5.0 degrees to +5.0 degrees for the third harmonic region.
The recorded peak gain for cross polarization data were recorded only for
elevation angles of ±2.0 degrees and 0 degrees for the second harmonic region
and for ±1.0 degree and 0 degrees for the third harmonic region. However, the
significantly high peak gains that were recorded for the cross polarization
sense indicate that the cross polarized data should be measured as extensively
as the parallel polarization data during future out-of-band measurements.

The values of average gain and standard deviation presented in the tables
were computed from the maximum azimuth pattern rather than from the entire
data set because the elevation pattern data do not extend into the sidelobe
regions. Values of the average gain and standard deviation computed from the
entire data set would be difficult to interpret and may not be meaningful due
to the truncation of the elevation pattern data. However, it appears that the
average gain and standard deviation for the maximum azimuth pattern is a
useful interim approximation to the statistics of the measured pattern data
pending the collection of data for larger elevation sectors. In particular,
elevation and azimuth sectors of at least 120 degrees of the antenna are
recommended for future investigations in order to obtain more useful and
accurate values of average gain and standard deviation for EMC applications.

It should be emphasized that the average gain values tabulated in the tables should be compared with the corresponding average gain for the in-band 3.0 GHz frequency over the same 80-degree sector. The average gain and standard deviation for 3.0 GHz for parallel polarization are +3.5 dB and ±10.6 dB, respectively, for the front 80-degree azimuth sector. The average gain and standard deviation 3.0 GHz for cross polarization are -5.8 dB and ±6.8 dB, respectively, over this same azimuth sector.

The cumulative probability distributions computed directly from the out-of-band frequencies differ noticeably from a Gaussian distribution and do not appear to have a simple analytical form. Plots of the directly computed and the approximated cumulative probability distribution for the maximum azimuth pattern at 9.2 GHz are shown in Figure 47. The numerical average gain and standard deviation presented in the tables provide marginally acceptable interim estimates for the actual cumulative probability distributions when used in the Gaussian approximation.

Inspection of the data presented in TABLE 1 for the second harmonic region and in TABLE 2 for the third harmonic region for the parallel polarization reveals several interesting trends. In particular, the peak gain for the second harmonic region varies from a lowest recorded value of 27.7 dB at 6.3 GHz to a highest recorded value of 33.7 dB at 7.3 GHz. However, the peak gain is typically ≈ 31 dB for the majority of the frequencies. The largest recorded azimuth shift is +3.0 degrees at 7.5 GHz; the largest recorded elevation shift is -4.0 degrees at 7.4 GHz. The average gain over the front ±40-degree sector varies from about -1.0 dB at 6.7 GHz to 4.5 dB at 5.7 GHz. Most of the average gain values are comparable, with the average gain of 3.5 dB obtained for the in-band 3.0 GHz pattern. Similarly, the standard deviations for the second harmonic region range from ±9.7 dB at 6.6 GHz to ±12.7 dB at 6.2 GHz. The tabulated standard deviations are commensurate with the in-band 3.0 GHz standard deviation of 10.6 dB.

The peak gain values shown in TABLE 2 for the third harmonic region vary more significantly than do the peak gain values for the second harmonic region

GAIN ABOVE ISOTROPIC (dB)

PROBABILITY THAT THE GAIN IS LESS THAN OR
EQUAL TO THE ABSCISSA
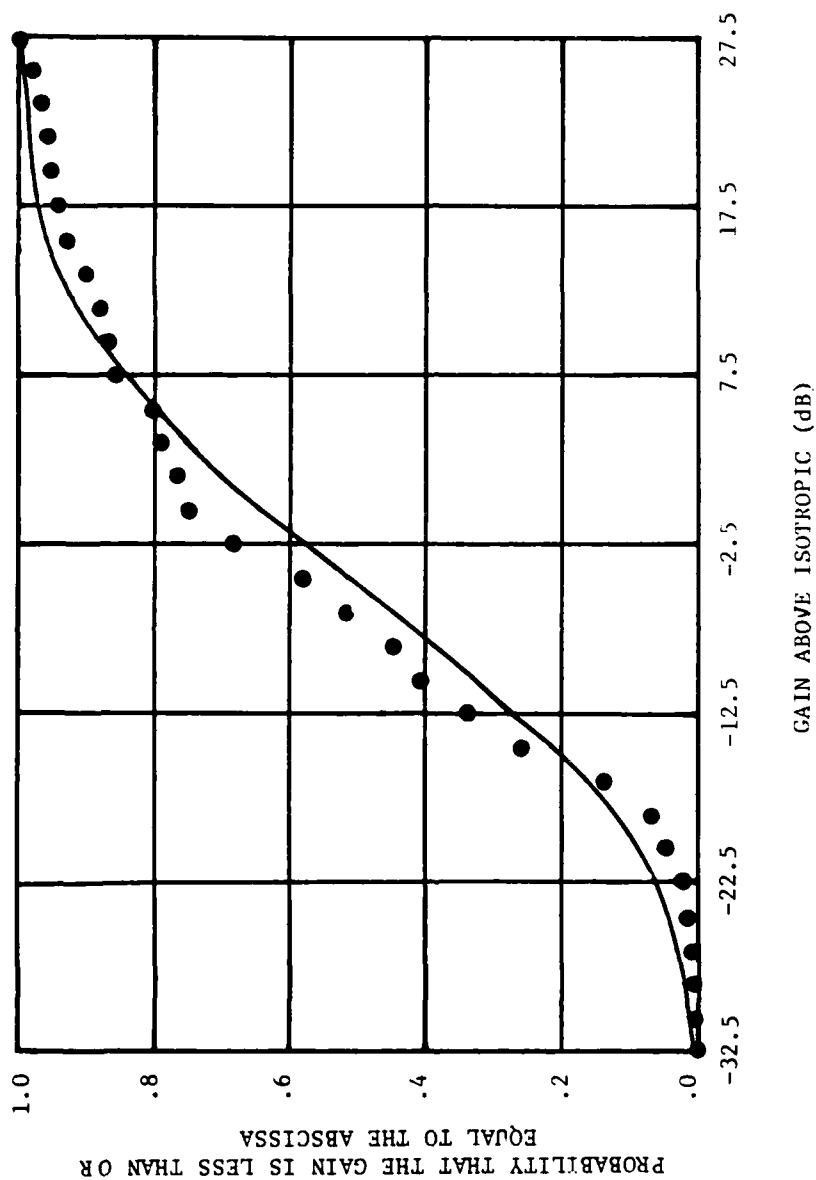
Figure 47. Plots of the cumulative probability distribution function constructed
from direct statistical analysis (dots) and the Gaussian cumulative
probability distribution function (solid line) constructed from the
average gain and standard deviation for the maximum azimuth pattern
for parallel polarization at the out-of-band frequency of 9.2 GHz.

just discussed. In particular, the recorded peak varies from 16.5 dB at 8.7 GHz to about 33.5 dB at both 8.0 GHz and 9.8 GHz. The largest recorded azimuth shift is -1.5 degrees at 10.0 GHz; the largest recorded elevation shift is +3.5 degrees at 9.9 GHz. The average gain varies from about -19.8 dB at 8.7 GHz to about +1.2 dB at 9.3 GHz. The average gain is below isotropic for all frequencies except 9.3 GHz. The standard deviations range from about 12.0 dB at 9.2 GHz to about ±15.0 dB at 9.5 GHz; thus, the average gains are typically lower than the in-band average gain, and the standard deviations are typically greater than the in-band standard deviation.

The tabulated values of peak gain, angular coordinates of the peak, and the average gain and standard deviation (shown in TABLES 3 and 4 for the second and third harmonic regions, respectively, for the cross polarization sense) also reveal important trends even though the data were obtained from only three selected elevation angles. In particular, the peak gain for the second harmonic region ranges from 13.1 dB at 6.3 GHz to 24.4 dB at 6.7 GHz. The azimuth shifts range from -3.5 degrees at 6.3 GHz to about +3.0 degrees at 6.6 GHz. Note that the maximum azimuth patterns for the cross polarization sense typically have two beams located approximately symmetrically either side of zero degrees azimuth, and that their peak gain values are often approximately equal. The average gain varies from about -12.0 dB at 6.4 GHz to about +0.7 dB at 6.7 GHz, and the standard deviation varies from about 9.0 dB for both 6.3 GHz and 6.7 GHz. The average gain values are commensurate with the in-band average gain of -5.8 dB for the cross polarization sense, and the standard deviations are significantly greater than the standard deviation of ±6.8 dB for the in-band cross polarized pattern.

The peak gain for the third harmonic region varies from 7.3 dB at both 8.7 GHz and 9.4 GHz to 22.5 dB at 9.3 GHz. Most of the peak gain values are in excess of 10 dB. The azimuth shift varies from -4.0 degrees at 9.6 GHz to +3.0 degrees at both 9.4 GHz and 9.5 GHz. The elevation shift ranges from -1.0 degree for about half of the frequencies to about +1.0 degree for the remainder. However, there was no elevation shift for the 8.7 GHz frequency. The average gain values for the third harmonic region vary from -21.8 dB at

3-48

both 8.8 GHz and 10.0 GHz to -8.3 dB at both 8.0 GHz and 9.9 GHz.   The
standard deviation varies from 10.9 dB at 8.4 GHz to 15.3 dB at 9.2 GHz.

POWER PATTERN DISPLAYS

The power patterns displayed in Figures 8 and 9 for the in-band frequency
of 3.0 GHz show the typical behavior expected for the parallel polarization
pattern at the design frequency.   Namely, there is a single pencil beam whose
peak gain is 28.2 dB, and the close-in sidelobes are about -22 dB relative to
the peak value located at zero degrees in azimuth and elevation.

The general behavior of the parallel-polarized patterns over the second
harmonic region is shown in Figures 10 through 25.   A rapid assessment of the
two dimensional patterns may be made by scanning the plots shown in Figures
10, 12, 14, 16, 18, 20, and 24 for the frequencies of 5.5 GHz, 6.0 GHz,
6.2 GHz, 6.3 GHz, 6.4 GHz, 6.5 GHz, and 6.6 GHz, respectively.   The
characteristics of each pattern in the vicinity of the pattern peak are
displayed in the azimuth and elevation plots presented in the odd-numbered
figures immediately following each plot.

Several interesting facts can be derived from inspection of the plots in
Figures 10 through 25.   In particular, the pattern details change
significantly with changes in frequency, even for test frequencies for which
the same number of higher-order modes can propagate.   This behavior may be
discerned (1) by comparing the plots for 5.5 GHz, 6.0 GHz, and 6.1 GHz with
each other and (2) by comparing the plots for 6.6 GHz with the plots for 6.5
GHz.   In the first instance, only the first five modes can propagate; in the
second instance, the first eight modes can propagate.   In both instances, the
pattern details are seen to be noticeably different for two frequencies which
have common allowed mode excitations.   This behavior is attributed to changes
in the complex excitation coefficients of the propagating modes with
frequency.

3-49

Furthermore, comparison of the patterns for frequencies 6.2 GHz, 6.3 GHz, and 6.4 GHz (which have differing numbers of allowed modes) reveals that the pattern details vary considerably for these three frequencies. However, without a much deeper analysis than is provided for in this measurements study, it is not possible to discern whether the pattern changes are due mainly to the appearance of new modes or merely to changes in the relative amplitudes and phases of the previously existing modes. Nevertheless, it is clear from the pattern plots that small changes of 0.1 GHz at out-of-band frequencies can cause significant changes in the antenna pattern details.

All of the interacting pattern characteristics cited above for the second harmonic frequency region also apply to the patterns displayed in Figures 26 through 42 for the third harmonic region. For example, the pattern details for the out-of-band frequencies of 8.8 GHz and 9.0 GHz differ noticeably despite having the same number of allowed modes. The sensitivity of the third harmonic patterns to changes in the number of modes may be discerned by inspecting the patterns for 8.0 GHz, 9.0 GHz, 9.2 GHz, 9.4 GHz, 9.6 GHz, and 10.0 GHz for which energy can propagate in the first 10, 11, 12, 14, 15, and 17 modes, respectively. Again, it cannot be readily determined if the observed changes in pattern details are due primarily to the appearance of additional modes or to changes in the relative amplitudes and phases of previously existing modes.

The cross-polarized maximum azimuth pattern recorded for the in-band frequency of 3.0 GHz displayed in Figure 38 has the characteristic "split-beam" shape associated with cross-polarized patterns. The recorded peak gain value of 6.8 dB is perhaps higher than expected and may be partially due to compact range effects arising from the cross-polarization characteristics of the range. Nevertheless, the cross-polarized pattern serves as a useful reference pattern for gauging the relative significance of cross-polarized patterns at out-of-band frequencies.

The cross-polarized patterns for the recorded maximum azimuth patterns shown in Figures 39 through 44 for the out-of-band frequencies of 5.5 GHz, 6.5

GHz, 7.5 GHz, 8.0 GHz, 9.0 GHz, and 10.0 GHz, all have the characteristic
"split-beam" shape. However, the recorded peak gains are significantly
greater than the recorded peak gain for the in-band frequency. This result is
attributed primarily to the excitation of the TE_{mn} and TM_{mn} modes having both
indices greater than zero and possibly the TE_{0m} modes having odd values of m
greater than one. A Fourier analysis of the complex (amplitude and phase)
pattern data recorded over at least +60 degrees in azimuth and elevation would
be required in order to identify confidently the waveguide mode excitations
for the cross-polarized and the parellel-polarized patterns.

STATISTICAL AVERAGE PATTERNS

The statistical average patterns for the parallel polarization sense for
the second and third harmonic frequency regions displayed in Figures 45 and
46, respectively, provide a succinct description of the measured out-of-band
pattern characteristics over the second and third harmonic regions. The
patterns were obtained by computing the numerical average value of the
measured pattern data for all of the frequencies in the measured frequency
band at each recorded azimuth and elevation angle. The standard deviation at
each azimuth and elevation was also computed.

The average peak gain value of 28.2 dB occurs at an azimuth angle of +0.5
degree and elevation angle of -2.0 degrees for the second harmonic average
pattern. The standard deviation at the average peak gain level is ±4.0 dB.
The standard deviation in the sidelobe regions varies from about ±3.0 dB to
±8 dB.

The average peak gain value of 24.0 dB occurs at an azimuth angle of -0.5
degree and elevation angle of 0 degrees for the third harmonic average
pattern. The standard deviation at the average peak gain level is ± 5.6 dB.
Again, the standard deviation in the sidelobe regions varies from about ±3 to
about ±8 dB.

The cumulative probability distribution function associated with each point in angular (θ,ϕ) space is, in fact, a function of the angular coordinates (θ,ϕ). However, analysis of the cumulative probability distribution function at the angular coordinates of the peak average gain (and at one point in the sidelobe region) indicates that the Gaussian approximation provides satisfactory estimates for most engineering applications. More accurate estimates of the cumulative probability density functions can, of course, be constructed directly from the measured data at each point in angular space. Alternatively, one could compute, for example, the first 4 or 5 "cumulants" to approximate the "characteristic functions" and obtain the probability density functions at each point as the Fourier transform of the approximate "characteristic function".[7] The cumulative probability distribution at each point in angular space is then obtained by integrating the probability density function (see Reference 7). Both methods require considerable amounts of computer time in order to process the large mass of measured data for the second and third harmonic regions. However, it may be possible to derive relatively simple estimates of the angle-dependent cumulative probability distribution functions through further analytical and numerical investigations.

---

[7] Papoulis, A., Probability, Random Variables, and Stochastic Processes, McGraw-Hill, Inc., 1965.

SECTION 4

RESULTS AND RECOMMENDATIONS

RESULTS

The out-of-band antenna patterns measured during this research program
for a reflector antenna illuminated by a small horn antenna excited via a
coax-to-waveguide adapter represent a significant first step toward the goal
of attaining a comprehensive measured data base for the out-of-band radiation
characteristics of reflector antennas. The effects of higher-order mode
excitations in the waveguide feed horn assembly are clearly evident in the
measured antenna patterns over the tested second and third harmonic frequency
regions. The general characteristics of the measured data that are important
for EMC applications may be summarized as follows:

1. The peak gains of the out-of-band patterns are generally
comparable with the peak gain at the in-band design frequency and frequently
exceed the in-band peak gain. Most of the peak gains are greater than 25 dB
above isotropic.

2. A substantial cross-polarized pattern is radiated for the out-of-
band frequencies. The peak gains of the cross-polarized patterns are greater
than 10 dB above isotropic for the majority of the tested frequencies.

3. The peak of the out-of-band radiation is typically shifted in
azimuth and elevation away from the in-band electrical boresight direction.
However, the azimuth and elevation shifts are usually less than the 3-dB
beamwidth of the shifted "beam".

4. The out-of-band patterns typically have several prominent
secondary lobes whose peak gains are also significant for EMC applications.

5. The computed average gains over the front 80-degree azimuth
sector are typically greater than isotropic for the second harmonic
frequencies, but they are typically below isotropic for the third harmonic
frequencies.

6. The cumulative probability distributions computed directly from
the measured out-of-band data differ noticeably from a Gaussian distribution
and do not appear to have analytical form, but the Gaussian approximation can

nonetheless provide useful interim engineering estimates for the cumulative
probability distributions.

The out-of-band data supplied to ECAC under this contract are immediately
useful for EMC analysis of cosited antenna coupling and should enhance the
validity and confidence of out-of-band antenna coupling estimations for
applicable real-world situations. However, further empirical and analytical
research efforts are needed in order to obtain a more comprehensive data base
and to derive efficient and reliable analytical models for analyzing and
subsequently improving the electromagnetic effectiveness of cosited
antennas. Toward that end, it is recommended that the following additional
research tasks be undertaken.

RECOMMENDATIONS

1. Additional Out-of-Band Pattern Measurements. Additional measurements
of the out-of-band pattern performance of reflector antennas are needed to
determine the effects of transmission line components. The out-of-band
pattern performance has been shown to be sensitive to the type of waveguide
transmission components employed in the feed system. To date, measurements
have been performed using a simple coaxial cable-to-waveguide adapter feed
system. It is proposed that additional measurements be performed using a feed
system incorporating:

    a. coaxial cable-to-waveguide adapter and E-plane bend,
    b. coaxial cable-to-waveguide adapter and H-plane bend,
    c. a coaxial cable-to-waveguide adapter attached to a typical
waveguide feed which extends from the reflector rim to the feed horn.

Statistical processing will be performed on the data to determine whether the
different transmission line devices result in significant changes in the out-
of-band statistical average pattern performance. These measurements will be
performed over frequency bands centered about the fundamental, the second, and
the third harmonic frequecies.

2. Computer Model Simulations. A Monte Carlo computer model has been developed under a companion program (see Reference 1) to compute statistical average out-of-band reflector antenna patterns. Preliminary computer simulations have demonstrated that the out-of-band patterns are particularly sensitive to the relative phase deviation of the higher-order transmission line mode. However, the sensitivity of the model results as a function of variables such as the mode amplitudes, mode phases, and "mixture" of modes has not yet been tested against measured data. It is proposed that the following numerical simulations be performed to determine the computer model sensitivity:

   a. Exercise the computer model to determine the effects of mode amplitudes, mode relative phases, and mode mixture on the out-of-band pattern statistics -- specifically, the mean pattern and standard deviations.

   b. Modify the model to account for the effects of waveguide feed system length on the relative model phases by using the higher-order mode phase velocity equations.

   c. Compare the computer model mean patterns and standard deviations with the measured data obtained during the measurement program.

3. Extension of the Out-of-Band Reflector Antenna Pattern Model. The present computer model performs a vector calculation of the average pattern and standard deviation over an approximately ±50° to ±80° field-of-view centered on the antenna boresight. In many applications, it is desirable to determine the complete pattern statistics including the back-lobe regions. Also, it is often necessary to compute pattern statistics such as the median gain and standard deviation over either a complete 4π steradian or partial angular sector. However, with the present model, these computations can be time-consuming and expensive. Thus, it is proposed that the model be extended to:

   a. Include the effects of reflector rim edge diffraction and strut and feed horn blockage on the out-of-band antenna pattern. This

extension will make it possible to compute the out-of-band pattern over a full
4π steradian angular sector, or over any selected subsector of the pattern.

   b.   Incorporate routines to determine the median gain and
standard deviation of the out-of-band pattern for the full 4π steradian
angular sector.

   c.   Examine computational methods to decrease the computer run
time required by the model. These methods might incorporate some recently
published techniques which are particularly suited to circular aperture-type
antennas.

   4.   Out-of-Band Antenna Coupling. Presently, under U.S. Army CORADCOM
sponsorship through the Army Research Office, a theoretical model for out-of-
band, near-field antenna coupling is under development. However, no measured
data are available to validate the theoretical analysis. It is, therefore,
proposed to perform a limited set of out-of-band antenna coupling
measurements, including the following:

   a.   Out-of-band coupling measurements as a function of azimuth
angle for two reflector antennas located at the same elevation. (Note: this
corresponds to the "common boresight" case.) These measurements will be
performed over frequency bands centered on the second and third harmonics.

   b.   Antenna coupling measurements as a function of azimuth angle
for two reflector antennas separated by approximately one-to-two antenna
diameters in elevation. These measurements will be performed over frequency
bands centered on the second and third harmonics.

The measured data will be processed to determine the mean and standard
deviation of the out-of-band coupling as a function of azimuth angle. It is
proposed that "identical" antennas be employed whose out-of-band far-field
pattern statistics are known. By employing known, "identical" antennas, a
correlation between the far-field pattern median gain and the near-field
coupling can be readily examined.

APPENDIX A
DESCRIPTION OF THE TEST ANTENNA

The test antenna used in this study (see Figure 1) is a horn-fed, 4-foot-diameter paraboloidal reflector antenna having an F/D ratio of 0.4. A detailed description of the feed and feed support assembly is provided by the sketches in Figures A-1 through A-4. Figure A-1 shows a front view of the antenna; Figure A-2 presents a side view of the antenna. The feed horn assembly and mounting ring are profiled in Figure A-3. Finally, Figure A-4 is a sketch of the feed horn aperture.
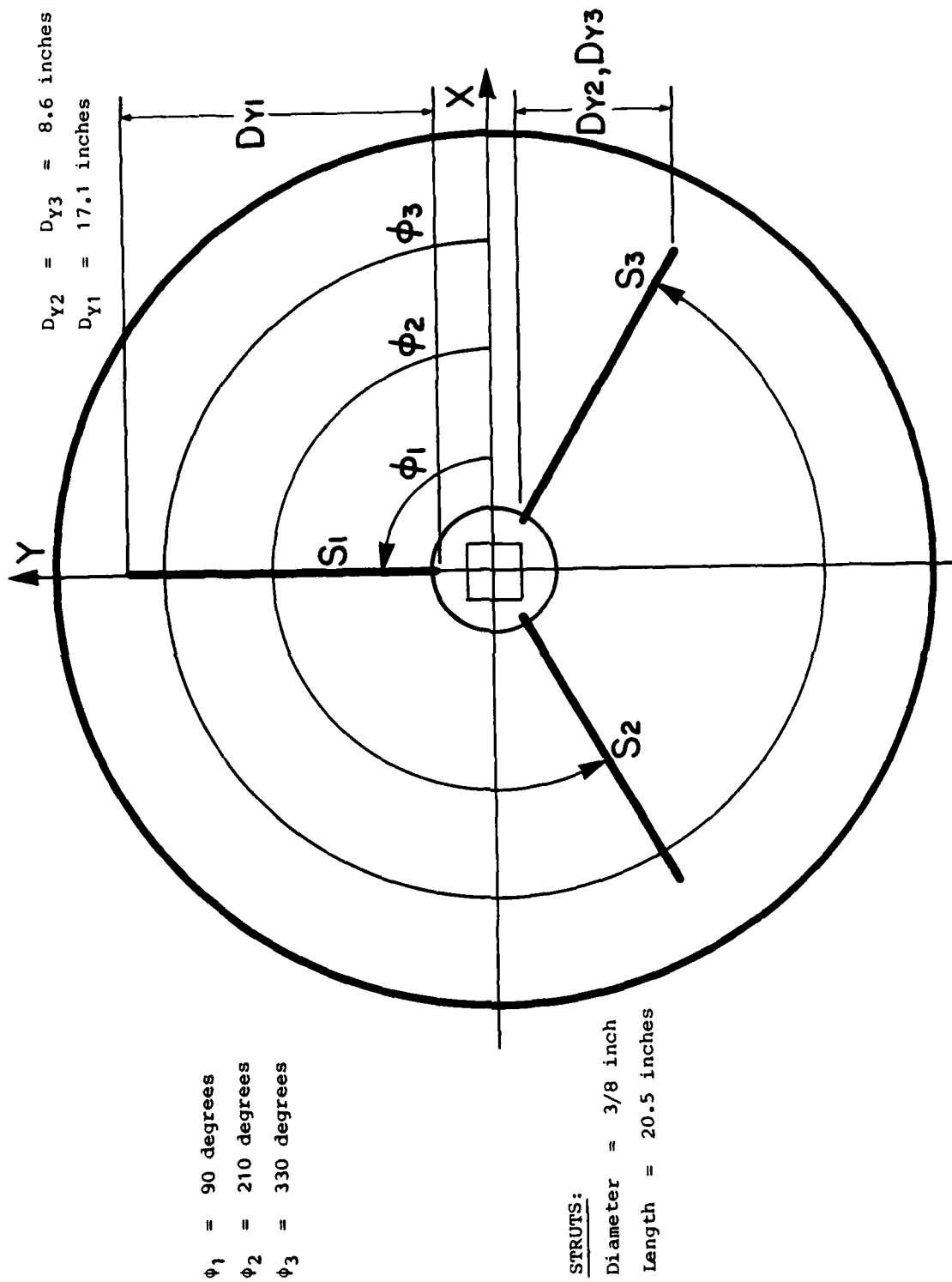
Figure A-1. Front view of the test antenna.

D_{Y2} = D_{Y3} = 8.6 inches

D_{Y1} = 17.1 inches

ϕ_1 = 90 degrees

ϕ_2 = 210 degrees

ϕ_3 = 330 degrees

STRUTS:

Diameter = 3/8 inch

Length = 20.5 inches

A-2
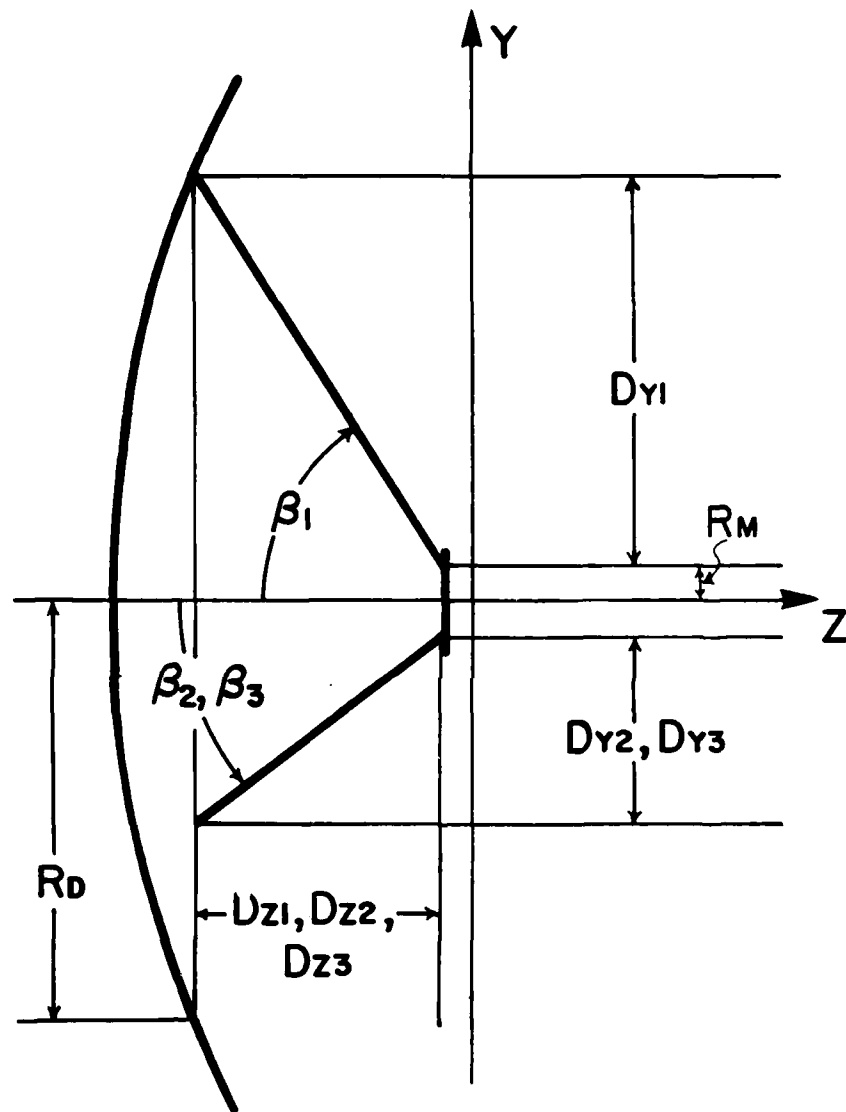
D_{Y1} = 17.1 inches β_1 = 56.6 degrees

D_{Y2} = D_{Y3} = 8.6 inches β_2, β_3 = 37.3 degrees

D_{Zall} = 11.3 inches R_D = 20 inches

R_M = 2.9 inches

Figure A-2. Side view of the test antenna.

w_N = 1.5 inches

w_F = 2 1/8 inches

γ = 5.1 degrees

L flare = 3.5 inches
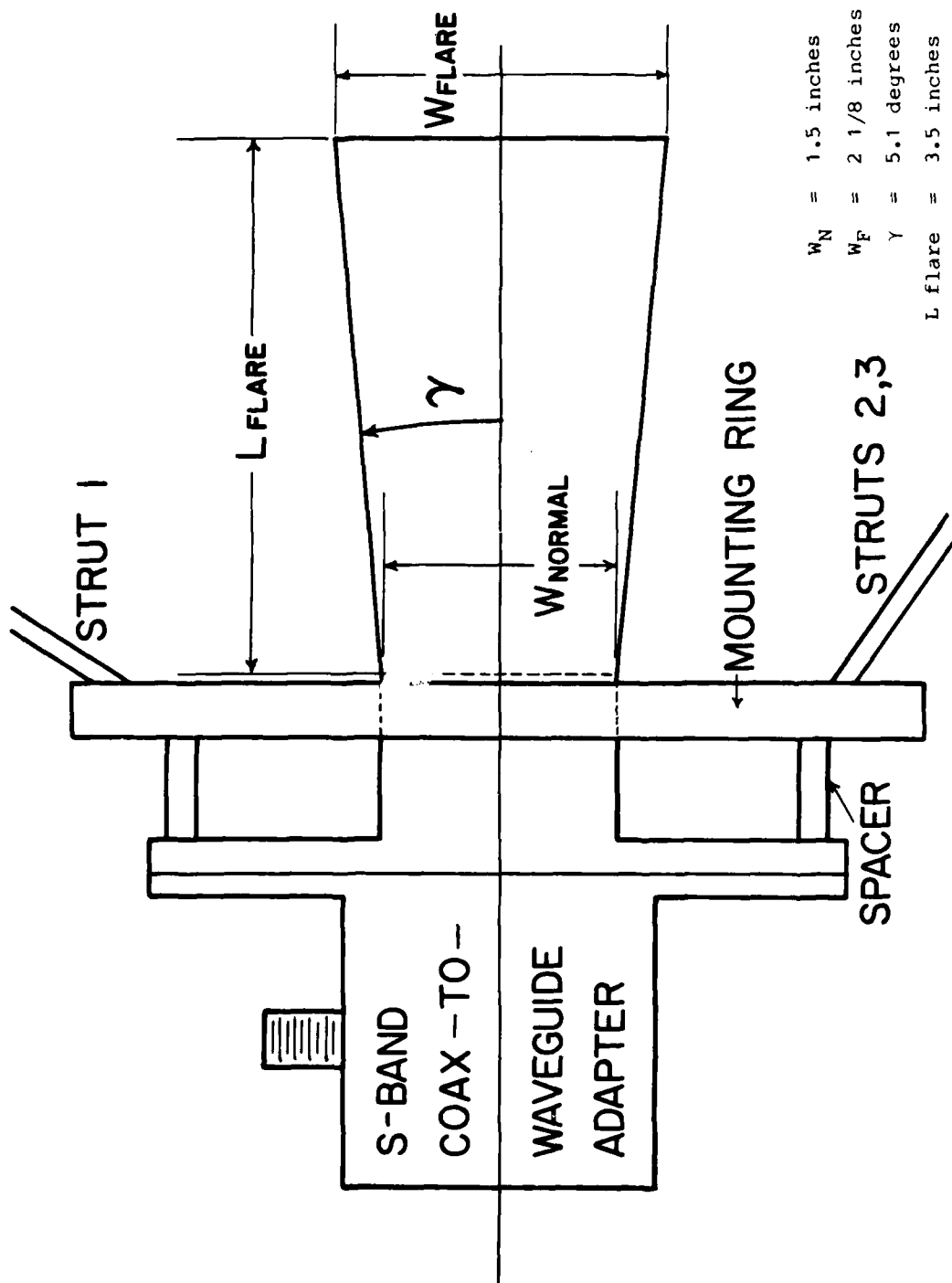
Figure A-3. Side view of the feed horn and mounting ring.

Figure A-4.   Inside dimensions of the feed horn aperture.
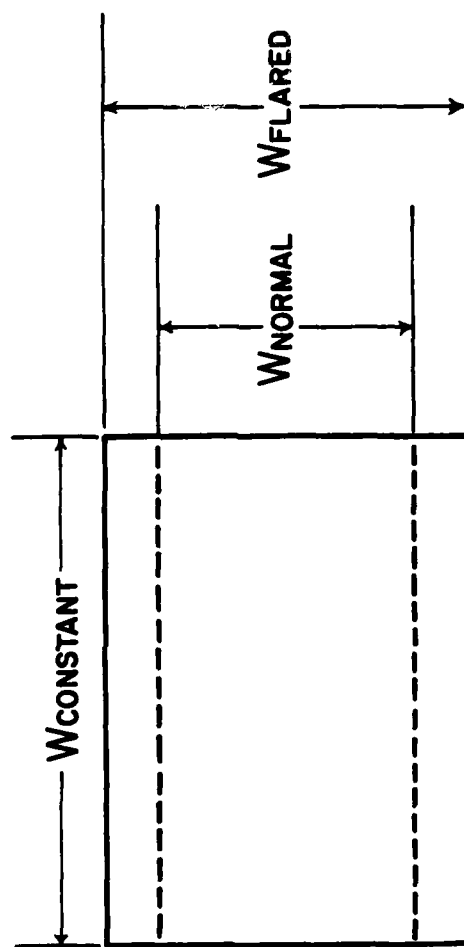
W_C = 2.84 inches

W_N = 1.34 inches

W_F = 1.97 inches

MICROCOPY RESOLUTION TEST CHART

NATIONAL BUREAU OF STANDARDS 1963 A
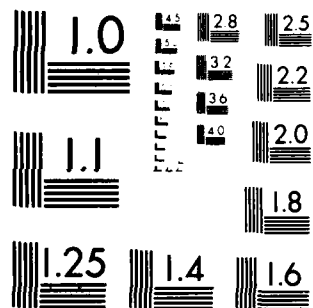
APPENDIX B
LIST OF CONTRIBUTING PROFESSIONALS

The following engineers/scientists (listed in descending order of person-hours devoted to this research program) made major contributions to the research efforts on this contract:

B. J. Cown

E. E. Weaver

R. C. Rogers

C. E. Ryan, Jr.

F. L. Cain

D. R. Blount.

APPENDIX C

LIST OF RELATED CONTRACTS

TABLE C-1 lists contracts performed by the Electronics and Computer System Laboratory of the Engineering Experiment Station of the Georgia Institute of Technology that are related to the measurements presented in this report.

TABLE C-1

CONTRACTS RELATED TO RADAR ANTENNAS
(Page 1 of 2)

Project No.	Contract Number & Sponsor	Title	Funding Level ($)	Period
A-579	NObsr-85387 BuShips	Antenna Characteristics (A Study of Interference Susceptibility of Radar Antennas)	185,000	1961-1963
A-750	NObsr-91070 BuShips	Improved Antenna Characteristics of Shipboard Radar Antenna	114,000	1963-1966
A-958	NObsr-95379	Statistical Gain Characteristics of Radar Targets	80,000	1966-1968
A-1080	N00024-68-C-1126 NSSC	Statistical Median and Mutual Gain and Modes in Rotary Joints of Radar Antennas	85,000	1968-1969
A-1301	N00024-71-1120 NSEG	Near-Field Obstacle Effects and Phased-Array Studies	75,000	1971-1971
A-1399	N00024-72-1274 NSSC	Near-Field Obstacles Effects and Phased-Array Studies	100,000	1972-1973
A-1433	DAAH01-72-0950 AMC	An Investigation of the Accuracy of Far-Field Radiation Patterns Determined from Near-Field Measurements	62,000	1972-1973
A-1504	N00024-73-C-1141 NSSC	Near-Field Obstacle Effects and Phased-Array Studies Phase III - Data Collection and Analysis	75,000	1973-1974
A-1588	DAAH01-74-C-0367 MICOM	A Study of Phased-Array Antenna Patterns Determined by Measurements on a Near-Field Range	99,000	1973-1974

TABLE C-1

(Page 2 of 2)

Project No.	Contract Number & Sponsor	Title	Funding Level ($)	Period
A-1611	Atlantic Res. Corp.	DG/AEGIS Electromagnetic Effectiveness Analysis Program	5,000	1974-1974
A-1613	N00024-74-C-1215 NRFC	Effects of Near-Field Structures on Antennas Performance and Phased-Array Studies	75,000	1974-1975
A-1694	F30602-75-0065 RADC	Broadband Antenna Measurement Techniques, Phase II	96,000	1974-1975
A-1703	Selenia, S.p.A. Rome, Italy	Modeling of Near-Zone Scattering for Selenia Applications	8,000	1974-Open
A-1715	N00024-75-C-5099 NASC	Main-Beam Distortion Effects of Ship Superstructures on Radar Antenna Performance	100,000	1975-1976
A-1830	N00024-76-C-7147 NSSC	Main Beam Distortion Effects of Near-Field Ship Stuctures	100,000	1976-1976
A-1885	F30602-75-C-0118 RADC	Broad Band Measurement System Studies	15,000	1976-1977
A-2179	DAAG29-78-C-0029 ARO	Out-of-Band EMC Measurement Techniques and Instrumentation for Phased-Array Antenna System	150,000	1978-1981
A-2610	DAAG-29-80-C-0083 ARO	Out-of-Band Reflector Model	50,000	1980-1981

LIST OF REFERENCES

1. Wells, T. B., and Ryan, C. E., Jr., Out-of-Band Reflector Antenna Model, Georgia Institute of Technology, Final Technical Report, Contract DAAG29-80-C-0083, May 1981.

2. Cown, B. J. and Ryan, C. E., Jr., Near-Field Theory and Techniques for Wideband Radiating Systems at In-Band and Out-of-Band Frequencies, Georgia Institute of Technology, Interim Technical Report No. 2, Contract No. DAAG29-78-C-0029, March 1980.

3. Johnson, R. C., "Antenna Range for Providing a Plane Wave for Antenna Measurements," U.S. Patent 3 302 2-5, January 31, 1967.

4. Johnson, R. C., Ecker, A., Moore, R. A., "Compact Range Techniques and Measurements, "IEEE Transactions on Antennas and Propagation, Vol. AP-17, pp. 568-576, September 1969.

5. Collin, R. E., Field Theory of Guided Waves, McGraw-Hill, Inc., 1960.

6. Cown, B. J. and Ryan, C. E., Jr., "Near-Field Theory and Techniques for Wideband Radiating Systems at In-Band and Out-of-Band Frequencies, Georgia Institute of Technology, Final Technical Report, Contract no. DAAG29-78-C-0029, January 1982.

7. Papoulis, A., Probability, Random Variables, and Stochastic Processes, McGraw-Hill, Inc., 1965.

DISTRIBUTION LIST FOR
ANTENNA PATTERN MEASUREMENTS TO CHARACTERIZE THE OUT-OF-BAND
BEHAVIOR OF REFLECTOR ANTENNAS
ECAC-TR-83-003

External	No. of Copies
Dr. Barry Cown Engineering Experiment Station Georgia Institute of Technology Atlanta, GA 20332	10
Dr. Raymond C. Baird National Bureau of Standards Electromagnetic Fields Division 723.05 Boulder, CO 80303	1
Chief of Naval Operations (OP-941F) Navy Department Washington, DC 20350	1
Director Navy Electromagnetic Spectrum Center Naval Communication Unit Washington Washington, DC 20390	1
Commanding Officer (Code 5341/Tompkins) Naval Research Laboratory Washington, DC 20375	1
Commanding Officer (Code 4108/Balthasar) Naval Research Laboratory Washington, DC 20375	1
Commander (Code 6174D) Naval Ship Engineering Center Washington, DC 20362	1
Commander (Code 6174E) Naval Ship Engineering Center Washington, DC 20362	1
Commander (SEA-06T) Naval Sea Systems Command Washington, DC 20362	1
Commander (SEA-034) Naval Sea Systems Command Washington, DC 20362	1

External	No. of Copies
Commander (SEA-03412/Demattia) Naval Sea Systems Command Washington, DC 20362	1
Commander (PMS-404-30) Naval Sea Systems Command Washington, DC 20362	1
Naval Sea Systems Command Department of the Navy Washington, DC 20362 Attn: Mr. Oz White	1
Commander (SY-83/Lane) Naval Air Test Center Patuxent River, MD 20670	1
Commanding Officer Naval Electronic Systems Engineering Activity, St. Inigoes St. Inigoes, MD 20684	1
Commander (Code 8105/Jensen) Naval Ocean Systems Center San Diego, CA 92152	1
Commander (Code 8105/Rockway) Naval Ocean Systems Center San Diego, CA 92152	1
Commander (Code 8122/Peter Li) Naval Ocean Systems Center San Diego, CA 92152	1
Commander (I. Olsen) Naval Ocean Systems Center San Diego, CA 92152	1
Superintendent (Dr. R. Adler) Naval Postgraduate School Monterey, CA 93940	1
Commander (Code 3525/Harris) Naval Weapons Center China Lake, CA 93555	1

External	No. of Copies
Western Area Frequency Coordinator Point Mugu, CA 93042	1
Commanding Officer Naval Avionics Center 21st and Arlington Ave. Indianapolis, IN 46218	1
Commander (Code CF-54/Needy) Naval Surface Weapons Center Dahlgren, VA 22448	1
Commander (Code CF-52/Lenzi) Naval Surface Weapons Center Dahlgren, VA 22448	1
Commander Pacific Missile Test Center Point Mugu, CA 93042	1
Commanding Officer Naval Underwater Systems Center Newport, RI 02840	1
Officer in Charge New London Laboratory Naval Underwater Systems Center New London, CT 06320	1
CDR, USACECOM Attn: DRSEL-COM-RY-3 Fort Monmouth, NJ 07703	1
CDR, USACECOM Attn: DRSEL-SEI-A (S. Segner) Fort Monmouth, NJ 07703	1
Dr. James Mink Code DRXRO-EL U.S. Army Research Office Post Office Box 12211 Research Triangle Park, NC 27709	1
CDR, USACECOM Attn: DRSEL-COM-RF-2 (P. Sass) Fort Monmouth, NJ 07703	1

External	No. of Copies
CDR, USAEPG Attn: STEEP-MT-M (LTC Turpin) Fort Huachuca, AZ 85613	1
Paul Major CECOM/CENSEI Fort Monmouth, NJ 07703	1
Warren Kesselman CAA36 Fort Monmouth, NJ 07703	1
HQ USAF/FMC Washington, DC 20330	1
USAF TAWC/EWCE Attn: J. H. Smith, Jr. Eglin AFB, FL 32541	1
HQ ASD/ENACE Wright-Patterson AFB, OH 45433	1
HQ RADC/RBC Griffiss AFB, NY 13441	1
1839th EIG/EIE Keesler AFB, MS 39534	1
HQ AFCC/DOYF Scott AFB, IL 62225	1
1842 EEG/EEITE Scott AFB, IL 62225	1
HQ AFEWC/ESRI San Antonio, TX 78243	1
JEWC/TAM San Antonio, TX 78243	1
EIC/EIEUS Oklahoma City AFB, OK 73145	1
HQ ESC/SD San Antonio, TX 78243	1
Defense Technical Information Center Cameron Station Alexandria, VA 22314	2

External	No. of Copies
Air University Library	1
Maxwell AFB, AL 36112	

Internal	
CC	1
CD	1
CCN	1
CA	1
CF	1
CM	1
CN	1
XM	1
XMT	1
XMT/J. Janoski	2
DO	1
DO-1	1
DO-2	1
DQ	1
DQT/D. Madison	1
DQT/M. Aasen	1
DC	1
DF	1
DI	1
DN	1
DS	1
DR	1
DRD	1
DRD/W. Stuart	5
DRD/R. Albus	1
DRD/B. Campbell	1
DRD/K. O'Haver	1
DRD/E. Kaita	1
DRD/R. Meidenbauer	1
DRD/W. Kuebler	1
DRD/R. Adams	1
DRM	1
DRM/A. Johnstone	1
DRS	1
DRC	1
DIL	10
DIL	Camera-Ready

ATE
MED
8